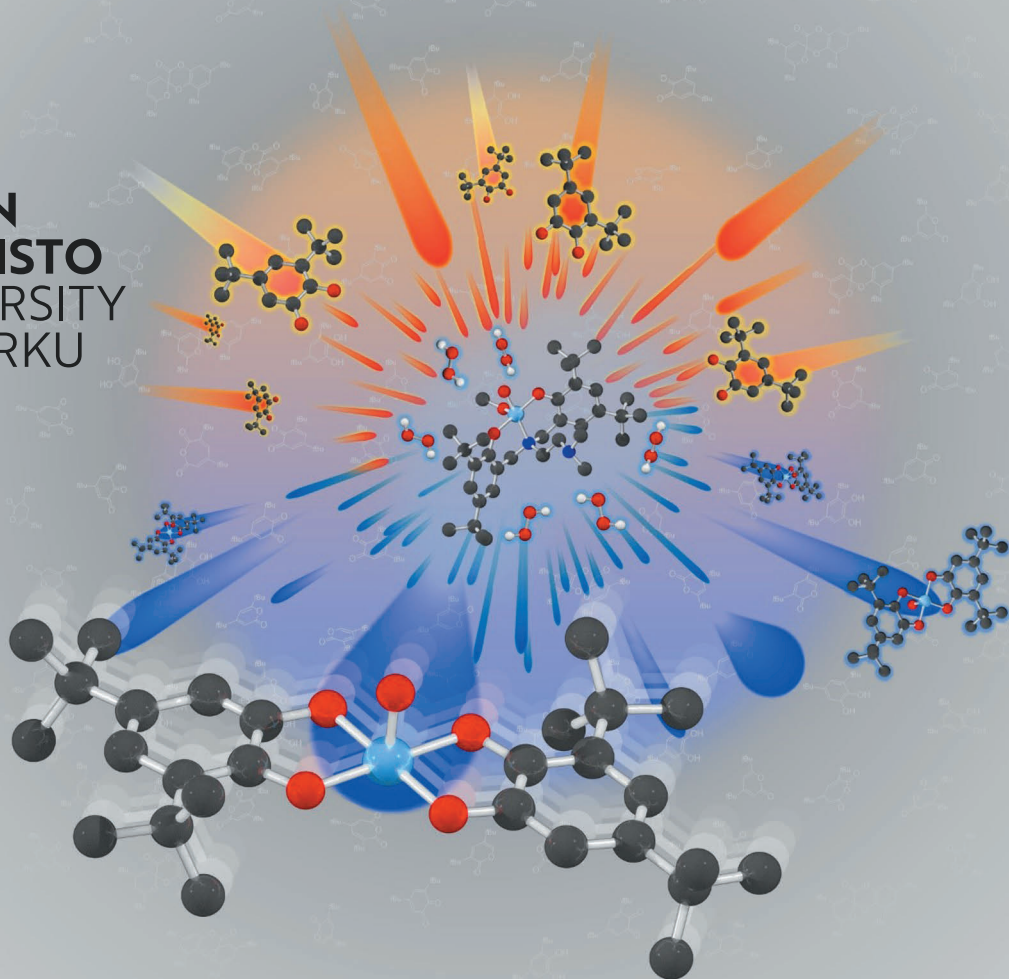




**TURUN  
YLIOPISTO**  
UNIVERSITY  
OF TURKU



# AMINOPHENOLATO COMPLEXES OF Mo, W, AND V

In Catalytic Alkene Epoxidation and  
Catechol Oxidation

Pasi Salonen





**TURUN  
YLIOPISTO**  
UNIVERSITY  
OF TURKU

# **AMINOPHENOLATO COMPLEXES OF Mo, W, AND V**

In Catalytic Alkene Epoxidation and Catechol Oxidation

---

Pasi Salonen

## University of Turku

---

Faculty of Science  
Department of Chemistry  
Intelligent Materials Chemistry Group  
Doctoral Programme of Physical and Chemical Sciences

## Supervised by

---

Doctor, Ari Lehtonen  
Intelligent Materials Chemistry Group  
Department of Chemistry  
University of Turku  
Turku, Finland

## Reviewed by

---

Professor, Timo Repo  
Chemical Synthesis and Analysis  
Department of Chemistry  
University of Helsinki  
Helsinki, Finland

Associate Professor, Anders Thapper  
Synthetic Molecular Chemistry  
Department of Chemistry  
Uppsala University  
Uppsala, Sweden

## Opponent

---

Senior Associate Professor, Dominique Agustin  
IUT Paul Sabatier  
Paul Sabatier University (Toulouse III)  
Toulouse, France

The originality of this thesis has been checked in accordance with the University of Turku quality assurance system using the Turnitin OriginalityCheck service.

Front cover by Pasi Salonen & Anssi Peuronen; Dalton Transactions 14 May 2021  
Issue 18 pp. 5991–6358, copyright Royal Society of Chemistry

ISBN 978-951-29-8654-5 (Print)  
ISBN 978-951-29-8655-2 (PDF)  
ISSN 0082-7002 (Print)  
ISSN 2343-3175 (Online)  
Painosalama, Turku, Finland 2021

*"In the fields of observation chance  
favors only the prepared mind"  
(Louis Pasteur)*

UNIVERSITY OF TURKU

Faculty of Science

Department of Chemistry

Chemistry

PASI SALONEN: Aminophenolato Complexes of Mo, W, and V in Catalytic Alkene Epoxidation and Catechol Oxidation

Doctoral Dissertation, 187 pp.

Doctoral Programme in Physical and Chemical Sciences

October 2021

## ABSTRACT

Mo, W and V are found naturally in metalloenzymes such as the Mo/W oxotransferases and the V haloperoxidases (VHPOs). These enzymes catalyze oxidation reactions related to C, N, S metabolism as well as halogenation. Cu and Fe are found in metalloenzymes such as the catechol oxidase (CO) and -dioxygenases (CDOs), which are responsible for oxidation of aromatic compounds. Bioinspired and -mimetic chemistry involves the use of synthetic transition metal complexes as structural and/or functional models of natural metalloenzymes. Called bioinorganic chemistry, the approach of modeling metalloenzymes allows harnessing some properties of the enzymes for use *e.g.*, in catalysis. Models allow indirect studies of metalloenzymes to learn aspects related to their structure and mechanism of action *i.e.*, function. The knowledge from the studying of metalloenzymes may be used to improve synthetic processes with more economical and environmentally friendly pathways following the principles of Green Chemistry. Catalysis is utilized to reach good sustainability, efficiency and selectivity and is applied in as much as 90% of all industrial syntheses of fine and bulk chemicals.

In this PhD thesis, several Mo, W and V based model complexes based on aminophenolato and similar ligands were synthesized, characterized, and studied as structural and/or functional models of VHPOs and CO/CDOs. Reflecting the properties of the enzymes, these model complexes were applied as catalysts in catechol oxidation and in the industrially significant epoxidation of alkenes. A recent development is the application of V complexes as functional models of the Cu dependent CO. This thesis work provides compelling evidence implying these reports may be at least partly erroneous. Moreover, substantial links between V mediated CO and CDO studies were revealed for the first time. Mo and W complexes were in turn utilized as catalysts in the epoxidation of alkenes. Several new phenomena, such as the beneficial impact of low catalyst loading was uncovered. Similar reactivity was additionally discovered for known Mo complexes. A novel epoxidation mechanism has been proposed for the studied class of Mo/W complexes based on experimental and computational results. The proposal is in line with recent suggestions that the epoxidation mechanism varies depending on the catalyst.

**KEYWORDS:** Oxidation catalysis, bioinorganic chemistry, enzyme mimetics, molybdenum, tungsten, vanadium

## TURUN YLIOPISTO

Matemaattis-luonnontieteellinen tiedekunta

Kemian laitos

Kemia

Pasi Salonen: Mo, W ja V aminofenolaattokompleksit katalyyttisessä alkeiden epoksidaatiassa ja katekolin hapetuksessa

Väitöskirja, 187 s.

Fysikaalisten ja kemiallisten tieteiden tohtoriohjelma

Lokakuu 2021

### TIIVISTELMÄ

Luonnossa molybdeenia (Mo), volframia (W) ja vanadiinia (V) esiintyy metalloenstyyimeissä kuten Mo/W oksotransferaaseissa sekä V haloperoksidaaseissa (VHPO:t). Nämä entsyymit katalysoivat organismien metaboliaan liittyviä hiilen, typen ja rikin hapetusreaktioita, sekä orgaanisten yhdisteiden halogenaatiota. Kuparia (Cu) ja rautaa (Fe) sisältäviä metalloentsyymejä ovat puolestaan mm. katekolioksidaasi sekä -dioksygenaasit (CO ja CDO:t). Bioepäorgaanisessa kemiassa siirtymämetallikomplekseilla voidaan rakenteellisesti (biomimetiikka) ja/tai toiminnallisesti (biovirikkeisyys) mallintaa metalloentsyymejä. Mallien keinoin voidaan saavuttaa joitain mallinnettavien metalloentsyymien ominaisuuksia, joita voidaan niin ikään hyödyntää vaikka katalyysissä. Lisäksi malleilla voidaan epäsuorasti tutkia tarkasteltavien entsyymien toimintaa ja/tai rakennetta, mistä saadun tiedon avulla voidaan edelleen parantaa synteesiprosessien kannattavuutta ja ympäristöystävällisyyttä Vihreän Kemian periaatteiden mukaisesti. Teollista hieno- ja peruskemikaalien valmistukseen käytetyistä menetelmistä 90% hyödyntää katalyysiä, sillä näin prosesseista saadaan kestäviä, tehokkaita sekä selektiivisiä.

Väitöskirjatyössä valmistettiin useita VHPO, CO ja CDO entsyymejä rakenteellisesti/ toiminnallisesti mallintavia aminofenolaattoligandihin pohjautuvia Mo, W ja V komplekseja, joita käytettiin katalyytteinä katekolin hapetuksessa sekä teollisesti merkittävässä alkeiden epoksidaatiassa em. entsyymien ominaisuuksia jäljitellen. Monien V yhdisteiden on sittemmin osoitettu olevan CO:n toiminnallisia malliyhdisteitä. Väitöskirjatyössä saadut tutkimustulokset kuitenkin viittaavat vahvasti siihen, ettei näin välttämättä ole, sillä V pohjaisten CO ja CDO malliyhdisteiden reaktiivisuuden välillä löydettiin merkittäviä yhtymäkohtia. Mo ja W aminofenolaattokomplekseja tutkittiin puolestaan alkeiden epoksidaatiokatalyytteinä. Yhdisteille löydettiin uusia ominaisuuksia, kuten katalyysiominaisuuksien parantuminen katalyytin määrää pienennettäessä. Samanlaisia ominaisuuksia löydettiin lisäksi jo entuudestaan tunnetuille Mo komplekseille. Kokeellisten sekä laskennallisten tulosten perusteella tutkituille komplekseille kyettiin esittämään uudenlaista epoksidaatiomekanismia. Esitys on linjassa muiden viime aikaisten tulosten kanssa, joiden mukaan mekanismi vaihtelee katalyytin mukaan.

ASIASANAT: Hapetusreaktio, bioepäorgaaninen kemia, entsyymimallinnus, molybdeeni, volframi, vanadiini

# Table of Contents

<b>Abbreviations and Symbols .....</b>	<b>8</b>
<b>List of Original Publications .....</b>	<b>12</b>
<b>List of Relevant Publications .....</b>	<b>13</b>
<b>1 Introduction.....</b>	<b>14</b>
<b>2 Literature Review.....</b>	<b>16</b>
2.1 Bioinorganic Chemistry Aspects.....	16
2.1.1 Vanadium Haloperoxidases.....	17
2.1.2 Catechol Dioxygenases.....	18
2.1.2.1 Catechol Dioxygenase Mechanism .....	20
2.1.3 Catechol Oxidase .....	21
2.1.3.1 Catechol Oxidase Mechanism .....	23
2.1.4 Molybdenum and Tungsten Oxotransferases.....	24
2.2 Catalysis – General Aspects.....	25
2.2.1 Activity Metrics: TON and TOF.....	26
2.2.2 Stability of Catalysts .....	27
2.2.3 Green Chemistry .....	27
2.2.3.1 Atom Economy and the E-factor.....	28
2.2.3.2 Choice of Solvent.....	29
2.2.3.3 Choice of Oxidant .....	30
2.3 Alkene Epoxidation .....	32
2.3.1 Utilization of Epoxides .....	33
2.3.2 Preparation of Epoxides .....	34
2.3.3 Alkene Model Compounds .....	34
2.3.4 Alkene Epoxidation Mechanism .....	35
2.3.4.1 Mimoun, Sharpless and Thiel Mechanisms ...	36
2.3.5 Mo & W Based Epoxidation Catalysis .....	38
2.3.5.1 Organometallic Systems.....	39
2.3.5.2 [MO <sub>2</sub> X <sub>2</sub> L <sub>2</sub> ] Systems.....	41
2.3.5.3 Schiff-Base and Porphyrin Systems .....	43
2.4 Catechol Oxidation .....	47
2.4.1 Vanadium Catechol Dioxygenase Mimetics .....	47
2.4.1.1 Finke’s “Common Catalyst Hypothesis” .....	50
2.4.1.2 Common Catalyst Identification .....	51
2.4.2 Vanadium Catechol Oxidase Mimetics.....	54
<b>3 Aims of the Studies .....</b>	<b>56</b>



<b>4</b>	<b>Materials and Methods</b> .....	<b>57</b>
4.1	General Instrumentation .....	57
4.2	Syntheses and Characterization .....	58
4.2.1	Proligand Syntheses .....	58
4.2.2	Complex Syntheses .....	59
4.3	Catalysis .....	61
4.3.1	Catechol Oxidase Mimetics .....	61
4.3.2	Catechol Dioxygenase Mimetics .....	61
4.3.3	Alkene Epoxidation .....	62
<b>5</b>	<b>Results and Discussion</b> .....	<b>64</b>
5.1	Syntheses and Characterization .....	64
5.1.1	Proligands .....	64
5.1.2	Complexes .....	65
5.1.3	Description of Crystal and Molecular Structures .....	68
5.2	Catalysis – Catechol Oxidation .....	72
5.2.1	Catechol Oxidase Mimetics .....	72
5.2.1.1	Detection and Role of H <sub>2</sub> O <sub>2</sub> .....	75
5.2.1.2	Mechanistic Considerations – ESI-MS and <sup>51</sup> V NMR .....	76
5.2.2	Catechol Dioxygenase Mimetics .....	78
5.2.2.1	Product Distribution – Column and Gas Chromatography .....	78
5.2.2.2	Product Distribution – Control Reactions .....	81
5.2.2.3	Vanadium Speciation: EPR and ESI-MS .....	83
5.2.3	Vanadium Catalyzed Catechol Oxidase vs. Dioxygenase Mimetism? .....	87
5.3	Catalysis – Alkene Epoxidation .....	89
5.3.1	Epoxidation Mechanism – Role of the Pendant Arm ....	96
5.3.1.1	Induction Period .....	99
5.3.1.2	“Dilution Effect” .....	100
5.3.1.3	Epoxidation Mechanism – DFT .....	102
5.3.1.4	Catalyst Decomposition? .....	104
<b>6</b>	<b>Summary and Conclusion</b> .....	<b>106</b>
<b>7</b>	<b>Future</b> .....	<b>108</b>
	<b>Appendix</b> .....	<b>110</b>
	<b>Acknowledgements</b> .....	<b>115</b>
	<b>List of References</b> .....	<b>118</b>
	<b>Original Publications</b> .....	<b>129</b>

# Abbreviations and Symbols

$\Xi$	Ratio (%) of measured NMR nuclide frequency vs. TMS in $\text{CDCl}_3$
$\square$	Free coordination site
$\delta$	Chemical shift (in ppm, in NMR spectroscopy)
1,2-DCE	1,2-Dichloroethane
1,2-CTD	Catechol 1,2-dioxygenase
2,3-CTD	Catechol 2,3-dioxygenase
3,5-DTBCH <sub>n</sub>	3,5-Di- <i>tert</i> -butylcatechol (n = 2), -catecholato anion/dianion (n = 1 or 0)
3,5-DTBQ	3,5-Di- <i>tert</i> -butyl-1,2-benzoquinone
3,5-DTBSQH <sub>n</sub> <sup>•</sup>	3,5-Di- <i>tert</i> -butyl-1,2-semiquinone (n = 1), -semiquinonato anion (n = 0)
3,6-DTBCH <sub>2</sub>	3,6-Di- <i>tert</i> -butylcatechol
<sup>3</sup> O <sub>2</sub>	Triplet (di)oxygen
4-TBCH <sub>2</sub>	4- <i>Tert</i> -butylcatechol
4-TBQ	4- <i>Tert</i> -butyl-1,2-benzoquinone
4-TBSQ <sup>•</sup>	4- <i>Tert</i> -butyl-1,2-semiquinonato anion
$A(^{51}\text{V})$	<sup>51</sup> V Hyperfine coupling constant in gauss (G) (in EPR spectroscopy)
aap	1-(2-Hydroxyphenyl)-1,3-butanedionato
acac	Pentane-2,4-dionato (acetylacetonato)
AFOR	Aldehyde: ferredoxin oxidoreductase
AH	Acetylene hydratase
Arg	Arginine
ATR	Attenuated Total Reflection
BAP	Bicarbonate activated peroxide
Bn	Benzyl
CD	Circular Dichroism
CDO	Catechol dioxygenase(s)
CHP	Cumene hydroperoxide
CO	Catechol oxidase

Cp/ Cp*	Cyclopentadienyl/ pentamethyl cyclopentadienyl
CV	Cyclic Voltammetry
cyclam	1,4,8,11-Tetraazacyclotetradecane
D	Donor (neutral atom or molecule)
dba	1,5-Diphenylpentane-1,3,5-trionato
DCM	Dichloromethane
DFT	Density Functional Theory
DIPP	2,6-Di- <i>iso</i> -propylphenyl
dmba	1,5-Bis( <i>p</i> -methoxyphenyl)pentane-1,3,5-trionato
DMF	Dimethylformamide
DMSO	Dimethylsulfoxide
DMSOR	Dimethylsulfoxide reductase
DNA	Deoxyribonucleic acid
L-DOPA	L-3,4-Dihydroxyphenylalanine
DQF-COSY	Double quantum filtered correlation spectroscopy
EBHP	Ethylbenzene hydroperoxide
egH <sub>n</sub>	Ethylene glycol (n = 2), ethylene glycolato anion/dianion (n = 1 or 0)
EO	Ethylene oxide
EPR	Electron Paramagnetic Resonance
ESI–(HR)MS(+/-)	(High-Resolution) Electrospray Ionization Mass Spectrometry in the positive or negative ionization mode
Fc/Fc <sup>+</sup>	Ferrocene/ferrocenium redox-couple
FDH	Formate dehydrogenase
FID	Flame ionization detector
⟨g⟩	g-Factor (in EPR spectroscopy)
His	Histidine
HMBC	Heteronuclear multiple-bond correlation
HMPA	Hexamethylphosphoric triamide
HSQC	Heteronuclear single-quantum correlation
ibCO	Catechol oxidase isolated from sweet potato ( <i>Ipomoea batatas</i> )
IL	Ionic liquid
<i>i</i> PPO	<i>Isotactic</i> polypropylene oxide
IR	Infrared
IUPAC	International Union of Pure and Applied Chemistry
<i>J</i>	Coupling constant in Hertz (Hz) (in NMR spectroscopy)
<i>k</i> <sub>cat</sub>	Enzymatic turnover number (frequency)
κ <sup>n</sup> -L	Ligand having n-denticity, where n = 1, 2, 3...
LMCT	Ligand to metal charge transfer
Lys	Lysine

<i>M</i>	Molar mass
<i>m</i> -CBA	<i>meta</i> -Chlorobenzoic acid
<i>m</i> -CPBA	<i>meta</i> -Chloroperbenzoic acid
Mes	Mesityl (2,4,6-trimethylphenyl) group
MPT	Molybdopterin = pyranopterin enedithiolato cofactor
MTO	Methyltrioxidorhenium(VII)
<i>m/z</i>	Mass-to-charge ratio (in mass spectrometry)
<i>n</i>	Amount of substance
NHC	<i>N</i> -heterocyclic carbene
NMR	Nuclear Magnetic Resonance
NOESY	Nuclear Overhauser effect correlation spectroscopy
OAT	Oxygen atom transfer
PAA	Peracetic acid
PO	Propylene oxide
POM	Polyoxometalate
PPO	Polypropylene oxide
ppm	Parts per million
Prg	Propargyl group
RT-DLaTGS	Room temperature deuterated lanthanum $\alpha$ -alanine doped triglycine sulfate
SAH	Salicylidenehydrazine
saldpt	<i>N,N'</i> -(3,3'-Dipropylamino)bis(salicylideneaminato)
salen	Ethylenebis(salicylideneaminato)
SA{T}P	Salicylideneamino{thio}phenolato
SO	Sulfite oxidase
<i>t</i> <sub>1/2</sub>	Reaction half-life
TACN	1,4,7-Triazacyclononane
TBHP	<i>Tert</i> -butyl hydroperoxide
TBHPaq	80 w-% ( <i>ca.</i> 8.0 M) aqueous <i>tert</i> -butyl hydroperoxide
TBHPdec	5.5 M <i>tert</i> -butyl hydroperoxide in <i>n</i> -decane
TBOH	<i>Tert</i> -butyl alcohol ( <i>tert</i> -butanol)
TCC	3,4,5,6-Tetrachlorocatecholato dianion
TCSQ <sup>•</sup>	3,4,5,6-Tetrachlorosemiquinonato anion
THF	Tetrahydrofuran
TLC	Thin-layer chromatography
tmh	2,2,6,6-Tetramethylheptane-3,5-dionato
TMS	Tetramethylsilane
TOF	Turnover frequency/ time of flight
TON	Turnover number
TPA	Tris(2-pyridylmethyl)amine

Tyr	Tyrosine
TYR	Tyrosinase
UV-Vis-(NIR)	Ultraviolet-visible-near-infrared
VBrPO	Vanadium bromoperoxidase
VCIPO	Vanadium chloroperoxidase
VHPO	Vanadium haloperoxidase(s)
VIPO	Vanadium iodoperoxidase
XAS	X-ray absorption spectroscopy
XOR	Xanthine oxidoreductase
XRD	X-ray diffraction (X-ray crystallography)

# List of Original Publications

This dissertation is based on the following original publications, which are referred to in the text by their Roman numerals:

- I **Salonen, P.**, Peuronen, A., Sinkkonen, J., Lehtonen, A. Oxidovanadium(V) complexes with L-proline-based amino acid phenolates. *Inorganica Chimica Acta*, 2019; 489: 108–114.
- II **Salonen, P.**, Peuronen, A., Lehtonen, A. Bioinspired Mo, W and V complexes bearing a highly hydroxyl-functionalized Schiff base ligand. *Inorganica Chimica Acta*, 2020; 503: 119414.
- III **Salonen, P.**, Savela, R., Peuronen, A., Lehtonen, A. Vanadium aminophenolates in catechol oxidation: conformity with Finke's common catalyst hypothesis. *Dalton Transactions*, 2021; 50: 6088–6099.
- IV **Salonen, P.**, Schachner, J., Peuronen, A., Belaj, F., Mösch-Zanetti, N., Lehtonen, A. Alkene epoxidation catalyzed by MoO<sub>2</sub>/WO<sub>2</sub> aminobisphenolato supported complexes: On their activity and reaction mechanism, manuscript.

The original publications have been reproduced with the permission of the copyright holders. Article I: Copyright (2019) Elsevier Ltd.; Article II: Copyright (2020) Elsevier Ltd.; Article III: Copyright (2021) Royal Society of Chemistry.

# List of Relevant Publications

**Salonen, P.**, Peuronen, A., Lehtonen, A. Oxidovanadium(V) amine bisphenolates as epoxidation, sulfoxidation and catechol oxidation catalysts. *Inorganic Chemistry Communications*, 2017; 86, 165–167.

# 1 Introduction

Molybdenum, tungsten, and vanadium are found naturally in several metalloenzymes such as the Mo/W oxotransferases and the V dependent haloperoxidases that catalyze biochemical oxidation reactions. Catechol oxidase and -dioxygenases are copper and iron dependent metalloenzymes that are responsible for the aerobic ( $O_2$  as the terminal oxidant) oxidative dehydrogenation and dioxygenation of aromatic 1,2-diols, respectively. Some of these metalloenzymes have been discovered to catalyze industrially important reactions such as alkene epoxidation and sulfide sulfoxidation, and thus are of high interest both academically and industrially. Investigation of the structure and function of metalloenzymes is challenging, and thus model compounds are used instead. Model compounds may be used to study the structure and/or function of a metalloenzyme. This approach, on one hand, allows indirect studying of the structure/function of a metalloenzyme, and, on the other hand, may give insight on how to improve the model system itself.

Efforts are being made to improve industrial synthetic processes with more economical and environmentally friendly pathways following the principles of *Green Chemistry*. Green Chemistry involves the use of catalysis, which is used to reach good sustainability, efficiency and selectivity and is applied industrially in about 90% of all syntheses of various chemicals. Mo, W, and V catalyzed alkene epoxidation is an industrially significant reaction that is used to produce ethylene oxide and propylene oxide. These chemicals in turn act as building blocks for various fine and bulk chemicals such as pharmaceuticals and plastics. Despite the high industrial importance of Mo/W/V mediated epoxidation, and continued academic work over the past 50 years, the actual mechanism(s) remains somewhat debated. Consequently, the topic is still interesting, and current work engages in developing high-activity catalysts, greener processes as well as mechanism elucidation involving the most state-of-the-art theoretical investigations. This PhD thesis summarizes most notable results of the past 50 years and delves into the catalytic alkene epoxidation chemistry of Mo/W complexes supported by aminobisphenolato ligands.

Metalloenzyme mediated  $O_2$  activation in the context of enzymes such as catechol oxidase and -dioxygenases is of high interest. This is in part due to on-going



efforts in developing enzyme mimicking transition metal-based catalysts that can activate O<sub>2</sub> for oxidation of unfunctionalized alkanes, alkenes, and aromatics. Achieving this is heralded as a singularly important technology for the chemical industry. Thus, modeling of O<sub>2</sub> activating metalloenzymes such as the catechol oxidase and -dioxygenases with models based on Cu and Fe, but also other metals, has been intensive. Vanadium complexes have quite recently been recognized to display catechol oxidase like activity; this PhD thesis will review the most relevant literature pertaining to V catalyzed catechol oxidase and -dioxygenase literature, and present results that show these claims may have at least partly been erroneously made.

## 2 Literature Review

### 2.1 Bioinorganic Chemistry Aspects

Over the past decades, the extraordinarily important role of metals in biology, the environment, and medicine has become increasingly evident.<sup>1</sup> Metal ions and their role in biology can only be studied *via* a multidisciplinary approach, termed “bioinorganic chemistry,” “inorganic biochemistry,” or as “biological inorganic chemistry,” depending on the source, which involves a plethora of branches from the chemical and biological sciences.<sup>2</sup> There has been significant advances in the general understanding of how enzymes, and metalloenzymes in particular, function. In part, this is due to developments in high-resolution X-ray crystallography (XRD) and related techniques,<sup>3</sup> X-ray absorption spectroscopy (XAS),<sup>4</sup> other spectroscopic methods such as electron paramagnetic resonance (EPR),<sup>5</sup> nuclear magnetic resonance (NMR),<sup>6</sup> UV-visible (UV-Vis), among others, which have made it possible to study the structures of metalloenzyme resting states and intermediates with increasing detail.

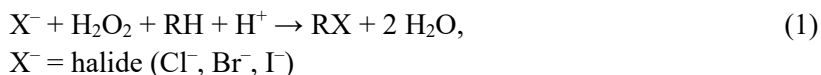
Metalloenzyme catalyzed biochemical reactions are often not only extremely substrate specific and very rapid, they also often express exquisite regio- and/or stereoselectivity, as well as convert difficult substrates such as  $N_2$ <sup>7</sup> to  $NH_3$  with relative ease under practically ambient or physiological conditions.<sup>8</sup> Structural knowledge of the active site structure of a metalloenzyme, being valuable information on its own, is however indispensable information when designing synthetic model catalysts. By synthesizing model compounds, some properties related to the natural metalloenzyme can be replicated in a laboratory setting. Modeling of natural metalloenzymes can be either “biomimetic” or “bioinspired,” or both.<sup>9</sup> The latter is concerned in duplicating the mode of action, or *function*, of the natural enzyme, whereas the former seeks *structural* analogy.<sup>9</sup> Although in nature the function of an enzyme is closely intertwined to its structure,<sup>10</sup> and vice versa, both models enable indirect studies, mechanistic or otherwise, of the natural enzymes, which may give important insight into the biological pathways, and thus completing a feedback loop pertaining studies of metalloenzymes to their synthetic models.<sup>8</sup> Some sacrifices need to be done when modeling the active sites of metalloenzymes, however:

“When reduced to practice, this approach necessitates the synthesis of relatively low molecular weight complexes, which, ideally, are obtainable in crystalline form and approach or duplicate the biological unit in terms of composition, ligand types, structure, and oxidation level(s). Such models, or synthetic analogues, of course, cannot simulate the environmental effects of and whatever structural constraints are imposed by the normal protein conformation.”<sup>11</sup>

In spite of these compromises, model compounds may have advantages over metalloenzymes insofar as scope of substrates, scale of production and tuning of structure of the model system is concerned, allowing superior control over selectivity and/or specificity of a reaction.<sup>8</sup>

### 2.1.1 Vanadium Haloperoxidases

Vanadium haloperoxidases (VHPOs) are metalloenzymes that catalyze the oxidation of halides (chloride, bromide and iodide) by H<sub>2</sub>O<sub>2</sub> into their corresponding hypohalous acids, and the subsequent oxidative halogenation of organic compounds according to equation (1).<sup>12-14</sup> Three VHPOs are known, namely the vanadium chloro-, bromo- and iodoperoxidases (VClPO, VBrPO, VIPO, respectively). From the enzymes, VBrPO and VIPO are encountered in marine environments, having been isolated and characterized from all types of marine algae *viz.* green, brown and red algae, whereas VClPOs have been found primarily from terrestrial fungi.<sup>15</sup> VHPOs synthesize most of the naturally occurring organohalogen compounds, most notably chloroform and bromoform.<sup>15</sup> However, other, more complex natural organohalogen compounds synthesized by the VHPOs are various chiral terpenes and indoles, among others.<sup>13,15</sup> These more sophisticated compounds are produced in smaller amounts, but they are often biologically active, possessing microbicidal activity, or pharmacological properties including anti-inflammatory or anti-cancer effects.<sup>13</sup>



Significantly, VHPOs have been described to catalyze industrially important reactions, such as the enantioselective variants of alkene epoxidation<sup>16,17</sup> as well as sulfide sulfoxidation.<sup>18</sup> As such, the structural and functional mimicking of VHPOs has been very active. The active sites of VClPO and VBrPO have been structurally characterized, and found to be remarkably similar.<sup>15,19</sup> The active sites of both enzymes can be described of containing a hydrogen vanadate(V) *i.e.*, HVO<sub>4</sub> center bound to a single axial histidine ligand in an overall trigonal bipyramidal coordination geometry.<sup>19</sup> Additionally, peroxido forms of the enzymes are

recognized. The three equatorial oxygen atoms carry a significant negative charge, and are stabilized by hydrogen bonding from a number of amino acid residues including glycine, serine, arginine, histidine (in VBrPO) and phenylalanine (in VCIPO), depending on the exact organism.<sup>15,19</sup> The active site of VBrPO, adapted from ref. <sup>15</sup>, is shown in the Figure 1A. Aminobisphenolato oxidovanadium(V) complexes **1** – **3** (Figure 1B) have been shown to structurally and functionally mimic VHPOs.<sup>20</sup> Moreover, groups of Licini, Crans, Pombeiro, and others, have thoroughly investigated catalytic and biochemical aspects of structurally very similar V complexes in epoxidation and sulfoxidation (ref. <sup>21</sup> and references cited therein).

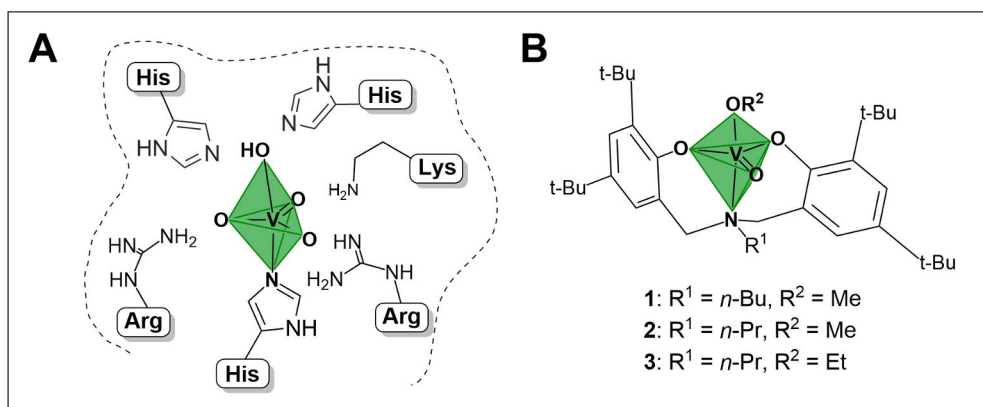
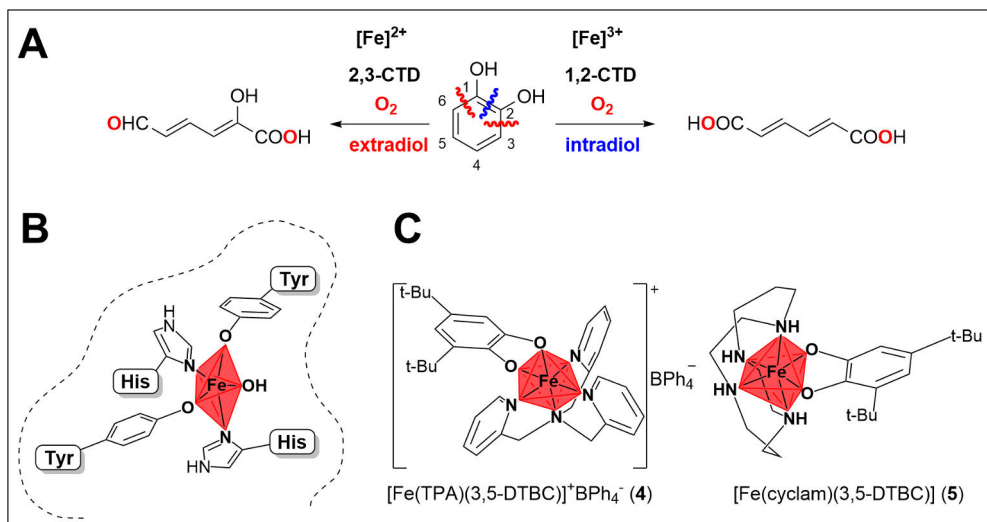


**Figure 1.** The active “oxido form” oxidovanadium(V) site in the VBrPO enzyme binding pocket (dashed line) containing histidine (His) lysine (Lys) and arginine (Arg) amino acid residues (**A**). The structures of generic aminobisphenolato oxidovanadium(V) model compounds **1** – **3** that functionally and structurally mimic VBrPO (**B**).

## 2.1.2 Catechol Dioxygenases

Catechol dioxygenases (CDOs) are Fe dependent bacterial enzymes that catalyze the oxidative degradation of catechol (benzene-1,2-diol) and other derivative aromatic compounds, reactions which are environmentally, pharmaceutically and medically significant.<sup>22–25</sup> Several Fe dependent CDO enzymes are recognized, from which catechol 1,2-dioxygenase (1,2-CTD) and catechol 2,3-dioxygenase (2,3-CTD) may be considered prototypical.<sup>22,24,25</sup> CDOs catalyze chemically difficult aerobic *i.e.*, dioxygen ( $O_2$ ) driven *dioxygenation* (dioxygen insertion) of catechols *via* incorporation of an  $O_2$  molecule into a substrate, a reaction that is essentially classified as C—C bond cleavage. Moreover, the reactions mediated by CDOs may be further categorized between intra- and extradiol C—C bond cleavage, reactions which produce linear unsaturated dicarboxylic acids and semialdehydes, respectively (Scheme 1A).<sup>23</sup> From the archetypical CDO enzymes, intradiol

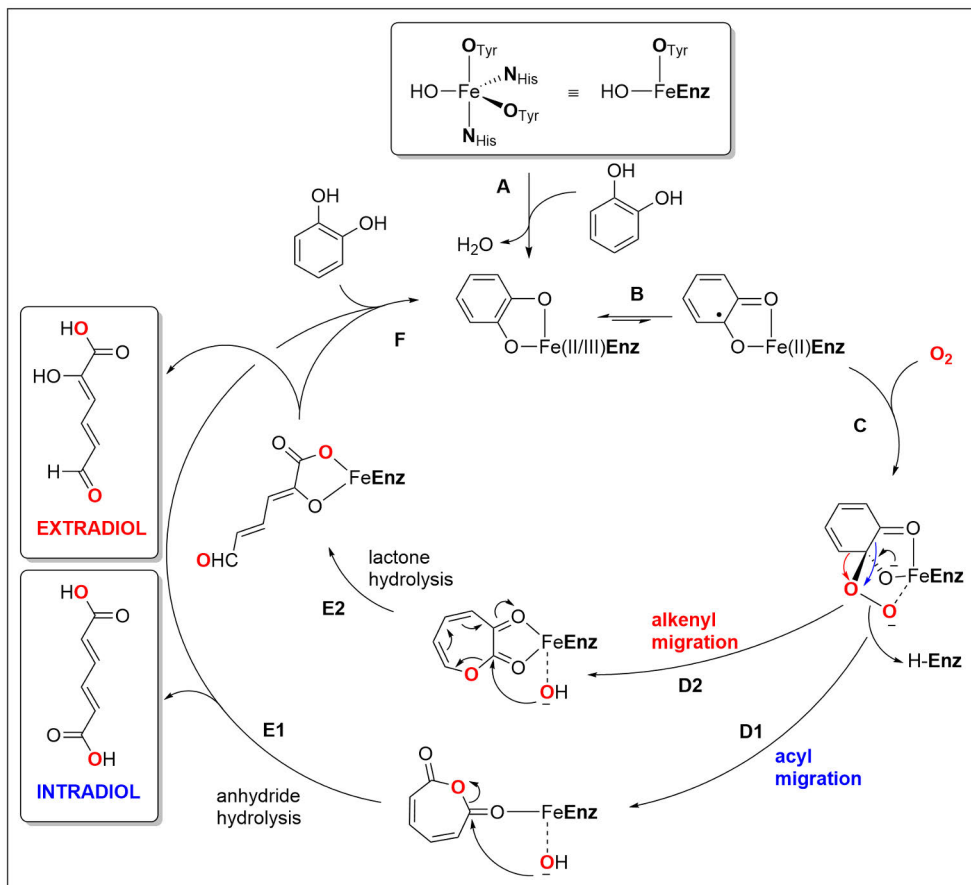
cleaving enzymes such as 1,2-CTD are iron(III) dependent, whereas extradiol cleaving enzymes *e.g.*, 2,3-CTD are iron(II) dependent.<sup>22–25</sup>



**Scheme 1.** Aerobic intra- and extradiol C—C bond cleavage and dioxygenation of a generic catechol by the prototypical CDO enzymes 1,2-CTD and 2,3-CTD, respectively (**A**). The active iron(III) site found in the enzyme 1,2-CTD binding pocket (dashed line) containing four tyrosine (Tyr) and histidine (His) amino acid residues as well as a hydroxido ligand (**B**). Iron(III) and iron(II) complexes **4** and **5** supported by multidentate aminopyridyl and cyclam type chelate and macrocyclic ligands, respectively, have been used to functionally mimic CDOs (**C**).

The capability of activating  $\text{O}_2$  using artificial transition metal catalysts for use in controlled (partial) oxidation of hydrocarbon feedstocks, such as alkanes, alkenes as well as aromatics, is one of the single most important and sought after “Holy Grail” chemical technologies.<sup>26,27</sup> As such, metalloenzymes including CDOs capable of dioxygenation have been extensively investigated with this goal in mind. In the active site of 1,2-CTD the iron(III) center, which adopts a distorted trigonal bipyramidal coordination geometry, is ligated by two axial histidine and tyrosine amino acid residues, as well as by additional histidine and tyrosine, and a water molecule derived hydroxido ligand in the equatorial positions (Scheme 1B).<sup>28</sup> A similar first coordination sphere has been obtained with iron(III) and iron(II) complexes supported by tetradentate tris(2-pyridylmethyl)amine (TPA) and cyclam (1,4,8,11-tetraazacyclotetradecane) type or similar ligands.<sup>29–32</sup> For example, iron(III) and iron(II) complexes such as  $[\text{Fe}(\text{TPA})(3,5\text{-DTBC})]^+\text{BPh}_4^-$  (**4**) or  $[\text{Fe}(\text{cyclam})(3,5\text{-DTBC})]$  (**5**) (where 3,5-DTBC = 3,5-di-*tert*-butylcatecholato dianion) have been successfully used as functional models of intra- and extradiol CDOs, respectively (Scheme 1C).<sup>31,32</sup>

## 2.1.2.1 Catechol Dioxygenase Mechanism



**Scheme 2.** The accepted mechanisms of aerobic intra- and extradiol dioxygenation of catechols. Not all reactions and intermediates are shown. The N<sub>His</sub> and O<sub>Tyr</sub> groups stand for histidine and tyrosine amino acid residues, and some ligands have been omitted for clarity and designated “Enz” for “enzyme”. Drawn according to refs <sup>24,33,34</sup>.

The mechanisms of intra- and extradiol catechol dioxygenase reactions have been investigated extensively using model systems and oxygen heavy isotope labeling experiments.<sup>31,33,34</sup> According to the currently accepted hypotheses, both intra- and extradiol mechanisms first involve bidentate coordination of a catechol substrate molecule to the iron(II/III) center, displacing an amino acid residue such as tyrosine, and water (Scheme 2 stage A). To facilitate reaction with O<sub>2</sub> (see section 2.2.3.3) the bound catechol substrate first undergoes metal-mediated one-electron oxidation to yield a 1,2-semiquinonate radical (Scheme 2 stage B). While it is generally agreed upon that the exact mechanism of O<sub>2</sub> activation varies between intra- and extradiol

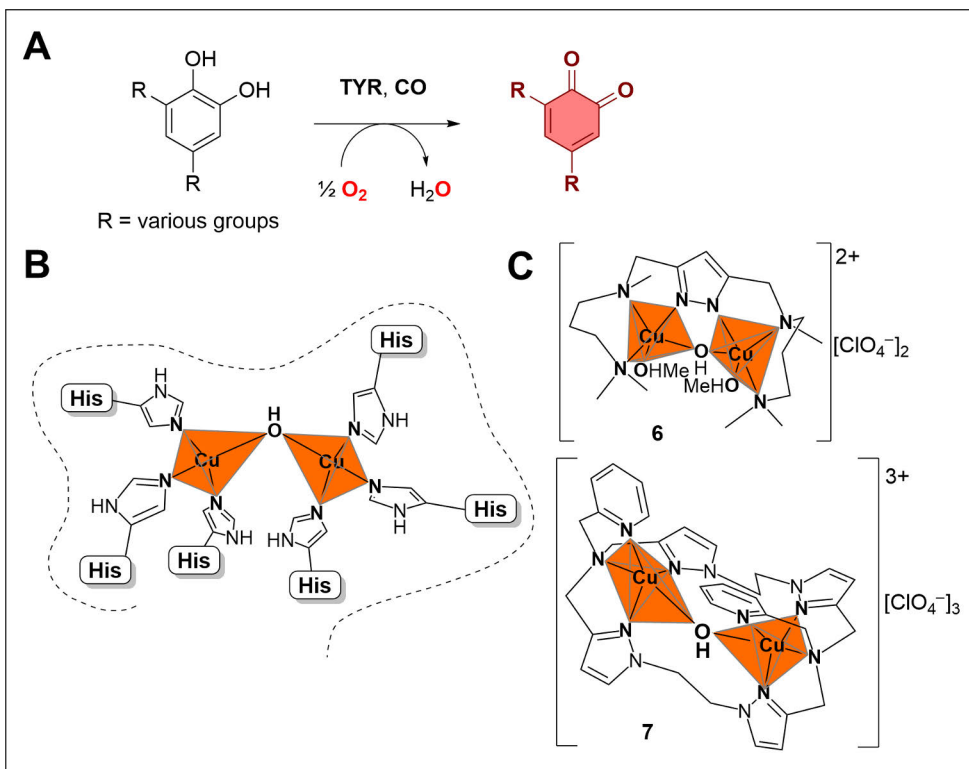
mechanisms,<sup>35</sup> it is currently understood that both pathways ultimately proceed *via* the formation of a common transient ternary iron(II)-semiquinonato-superoxido intermediate (Scheme 2 stage C).<sup>34</sup> Through extensive substrate heavy-oxygen labeling, it has been determined that the intra- and extradiol mechanisms diverge from this point forward. In the intradiol pathway, in the presence of the (su)peroxide, the bound catechol undergoes a Baeyer-Villiger like acyl migration reaction, yielding an anhydride intermediate (Scheme 2 stage D1), followed by hydrolysis, forming the dicarboxylic acid end-product (Scheme 2 stage E1). In contrast, in the extradiol pathway, the bound catechol undergoes alkenyl migration *via* 1,2-rearrangement (namely, the Criegee rearrangement), into a lactone intermediate (Scheme 2 stage D2), followed by subsequent hydrolysis and release of the semialdehyde product in the next step (Scheme 2 stage E2). The catalytic cycle restarts in both mechanisms by the coordination of next catechol substrate, in the Scheme 2 stage F.<sup>31,33,34</sup>

### 2.1.3 Catechol Oxidase

Amongst the multi-copper dependent oxidases Tyrosinase (TYR) and Catechol Oxidase (CO) are two metalloenzymes found in plants that catalyze the oxidation (oxidative dehydrogenation) of catechols and derivatives thereof into their corresponding 1,2-benzoquinones (*o*-quinones), compounds having a characteristic brown/red color (Scheme 3A).<sup>36-38</sup> From these enzymes CO is only capable of oxidizing catechols (catecholase activity), whereas TYR additionally oxidizes phenols to catechols *via* cresolase activity.<sup>37</sup> Catechols are a large group of small bioactive molecules with high physiological significance. For example, they are found as a structural motif in a variety of bronchodilator, adrenergic, anti-hypertensive, and anti-parkinsonian medication such as L-DOPA, as well as in neurotransmitters such as dopamine, and in hormones such as adrenaline (epinephrine), estrogen and metabolites thereof.<sup>39</sup> Moreover, catechols have a rich redox-chemistry, whereby they can be reversibly (electrochemically) oxidized to semiquinones and further to *o*-quinones.<sup>40</sup>

Enzymatic browning plays key physiological roles in fruits, vegetables and seafoods by producing melanins, dark colored polymeric pigments with diverse structure possessing anti-bacterial, anti-fungal, anti-cancer and anti-oxidant properties.<sup>41</sup> Enzymatic browning also negatively affects the color, flavor and nutritional value of various foods, and it is estimated that over 50% of produce is lost before reaching the consumer as a result, representing massive economic losses for the food industry.<sup>41</sup> Since CO is one of the key enzymes responsible for enzymatic browning, and in light of the economic impacts associated with it, research into CO, its catalytic mechanism, and inhibition thereof in particular, has

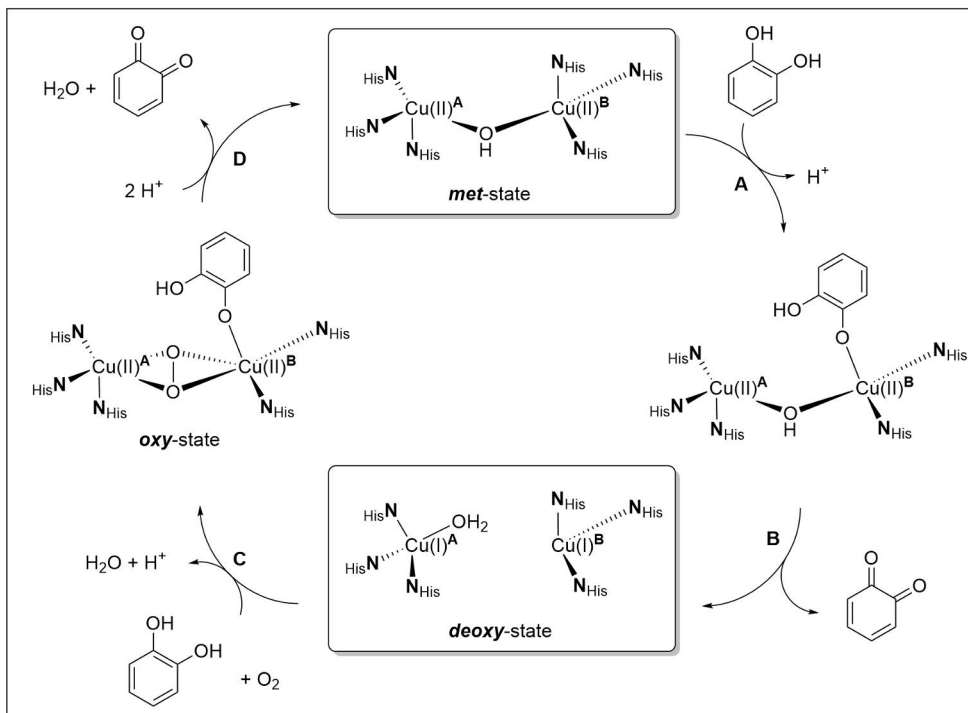
been very active. The active site of CO in the resting *met*-state consists of two copper(II) ions ligated by three histidine residues each, and bridged by a  $\mu$ -hydroxido ligand (Scheme 3B), with an approximate trigonal pyramidal coordination geometry at both metal centers.<sup>42</sup> Consequently, the active site of CO has been structurally modeled by architecturally very diverse dicopper complexes, such as **6** and **7**, which are based on multidentate (and for **7** macrocyclic) pyrazole ligands (Scheme 3C).<sup>43–50</sup>



**Scheme 3.** Aerobic oxidation of a generic catechol to the corresponding 1,2-benzoquinone as mediated by the enzymes TYR and CO (**A**). The active dicopper(II) site in the resting *met* state as found in the enzyme CO binding pocket (dashed line) containing six histidine (His) amino acid residues (**B**). Dicopper(II) complexes **6** and **7** supported by multidentate pyrazole based chelate and macrocyclic ligands, respectively, have been used to structurally and functionally mimic CO (**C**).



## 2.1.3.1 Catechol Oxidase Mechanism



**Scheme 4.** Catalytic cycle of ibCO as proposed by Krebs and co-workers based on structural, spectroscopic, and biochemical data. The met- and deoxy-states (boxed) have been characterized by XRD. The  $N_{\text{His}}$  groups stand for histidine amino acid residues. Adapted from <sup>36</sup>.

Although the exact details concerning the mechanism of CO are not fully known, biochemical and spectroscopic evidence, including X-ray structures obtained from the met/deoxy states of the dicopper centers in IbCO isolated from sweet potato (IbCO, catechol oxidase from *Ipomoea batatas*), have enabled detailed proposals to be made.<sup>51,52</sup> A mechanism suggested by Krebs and co-workers, shown in Scheme 4, has been widely accepted.<sup>36</sup> The start of the catalytic cycle entails the displacement of a histidine ligand by a monodentate catechol substrate at the dicopper(II) B-site of the oxidized catalytic resting, also known as *met*-state of CO (Scheme 4 stage A). Substrate oxidation and subsequent release of *o*-benzoquinone occurs concomitantly to one-electron reduction at both copper sites, and the *deoxy*-state of CO is thus obtained (Scheme 4 stage B). The bridging hydroxido ligand is converted to an aqua ligand at the copper A-site which adopts a distorted trigonal pyramidal geometry, whereas copper B-site may be described as distorted square planar with one missing ligand.<sup>52</sup> In the next step, molecular dioxygen is bound to both reduced copper

centers as a bridging peroxido ligand in a  $\mu\text{-}\eta^2\text{:}\eta^2$  fashion, displacing the aqua ligand at the copper A-site. The coordination of  $\text{O}_2$ , which re-oxidizes both copper centers in their cupric forms, occurs prior to coordination of a second catechol substrate at the copper B-site, yielding the dicopper(II) *oxy*-state of CO (Scheme 4 stage C). Finally, *o*-benzoquinone and water are released and the *met*-state of CO is regenerated, and the cycle starts anew (Scheme 4 stage D).<sup>36,51,52</sup>

## 2.1.4 Molybdenum and Tungsten Oxotransferases

Mo and W oxotransferases, or oxidoreductases, are a very large class of ubiquitous mammalian, bacterial and archaean enzymes that catalyze oxygen atom transfer (OAT) reactions.<sup>53,54</sup> OAT, by definition, involves transfer of a terminal oxido (oxide,  $\text{O}^{2-}$ ) ligand from an active metal site to a substrate in the course of the reaction according to equation (2).<sup>55</sup> Despite what the collective name of the enzymes (oxotransferases) would suggest, not all Mo/W enzymes actually perform OAT reactions. From the enzymes it is believed that sulfite oxidase (SO) and DMSO reductase (DMSOR) enzymes engage in true, *canonical* OAT.<sup>56</sup> Collectively, these enzymes are responsible of biochemical oxidation reactions related to carbon, nitrogen and sulfur metabolism.<sup>57,58</sup>



It is currently well-established that all mononuclear Mo containing enzymes, other than the Mo dependent nitrogenase, fall into three large and mutually exclusive enzyme families called xanthine oxidoreductase (XOR), SO and DMSOR (Figure 2).<sup>56</sup> The Mo enzymes are responsible for the oxidation of aldehydes, aromatic heterocycles, sulfites, and nitrites etc., which are physiologically important reactions *e.g.*, in relation to degradation of DNA. For example in humans, XOR catalyzes oxidation of xanthine to uric acid, as well as catabolism of other purines, whereas SO catalyzes degradation of cysteine and methionine.<sup>56,59</sup>

Likewise, the W containing enzymes may be divided into aldehyde: ferredoxin oxidoreductase (AFOR), formate dehydrogenase (FDH) and acetylene hydratase (AH) families (Figure 2).<sup>57</sup> The W enzyme AFOR catalyzes the oxidation of aldehydes and aldehyde derivatives of amino acids, and is thus similar to Mo XOR in that regard. The enzymes in the FDH family catalyze conversion of  $\text{CO}_2$  to acetate and methane, and the enzyme family AH catalyzes hydration of acetylene.<sup>57</sup> Structurally, the active sites of all Mo and W oxotransferases consist of metal centers in their highest oxidation states VI coordinated by one or two bidentate MPT (molybdopterin, pyranopterin enedithiolato cofactor) ligands (Figure 2).<sup>56</sup> Depending on the family, the active sites may contain only one of the MPT ligands, as is the case with XOR and SO, whereas the rest of the families contain two MPT

ligands.<sup>56</sup> The active site structures of all families (in the eponymous enzymes) are shown in Figure 2.

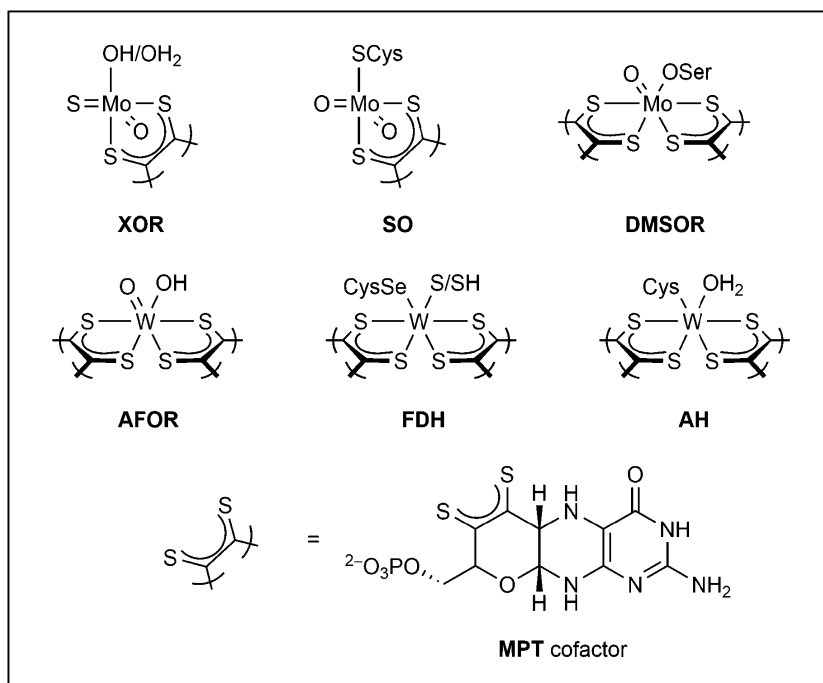
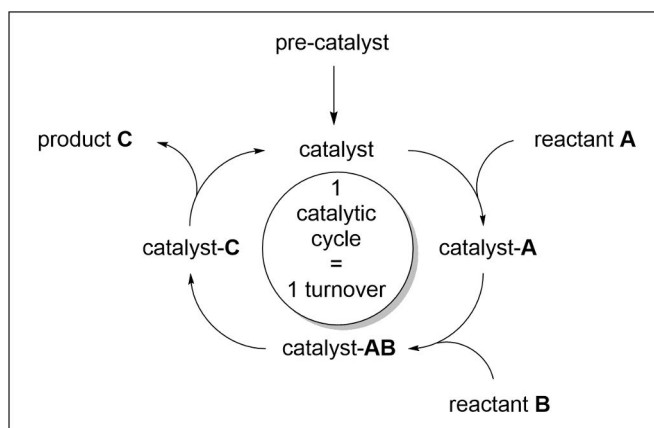


**Figure 2.** The active site structures of Mo/W oxotransferases. XOR = xanthine oxidoreductase, SO = sulfite oxidase, DMSOR = DMSO reductase, AFOR = aldehyde: ferredoxin oxidoreductase, FDH = formate dehydrogenase, AH = acetylene hydratase. Adapted from ref. <sup>60</sup>.

## 2.2 Catalysis – General Aspects

Catalysts, as defined by the IUPAC Golden Book, are reactants and *products* of any catalytic chemical reaction that increase the overall rate of the said chemical reaction without modifying the chemical equilibrium.<sup>61</sup> In essence, a catalytic reaction is a cyclic process wherein a catalyst is involved in chemical bonding with one or more reactants that convert into products during a single reaction cycle, or *turnover* (Scheme 5).<sup>62</sup> It is important to realize that the catalyst itself is both a reactant and a product of a catalytic reaction, because the catalyst is regenerated after a single turnover. Strictly speaking, and as shown in Scheme 5, a *pre-catalyst*, which may be a synthesized and fully characterized transition metal complex, is often transformed into the true active catalyst during the catalytic cycle. “Halpern’s rules”<sup>63</sup> – or rather guidelines intended as a useful heuristic device in the context of catalysis – state that if (the suspected catalyst) is isolable, it is probably not the catalyst; if it is metastable

and detectable *via* spectroscopic means, it *could* be the catalyst; and finally if it is highly unstable, unisolable and undetectable, then it most likely *is* the catalyst.<sup>64</sup> That is to say, the chemical composition of a true catalyst in any given catalytic reaction is rarely known precisely, because catalytically active species are usually fleeting and thus often impossible to detect by spectroscopic means. Nevertheless, the viability of a catalytic process, regardless of the identity of the “true catalyst,” is largely dependent upon two properties of a catalyst, namely activity and stability.<sup>62,65</sup> The selectivity of a catalyst in a catalytic process is sometimes recognized as the third most important property.<sup>62,65</sup>



**Scheme 5.** A schematic representation of a simplified catalytic reaction involving the catalyst and two reactants **A** and **B**. During a single reaction cycle (turnover), the reactants **A** and **B** are converted into the product **C**, whereas the catalyst is regenerated.

## 2.2.1 Activity Metrics: TON and TOF

The activity of a catalyst is a measure of how fast any given reaction proceeds under catalytic conditions and is one of the most important properties of a catalyst. Activity can be defined in terms of kinetics by monitoring the change of concentrations of reactants and products. Some of the most important metrics that measure activity are the turnover number (TON) and turnover frequency (TOF). TON is usually defined as the number of equivalents of product generated per equivalent of catalyst, and it may be calculated using equation (3).<sup>62,65</sup> TON is a dimensionless quantity, and it provides information about the stability of a catalyst. For a catalytic reaction that uses a 0.01 or 0.001 eqv. catalyst loading relative to a substrate (*i.e.*, denoted 1 and 0.1 mol-%, respectively), the TON may reach values no larger than 100 and 1000, respectively, after full conversion of the substrate. However, TON may be raised by adding more substrate. On the other hand, TOF is typically – although competing definitions exist<sup>66</sup> – defined as TON per unit of time ( $\text{h}^{-1}$ ,  $\text{min}^{-1}$ ,  $\text{s}^{-1}$ ), according to

equation (4).<sup>62,65</sup> TOF provides information about the reaction rate. For industrial applications, a TON should be in the range of no less than  $10^3$  and ideally over  $10^5$ , whereas the most robust industrial applications have a TOF ranging between 600 – 6000  $\text{h}^{-1}$ .<sup>62,65</sup>

$$\text{TON} = (n(\text{product})) \times (n(\text{catalyst}))^{-1} \quad (3)$$

$$\text{TOF} = \text{TON} \times \text{time}^{-1} \quad (4)$$

Where  $n$  = amount of substance.

## 2.2.2 Stability of Catalysts

The stability of a catalyst pertains to its chemical, thermal and in some cases mechanical stability during catalysis, and it is influenced by several factors including, but not limited to, (chemical/thermal) decomposition, leaching, and inactivation by poisoning or fouling.<sup>62</sup> It is usually considered the second-to-most important property of a catalyst, after activity.<sup>62</sup> However, the (in)stability of a catalyst has profound implications on its activity in cases where decomposition leads to catalytically *more* active species relative to the expected catalyst. For example, in the context of Mo catalyzed epoxidation there are numerous examples of (pre)-catalyst decomposition leading to ever more catalytically active species (see sections 2.3.5.1, and 2.3.5.2).<sup>26,67–69</sup> The phenomenon of *leaching*, more commonly associated with transition metal-based heterogeneous catalysis, involves removal of metal *i.e.*, by extraction, and dissolution (homogenization) thereafter, by the action of strongly complexing and solvolytic oxidants such as  $\text{H}_2\text{O}_2$  or organic hydroperoxides ROOH, rendering the heterogenous catalysts often inactive.<sup>70</sup> Leaching has been shown to affect homogeneous transition metal complexes as well (see sections 2.4.1.1 and 2.4.1.2), in some cases leading to formation of a catalytically extremely active species. Homogeneous transition metal complex associated leaching is the premise of the publication III.

## 2.2.3 Green Chemistry

Enormous efforts are being made to improve industrial synthetic processes with more economical and environmentally friendly pathways following the 12 principles of *Green Chemistry*.<sup>71</sup> One of the 12 tenets of Green Chemistry involves the use of catalysis, which is used to reach good sustainability, efficiency and selectivity and is applied industrially in about 90% of all syntheses of various chemicals.<sup>72</sup> Important considerations with regards to Green Chemistry are *atom economy*<sup>73</sup> and a term called *E-factor*<sup>74</sup>, which measure whether or not a process is (atom) economically feasible and environmentally acceptable. Other issues that are of concern in a laboratory preparative as well as in industry are the choice of solvents and oxidants,

which may have extremely important implications on the stability, activity, and selectivity of a catalysts and catalytic processes.

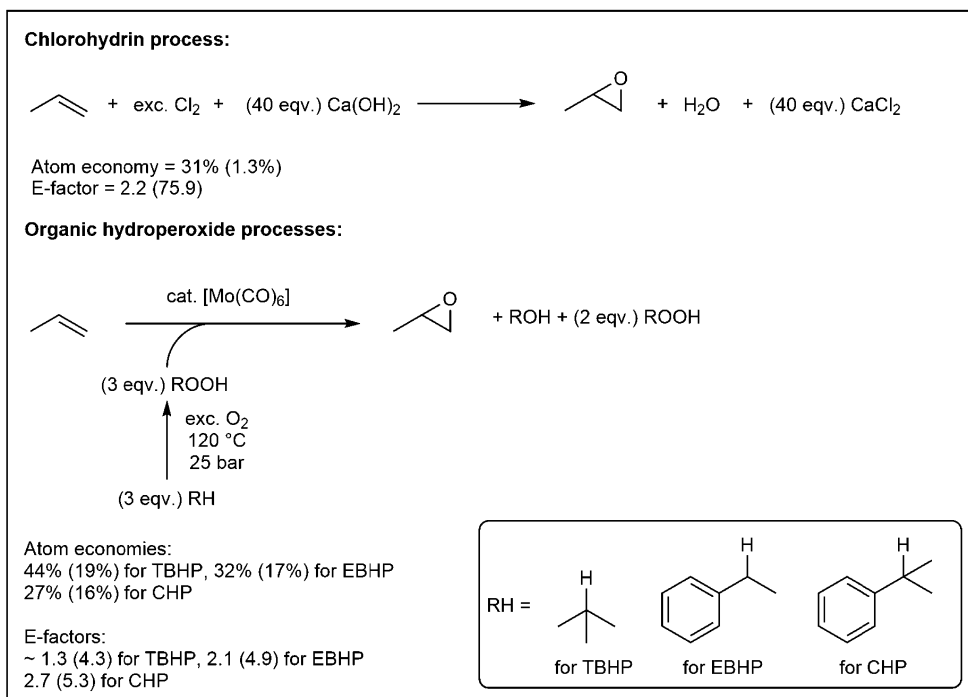
### 2.2.3.1 Atom Economy and the E-factor

Atom economy describes the percentage ratio between mass of desired product to the total mass of all products. It is calculated by dividing the molecular weight of the desired product by the molecular weight of all products formed in a stoichiometric reaction (equation 5).<sup>74</sup> The closely related E-factor (environmental factor) measures the percentage ratio of waste to desired product; it is a fully theoretical metric that assumes 100% chemical yield, exact stoichiometry, and it disregards substances that do not appear in the stoichiometric reaction.<sup>74</sup> Moreover, water is often excluded in the calculation of the E-factor in processes that involve aqueous waste streams. A theoretical E-factor can be derived from atom economy, *e.g.*, a reaction having a 40% atom economy corresponds to an E-factor of 1.5 (60/40). Although ideally the E-factor is close to zero, generally it ranges between 5 – 100 in the fine chemical industry (including pharmaceutical), and 0.1 – 5 in the bulk and oil refining industries.<sup>74</sup>

$$[M(\text{desired product})] \times [M(\text{all products})]^{-1} \quad (5)$$

Where  $M$  = molar mass.

Propylene oxide (PO) is produced industrially in the Halcon-ARCO/Sumimoto hydroperoxide processes (see section 2.3.2) *via* epoxidation of propene, supplementing the original non-catalytic chlorohydrin method that has a low atom economy and a very poor E-factor (see Scheme 6).<sup>71,74</sup> The chlorohydrin process is a multi-step process that suffers from poor selectivity per step and separation problems, reducing overall yield. The greatest disadvantage lies in the epoxidation step, as *ca.* 40 equivalents of  $\text{CaCl}_2$  is formed relative to PO.<sup>75</sup> Furthermore, the raw aqueous PO stream, containing many chlorinated hydrocarbons, must be fractionated by distillation, resulting to unavoidable hydrolysis of PO, further reducing yields.<sup>75</sup> While the atom economies of the chlorohydrin and hydroperoxide processes are similar, 31% *vs.* 27 – 44%, respectively, based on minimum stoichiometry, the E-factor of the chlorohydrin process rises to prohibitively large numbers especially if super stoichiometry is taken into account.<sup>76</sup> In comparison, for organic hydroperoxides, the E-factor remains low even under super stoichiometric conditions. This is further improved by the relatively easy oxidation (recycling) of the alcohol by-products back to hydroperoxides in the hydroperoxide processes.



**Scheme 6.** Overall reactions involved in non-catalytic chlorohydrin and catalytic Halcon-ARCO/Sumimoto hydroperoxide processes, all producing PO in the epoxidation of propene. TBHP = *tert*-butyl hydroperoxide, EBHP = Ethylbenzene hydroperoxide, CHP = Cumene hydroperoxide. Super stoichiometric atom economies and E-factors shown in parentheses.

### 2.2.3.2 Choice of Solvent

The use of solvents in small and large scale syntheses represent not only an issue with regards to feasibility of a chemical process, economic or otherwise, but it is of great concern to the environment, health, and safety.<sup>74,77</sup> It is estimated that *ca.* 85% of the total mass of chemicals involved in the synthesis of pharmaceuticals comprises solvents, with obviously detrimental effects to the E-factor in particular.<sup>74</sup> Moreover, solvent recovery *e.g.*, *via* distillation is energy-consuming, especially in the case of one of the most environmentally compatible solvent, water.<sup>78</sup> In light of these concerns, Pfizer Inc. has evaluated the most commonly used laboratory solvents based on their impact to worker and process safety as well as environmental and regulatory considerations (Table 1).<sup>77</sup> The solvents in the undesirable category typically show elevated carcinogenicity, mutagenicity, reprotoxicity, volatility, flammability as well as high ecotoxicity or high potential for ecologic contamination, and should be replaced with solvents from the usable and/or preferred categories.<sup>77</sup>

Relatively recently, ionic liquids (ILs) have attracted considerable attention as alternatives to volatile and toxic organic solvents such as haloalkanes.<sup>79,80</sup> Although ILs demonstrate many attractive properties such as high chemical and thermal stability, non-volatility, non-flammability, high polarity, and high solvating effects, their potentially ecotoxic nature towards aquatic environments, primarily due to their very good water solubility, has been recognized.<sup>80,81</sup> Nonetheless, other phenomena associated with ILs with regards to catalysis is the capability to immobilize soluble pre-catalysts, allowing tandem recycling of solvent and/or catalysts.<sup>79</sup> Additionally, some reactions show marked rate-enhancement if performed in an IL compared to traditional solvents, as demonstrated by Kühn and co-workers in Mo catalyzed epoxidation.<sup>82</sup>

**Table 1.** List of preferred, usable and undesirable solvents for use in medicinal and research based chemistry organization, as evaluated by Pfizer Inc.<sup>77</sup>

Preferred	Usable	Undesirable
Water	Cyclohexane	Pentane
Acetone	Heptane	Hexane(s)
Ethanol	Toluene	Di-isopropyl ether
2-Propanol	Methylcyclohexane	Diethyl ether
1-Propanol	Methyl <i>tert</i> -butyl ether	Dichloromethane
Ethyl acetate	Isooctane	Dichloroethane
Isopropyl acetate	Acetonitrile	Chloroform
Methanol	2-Methyl tetrahydrofuran	Dimethyl formamide
Methyl ethyl ketone	Tetrahydrofuran	<i>N</i> -methylpyrrolidinone
1-Butanol	Xylene(s)	Pyridine
<i>Tert</i> -butanol	Dimethyl sulfoxide	Dimethyl acetate
	Acetic acid	Dioxane
	Ethylene glycol	Dimethoxyethane
		Benzene
		Carbon tetrachloride

### 2.2.3.3 Choice of Oxidant

The choice of oxidant may also have profound effects on the viability of a catalytic reaction, notwithstanding economic and environmental implications. Table 2 lists some terminal oxidants commonly used in alkene epoxidation in both academia and industry.<sup>26,83</sup> The list has been divided between three sections, namely the benign green oxidant (O<sub>2</sub>), (in)organic hydroperoxides, and peracids with both atom economics and E-factors associated with the use of any given oxidant decreasing from the top of the list to bottom. The term “active oxygen” itself is closely related



to both atom economy and E-factor. From the list, it is instantly obvious that dioxygen offers by far the best mass utilization since it is incorporated either fully or halfway into the final product, depending on the exact mode of oxidation. The nature of possible co-products also make dioxygen perfectly compatible amidst increasing pressures to adopt more environmentally acceptable and sustainable industrial processes following the principles of Green Chemistry.<sup>71,84</sup> Indeed, most (catalytic) industrial processes use O<sub>2</sub> as the predominant oxidant for the aforementioned reasons.<sup>26</sup>

**Table 2.** A (non-exhaustive) list of some commonly used terminal oxidants in catalytic and non-catalytic alkene epoxidation.<sup>26,83</sup> E-factor and atom economy associated with the use of any given oxidant decrease from top to bottom in the respective groups. BAP = bicarbonate activated peroxide, TBOH = *tert*-butanol, MTBE = methyl *tert*-butyl ether, *m*-CPBA = *m*-chloroperbenzoic acid, *m*-CBA = *m*-chlorobenzoic acid.

Oxygen donor	Active oxygen (%)	<i>M</i> (g mol <sup>-1</sup> )	Co-product
O <sub>2</sub>	50.0 (100) <sup>[a]</sup>	32.00	H <sub>2</sub> O or none <sup>[a]</sup>
H <sub>2</sub> O <sub>2</sub> (+ BAP)	47.0 (14.1) <sup>[b]</sup>	34.01	H <sub>2</sub> O
TBHP	17.8 <sup>[c]</sup>	90.12	TBOH / MTBE / recycled
EBHP	11.6 <sup>[c]</sup>	138.17	1-phenylethanol / styrene / recycled
CHP	10.5 <sup>[c]</sup>	152.19	cumyl alcohol / recycled
PAA	21	76.05	acetic acid
<i>m</i> -CPBA	9.3	172.56	<i>m</i> -CBA

<sup>[a]</sup> Dioxygen insertion. <sup>[b]</sup> For 30 w-% aqueous hydrogen peroxide solution. <sup>[c]</sup> Similar to H<sub>2</sub>O<sub>2</sub>, the active oxygen values for organic hydroperoxides are nominal only; they are always supplied as aqueous or organic solutions due to inherent instability of pure organic hydroperoxides.

Despite this, however, the use of O<sub>2</sub> as an oxidant has some severe drawbacks. It is a very unreactive molecule due to having a diradical triplet electronic ground state: direct reaction of triplet-oxygen (<sup>3</sup>O<sub>2</sub>) with most non-radical organic molecules (possessing a singlet electronic ground state) is a spin forbidden process associated with a very low reaction rate at ambient conditions.<sup>27</sup> To overcome this kinetic barrier, high temperatures and pressures or catalysis is needed to activate it (*e.g.*, see Scheme 6). On the other hand, paramagnetic transition metal ions may react with relatively easily oxidizable organics, or additionally with <sup>3</sup>O<sub>2</sub>, producing highly reactive organic free radicals and metal-superoxide species, respectively (see *e.g.*, Scheme 2 in section 2.1.2.1).<sup>26</sup> However, oxygen activation processes typically promote intrinsically unselective organic radical reactions, although this problem can be alleviated to certain degree with simple substrates.<sup>83</sup>

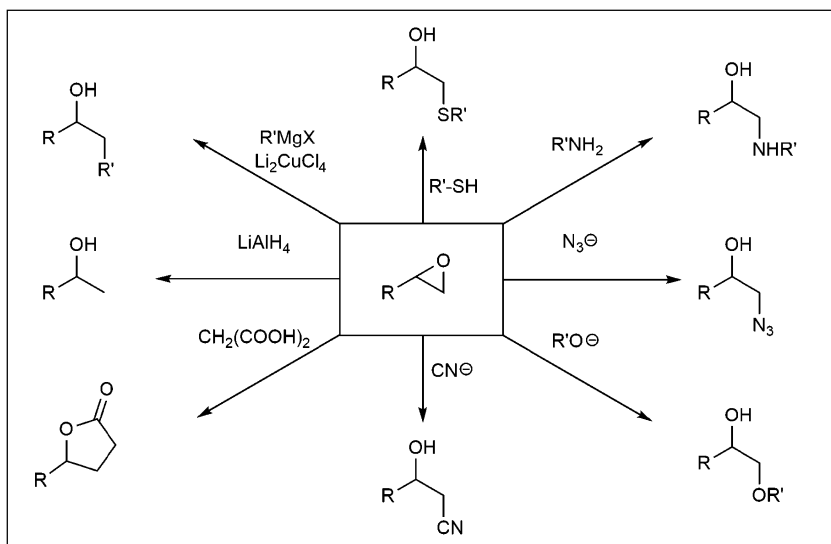
By far the most common oxidants used in an academic setting especially are the inorganic and organic hydroperoxides, such as H<sub>2</sub>O<sub>2</sub>, TBHP, EBHP and cumene

hydroperoxide (CHP), which can be thought of as “reduced dioxygen species”, sacrificing some oxidative power of singlet oxygen for far superior selectivity.<sup>27</sup> From the Table 2 it can be seen that all peroxides have similar active oxygen values, making H<sub>2</sub>O<sub>2</sub> by virtue of giving water as co-product, ostensibly<sup>78</sup> the hydroperoxide of choice.<sup>85</sup> Moreover, as reported by Richardson and co-workers, H<sub>2</sub>O<sub>2</sub> may be activated by NH<sub>4</sub>HCO<sub>3</sub> to obtain hydrogen percarbonate (HCO<sub>4</sub><sup>-</sup>), an oxidant with significantly better oxidative power than H<sub>2</sub>O<sub>2</sub>, in a so-called BAP reaction (BAP = bicarbonate activated peroxide), also permitting aqueous solvent mixtures as reaction media.<sup>86,87</sup> The use of H<sub>2</sub>O<sub>2</sub> is limited in cases where a transition metal catalyst, substrate and/or product, are prone to hydrolysis, or otherwise sensitive towards water, however. Furthermore, H<sub>2</sub>O<sub>2</sub> is obviously completely incompatible with some transition metals that catalyze its disproportionation into oxygen and water.<sup>88</sup>

Although organic hydroperoxides appear as less ideal oxidants than H<sub>2</sub>O<sub>2</sub>, they generally enjoy greater compatibility due to a number of reasons. In contrast to peracids and H<sub>2</sub>O<sub>2</sub>, organic hydroperoxides generally do not react with organics in the absence of a catalyst,<sup>89</sup> and show superior stability when compared to H<sub>2</sub>O<sub>2</sub> of similar grade (e.g. 70+ w-% aqueous solutions), and particularly so in comparison to peracids.<sup>90,91</sup> They are readily soluble in organic solvents, sparingly soluble in water, and the formed co-products, alcohols, generally demonstrate less deleterious effects to catalysts and other reactants compared to water. The structure of the organic hydroperoxide is generally regarded as having only minor effects on reaction rates and selectivities,<sup>92</sup> the choice between them being rather superficial. From the listed hydroperoxides use of TBHP is the most atom economical due to its lower molecular weight compared to the other organic hydroperoxides (see Table 2). There are some reports that suggest CHP induces higher enantiomeric excesses than TBHP in asymmetric sulfoxidation, however.<sup>93</sup>

## 2.3 Alkene Epoxidation

Epoxides, three-membered cyclic ethers, are amongst the most important of organic compounds. The epoxide functionality is highly reactive due to significant ring strain.<sup>94,95</sup> The high synthetic value of epoxides indeed springs from this reactivity, and the fact that they readily undergo highly stereo- and regioselective ring-opening and ring-expansion reactions with a vast array of different nucleophiles, giving rise to a multitude of 1,2-difunctional compounds, some of which are listed in Scheme 7.<sup>96,97</sup> Since epoxides are often *prochiral*, the end-products from epoxide functionalization find use in a variety of applications, particularly in synthetic pharmaceutical chemistry.



**Scheme 7.** Some reactions of epoxides with a multitude of nucleophiles en route to 1,2-difunctional compounds. Adapted from references <sup>96,97</sup>.

### 2.3.1 Utilization of Epoxides

The two industrially most widely manufactured epoxides in terms of mega tonnage per year are ethylene oxide (EO) and propylene oxide (PO).<sup>98</sup> The majority of EO, *ca.* 75%, is converted to glycols, such as ethylene glycol (egH<sub>2</sub>, ethane-1,2-diol), which is used as anti-freeze and in polyesters. Other glycols such as diethylene glycol and triethylene glycol as well as higher glycols find use as high-boiling solvents and as plasticizers. A small percentage of EO is polymerized for use as surfactants and as precursors for the synthesis of polyurethanes.<sup>98</sup> PO, in contrast to EO, is used as a raw material for many more end-products and intermediates in the chemical industry, however with similar applications. Most of PO (~ 65%) is converted to polyether polyols and used in the manufacture of polyurethanes. Other applications of PO include production of propylene glycol (*ca.* 20%), which is directly used as a high-boiling solvent, anti-freeze, or further polymerized to polypropylene oxide (PPO) for use as *e.g.* surfactants.<sup>99</sup> PO derivatives generally find extensive applications in food, cosmetic and pharmaceutical industries due to their relatively good biodegradability in comparison to EO, as well as due to high biocompatibility<sup>100</sup> with living organisms.<sup>98</sup> Recently, isotactic polypropylene oxide (*i*PPO), obtained by enantioselective catalytic chain transfer polymerization of PO, has been identified as photodegradable polymer having tensile strength comparable to that of nylon-6,6.<sup>101</sup> It is argued that *i*PPO may hold promise as substituent for nylon-6,6 in applications that require high strength and degradability, such as in fishing nets.<sup>101</sup>

## 2.3.2 Preparation of Epoxides

As a direct result of their vast synthetic utility, several ways to produce epoxides from alkenes have been developed. However, due to economic and environmental factors the methods differ significantly between academia and the industry. Industrial catalytic alkene epoxidation protocols include the Halcon/ARCO (Halcon International and Atlantic Richfield Company, later Lyondell-Chemical) TBHP/EBHP and Sumimoto CHP “organic hydroperoxide processes”<sup>75,102–104</sup> and the phased-out non-catalytic chlorohydrin processes that are the main industrial processes for the manufacture of both EO and PO (see Scheme 6 section 2.2.3.1).<sup>76</sup> The hydroperoxide processes employ complexes such as  $[\text{Mo}(\text{CO})_6]$  as the pre-catalysts, and are environmentally much more friendly than the chlorohydrin process.<sup>91</sup> However, a great disadvantage of the hydroperoxide processes is the stoichiometric production *tert*-butanol (TBOH), 1-phenylethanol or cumyl alcohol co-products, depending on the oxidant (see Table 2).<sup>75</sup> The various co-products such as TBOH and 1-phenylethanol can be, on one hand, sold as such or converted to other useful chemicals such as methyl *tert*-butyl ether (MTBE), a fuel octane-booster, and styrene, or they can be dehydrated and re-oxidized (recycled) by  $\text{H}_2\text{O}_2$ .<sup>92</sup> Thus, the economics of the hydroperoxide processes are dominated by the market situation of the co-product(s).<sup>75</sup>

However, in an academic laboratory setting, where substances are usually made in preparative scale, non-catalytic stoichiometric oxidation is more economically and environmentally acceptable, and consequently widely used. One of the most important methods with wide utility in this regard is the Prilezhaev reaction,<sup>105</sup> which involves the use of peracids such as peracetic acid (PAA) or *m*-chloroperbenzoic acid (*m*-CPBA) in particular, as a stoichiometric strong oxidizing agent (see Table 2).<sup>106</sup> Due to the particularly reactive and dangerous nature of peracids, there are no industrial scale stoichiometric epoxidation processes involving them.

## 2.3.3 Alkene Model Compounds

Although ethene (ethylene) and propene (propylene) are industrially the most important alkenes for epoxidation,<sup>107</sup> they are rarely used to evaluate the catalytic epoxidation potential of catalysts due to handling issues (both are gases). By far the most used model substrate in transition metal catalyzed epoxidation is *cis*-cyclooctene (**S1**), followed by cyclohexene (**8**).<sup>107</sup> Due to its “notoriously” high reactivity<sup>89</sup> and selectivity<sup>108</sup> for the cyclooctene (ep)oxide, **S1** is widely used to benchmark epoxidation catalysts in terms of TONs and TOFs, and it is consequently often the only studied substrate, in addition to **8**.<sup>109–111</sup> Terminal alkenes such as oct-1-ene (**S2**) and hex-1-ene (**9**) are significantly less reactive than their cyclic variants **S1** and **8**, respectively, but more prone to epoxide ring-opening reactions.<sup>107</sup> This is

due to electronic and steric properties of terminal alkenes *vs.* those of internal, and especially cyclic internal alkenes, for which ring strain may be pronounced.<sup>89</sup> Styrene (**S3**) is a commonly studied model substrate. It is a particularly unselective substrate, frequently affording over oxidation by-products such as phenylacetaldehyde, 1-phenylethane-1,2-diol (styrene glycol), benzaldehyde and benzoic acid aside from the desired styrene (ep)oxide.<sup>112</sup> (*cis/trans*)-Stilbene (*cis/trans*-**10**), prochiral styrene derivatives, are also frequently explored substrates that share some of the challenging reactivity characteristics of **S3**, in addition to often giving racemic mixtures upon oxidation.<sup>107</sup> There are only very few reports of epoxidation catalysts capable of selectively epoxidizing **S3** and **10**.<sup>113</sup> Some of the most challenging substrates for epoxidation are natural compounds such as mono- and bicyclic terpene derivatives including *L/D*-limonene (*D/L/rac*-**S4**),  $\alpha$ -terpineol (**S5**), norbornene (**11**), camphene (**12**),  $\alpha$ -pinene (**13**), among others.<sup>107</sup> In addition to being difficult to (ep)oxidize, **S4** and **S5** offer a measure of regioselectivity as well as functional group tolerance for epoxidation catalysts, having two olefinic sites and hydroxyl functionalities, respectively. Figure 3 shows some of the most widely used alkene substrates for epoxidation.

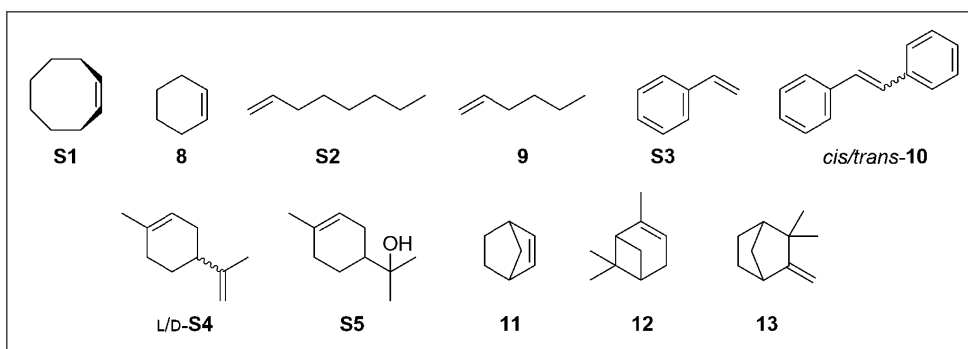


**Figure 3.** A (non-exhaustive) list of commonly used alkene substrates used in epoxidation. Substrates **S1** – **S5** were focused upon in the experimental part of this PhD thesis.

### 2.3.4 Alkene Epoxidation Mechanism

The mechanism(s) of Mo, W and V catalyzed alkene epoxidation has been under intensive study and a long-standing debate since the late 1960's. To date, there is still no definitive solution, and it remains an open problem to some degree. Modern consensus holds that an oxidant molecule, usually H<sub>2</sub>O<sub>2</sub> or TBHP, is activated by a metal center prior to oxygen transfer to a substrate *via* a peroxo-metal pathway.<sup>110</sup> Some of the most contemporary theoretical and experimental investigations by the groups including, but not limited to, Finney, Poli, Romão, Kühn, Calhorda and

Gonçalves in relation to Mo epoxidation revolve around Thiel's core epoxidation mechanism, which itself is highly complementary to the Sharpless mechanism (see next section).<sup>110,114–119</sup> Currently, special emphasis in these studies is directed towards subtleties involving oxidant activation, and most studies almost invariably show that an (alkyl)hydroperoxide is first coordinated to the metal, followed by proton transfer from the hydroperoxido ligand to a terminal metal oxido ligand, in a manner similar to what has been proposed<sup>114</sup> by Sharpless.<sup>115–118,120,121</sup> These mechanisms are, however, different to one another, and indeed, a notion is gaining ground which holds that there is no single, general mechanism, but ultimately it is dependent on the actual catalytic system.<sup>116</sup>

#### 2.3.4.1 Mimoun, Sharpless and Thiel Mechanisms

The groups of Mimoun and Sharpless were the first to study Mo catalyzed epoxidation mechanistically, and accordingly, two different proposals bearing their name were conceived (Scheme 8 reactions A1 – 3 and B1 – 2). Mimoun and Sérée De Roch showed in 1970 that an oxidobisperoxidomolybdenum(VI) complex  $[\text{MoO}(\text{O}_2)_2(\text{HMPA})]$  (**14**) (HMPA = hexamethylphosphoric triamide) stoichiometrically epoxidized **9**.<sup>122</sup> Based on the kinetics of the reaction, as well as on observations that coordinating solvents inhibit epoxidation, an organometallic multi-step mechanism involving initial alkene coordination to the metal was proposed (Scheme 8 reaction A1–3). In the first step of the Mimoun mechanism, an alkene is first coordinated to the metal (Scheme 8 reaction A1), displacing a HMPA ligand, followed by [3 + 2] cycloinsertion of the alkene across a Mo—O<sub>peroxido</sub> bond (Scheme 8 reaction A2), forming a metallacycle. Frequently observed in the chemistry of late transition metals, the involvement of a metallacycle was considered chemically sound. Furthermore, it was argued that these steps would explain the observed kinetics of the reaction, which hinted towards a stepwise process. In the final step of the reaction, the epoxide end-product would be obtained *via* cycloextrusion of the metallacycle (Scheme 8 reaction A3).<sup>123</sup>

In Mo, W and V catalyzed alkene epoxidation, there is currently overwhelming experimental and theoretical evidence to rule out the Mimoun epoxidation mechanism involving [3 + 2] cycloaddition, however. Sharpless and co-workers found experimentally that the reaction rate in the stoichiometric reaction between **14** and alkenes **8** or **11** closely parallels that observed if peracids PAA and *m*-CPBA were used instead of **14**.<sup>124</sup> Peracids are reagents that are known to react in the Prilezhaev alkene epoxidation reaction *via* the widely accepted Bartlett's *spirocyclic* "butterfly mechanism" involving [2 + 1] cycloaddition.<sup>125</sup> Moreover, the observed reaction rate differed significantly from known [3 + 2] cycloaddition reactions, most notably OsO<sub>4</sub> mediated alkene dihydroxylation.<sup>124,126</sup> A similar three-membered

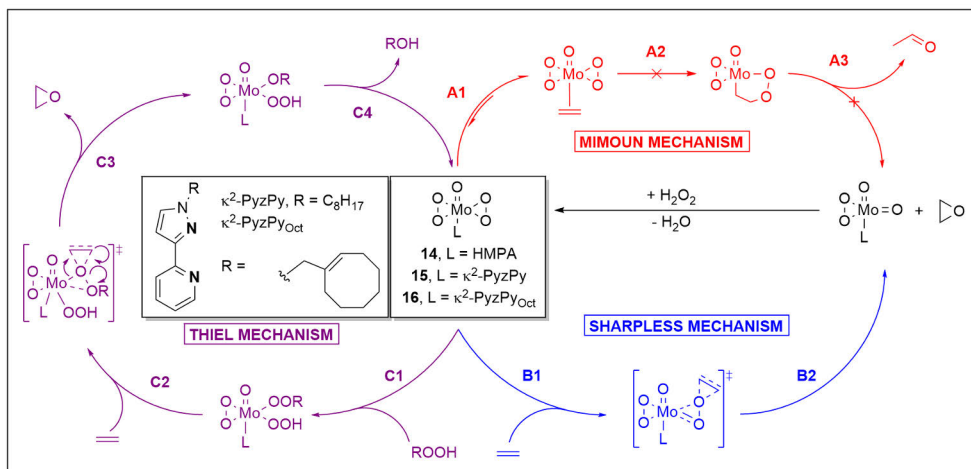
spirocyclic transition state was thus invoked to be the case with **14** mediated epoxidation of **8** and **11**, as shown in the Sharpless epoxidation mechanism (Scheme 8 reaction B).<sup>124</sup> An oxo-metal mechanism, similar to that observed in biological OAT, was also ruled out with <sup>18</sup>O labeling experiments.<sup>124</sup>

In the (catalytic) Sharpless mechanism, an alkene substrate is epoxidized in a single concerted step involving a three-membered spirocyclic transition state in a reaction ultimately closely resembling the Bartlett butterfly mechanism (Scheme 8 reaction B1), followed by generation of [MoO<sub>2</sub>(O<sub>2</sub>)(HMPA)] (Scheme 8 reaction B2).<sup>124</sup> Moreover, modern DFT quantum chemical calculations revealed that the Mimoun metallacycle mechanism is not only energetically unfeasible but the end-product obtained from a hypothetical metallacycle intermediate is an aldehyde, not an epoxide.<sup>123,127</sup> Similar DFT results have been obtained in V catalyzed epoxidation of ethylene, where the main product was observed to be acetaldehyde.<sup>128</sup> Moreover, a metallacycle mechanism could not explain the particularly high reactivity of allylic alcohols with Mo and V, especially in the presence of organic hydroperoxides.<sup>90</sup>

The Sharpless and Mimoun mechanisms cannot adequately explain the often vastly superior catalytic epoxidation performance of various early group 4 – 6 d<sup>0</sup> transition metal complexes in the presence of organic hydroperoxides, such as TBHP, as opposed to H<sub>2</sub>O<sub>2</sub>.<sup>114,129,130</sup> Thiel and co-workers employed an oxidobisperoxido molybdenum(VI) complex [MoO(O<sub>2</sub>)<sub>2</sub>(κ<sup>2</sup>-PyzPy)] (**15**) (κ<sup>2</sup>-PyzPy = bidentate pyrazolylpyridine ligand, see Scheme 8) and were able to show that, under *catalytic* conditions, the oxygen atom in the epoxide is derived from neither metal oxido nor peroxido ligands, but instead from TBHP.<sup>131</sup> Later work involving a complex [MoO(O<sub>2</sub>)<sub>2</sub>(κ<sup>2</sup>-PyzPy<sub>Oct</sub>)] (**16**), featuring an *internal* cyclooctene moiety in the ligand design, revealed that the ligand was not epoxidized prior to treatment of **16** with TBHP, decisively ruling out a direct oxygen transfer from oxido and peroxido ligands in a stoichiometric fashion, since an intramolecular oxygen transfer would be expected to be highly favored.<sup>132,133</sup>

Theoretical investigations involving complexes **15** and **16** are consistent with a “peroxo-metal”<sup>26</sup> mechanism that is complementary to the one originally proposed by Sharpless (Scheme 8 reaction C1 – 4).<sup>114,132,133</sup> The Thiel mechanism starts by coordination of the oxidizing agent (ROOH, such as TBHP) to a Lewis acidic Mo(VI) center followed by proton transfer from TBHP to one of the metal peroxido ligands (Scheme 8 reaction C1).<sup>133</sup> Reaction step C1 was experimentally determined to have a temperature dependent induction period, interpreted to be related to the formation of the [MoO(O<sub>2</sub>)(OOH)(OOR)(L)] species.<sup>133</sup> Moreover, there is marked competition between coordinating solvents and TBHP, and the more basic TBHP has a higher reaction rate than H<sub>2</sub>O<sub>2</sub>.<sup>133</sup> Rearrangement of the OOR ligand to a side-on η<sup>2</sup> coordination mode activates the alkyl hydroperoxide for oxygen transfer into the alkene (Scheme 8 reaction C2). An alkoxido ligand is generated concomitant

with the epoxidation step (Scheme 8 reaction C3), which in the last step abstracts the proton originally from the hydroperoxido ligand, releasing alcohol co-product and regenerating the initial oxidobisperoxido complex, and restarting the catalytic cycle (Scheme 8 reaction C4).<sup>133</sup>



**Scheme 8.** Mimoun, Sharpless and Thiel epoxidation mechanisms represented by red, blue, and purple reactions, respectively. Adapted from refs. <sup>123,127,132,133</sup>.

### 2.3.5 Mo & W Based Epoxidation Catalysis

Interest into Mo and W oxido complexes in epoxidation catalysis arose after Halcon and ARCO issued patents on the homogeneous  $[\text{Mo}(\text{CO})_6]$  TBHP/EBHP hydroperoxide processes.<sup>116</sup> The seminal mechanistic work by the groups of Sharpless, Mimoun, and later Thiel, on epoxidation has since sparked further interest on the topic. Contemporary Mo and W based epoxidation research focuses on developing greener processes in accordance with Green Chemistry. In practice, some of the ways to accomplish greener protocols is to develop high-activity complexes (high TON and TOF) or efficient processes involving complexes that remain highly active and selective in non-toxic polar solvents such as alcohols, or in solventless (neat) conditions. Furthermore, the stability and recoverability of catalysts has become an important focus. Some of the most notable types of studied Mo/W systems include a) Organometallic complexes having variable valence typically between II – VI; b) High-valent monomeric and dimeric  $[\text{MO}_2\text{X}_2(\text{L})_2]$  complexes; c) High-valent complexes based on multidentate Schiff-base ligands of variable donor count and N/O/S type.



## 2.3.5.1 Organometallic Systems

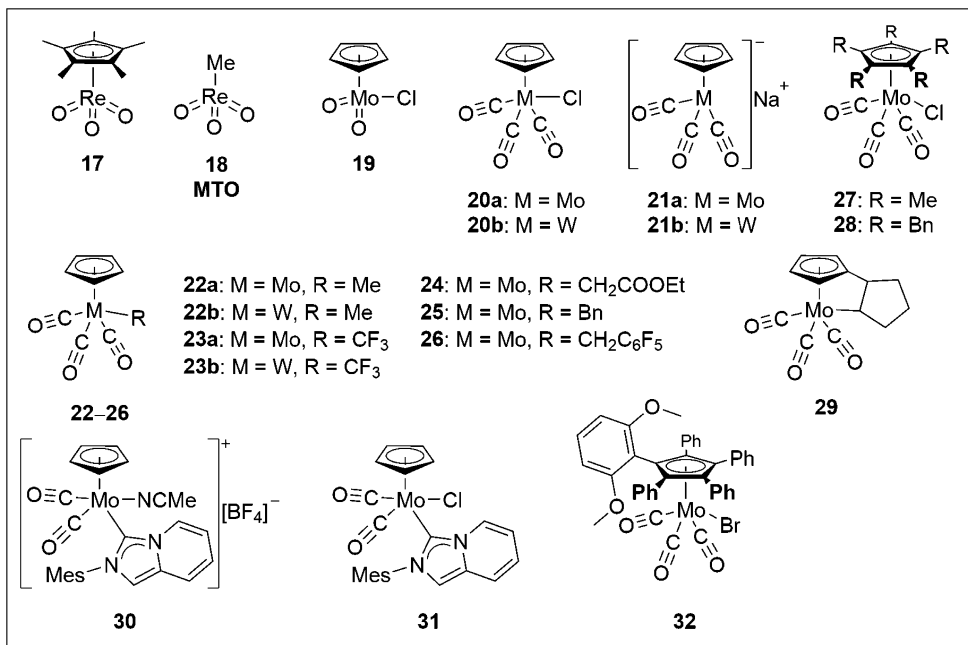


**Figure 4.** Some of the most active organometallic cyclopentadienyl-based Mo, W and Re pre-catalysts and synthetic precursors used in contemporary alkene epoxidation research. Bn = benzyl, Mes = mesityl (2,4,6-trimethylphenyl).

Organometallic molybdenum and tungsten complexes, often featuring cyclopentadienyl (Cp) and carbonyl ligands, are perhaps some of the most prominently investigated epoxidation pre-catalysts, having been extensively studied by the groups Herrmann, Romão, Kühn and Poli, and their co-workers, among others.<sup>109,120,121,134–140</sup> High interest in these complexes can at least partly be attributed to the high success of organometallic Mo derivatives in industrial epoxidation catalysis (Halcon-ARCO hydroperoxide processes), as well as [Cp\*ReO<sub>3</sub>] (**17**) (Cp\* = pentamethyl cyclopentadienyl), a derivative of [MeReO<sub>3</sub>] (**18**, MTO, methyltrioxidorhenium(VII)), one of the most active and selective epoxidation pre-catalysts known.<sup>141,142</sup> Similarly, Cp supported Mo complexes are amongst the most active Mo based epoxidation pre-catalysts ever reported. However, synthesis and handling of these types of complexes is challenging due to their sensitivity towards oxygen and water, especially after oxidation.<sup>134</sup> Upon discovery of the first organometallic molybdenum complex,<sup>143</sup> [CpMoO<sub>2</sub>Cl] (**19**), and subsequent innovations in synthesis optimization,<sup>111</sup> the research into Cp type Mo/W compounds has intensified dramatically.<sup>134,135</sup>

Starting from  $[\text{CpM}(\text{CO})_3\text{Cl}]$  ( $\text{M} = \text{Mo}$  (**20a**),  $\text{W}$  (**20b**)) or  $\text{Na}^+[\text{CpM}(\text{CO})_3]^-$  ( $\text{M} = \text{Mo}$  (**21a**),  $\text{W}$  (**21b**)), a vast number of derivatives can be obtained by employing different Cp ligands, or by introducing various ligands at the metal center *e.g.* by alkylation or *via* oxidative decarbonylation.<sup>135</sup> Reaction of **20** and **21** with MeI,  $\text{CF}_3\text{I}$ ,  $\alpha$ -chloroesters, benzyl chloride or (chloromethyl)pentafluorobenzene yields complexes **22** – **26** of the type  $[\text{CpM}(\text{CO})_3\text{R}]$  ( $\text{M} = \text{Mo}$ ,  $\text{R} = \text{Me}$  (**22a**);  $\text{M} = \text{W}$ ,  $\text{R} = \text{Me}$  (**22b**);  $\text{M} = \text{Mo}$ ,  $\text{R} = \text{CF}_3$  (**23a**);  $\text{M} = \text{W}$ ,  $\text{R} = \text{CF}_3$  (**23b**);  $\text{M} = \text{Mo}$ ,  $\text{R} = \text{CH}_2\text{COOEt}$  (**24**);  $\text{M} = \text{Mo}$ ,  $\text{R} = \text{Bn}$  (**25**,  $\text{Bn} = \text{benzyl}$ ) and  $\text{M} = \text{Mo}$ ,  $\text{R} = \text{CH}_2\text{C}_6\text{F}_5$  (**26**), respectively (Figure 4).<sup>120,137,138</sup> Highlighting the often observed drastic differences in epoxidation reactivity between Mo and W complexes, **22a** reaches a TOF  $\sim 6000 \text{ h}^{-1}$  in the epoxidation **S1**, whereas for the W-derivative **22b** only  $60 \text{ h}^{-1}$  is obtained.<sup>120,121,139</sup> Complexes **25** and **26** represent some of the most active  $[\text{CpMo}(\text{CO})_3\text{R}]$  type epoxidation pre-catalysts, reaching TOFs  $\sim 12000 \text{ h}^{-1}$  and  $18000 \text{ h}^{-1}$  in the epoxidation of **S1**, respectively.<sup>138</sup>

Additional reactivity in epoxidation may be obtained by different Cp ligands: complexes **27** and **28**, having a general formula  $[\text{Cp}'\text{Mo}(\text{CO})_3\text{Cl}]$  ( $\text{Cp}' = \text{Cp}^*$  (**27**),  $\text{C}_5\text{Bn}_5$  (**28**)) reach TOFs of 1200:1200:800  $\text{h}^{-1}$  in the epoxidation of **S1** at 1 mol-% catalyst loadings, for **20a:27:28**, respectively.<sup>111</sup> Interestingly, with **28** TOFs up to  $21000 \text{ h}^{-1}$  may be realized at 0.01 mol-% catalyst loading, surpassing that originally obtained for MTO/ $\text{H}_2\text{O}_2$  epoxidation benchmarking system, at  $\text{TOF} = 14000 \text{ h}^{-1}$  (although later enhanced to  $40000 \text{ h}^{-1}$  by Kühn and co-workers<sup>80</sup>).<sup>111</sup> *Ansa*-complexes such as **29** represent the pinnacle of “traditional” CpMo complexes when it comes to epoxidation activity. Having a modified Cp ligand fitted with a cycloalkyl bridge directly bound to the metal center such as in **29** leads to TOFs in the range of  $44000 \text{ h}^{-1}$  when the epoxidation of **S1** is performed in certain ILs.<sup>140</sup> *Ansa*-bridged complexes are currently under investigation as a potential platform for chiral catalysts, since the alkyl bridge offers good opportunities to attach stereogenic centers.<sup>135</sup> As a recent development, the most active Cp based Mo epoxidation catalysts are based on persistent carbenes, more specifically *N*-heterocyclic carbenes (NHCs), however.<sup>135</sup> Complexes **30** and **31** represent the state-of-the-art in Mo-catalyzed epoxidation, reaching TOFs of  $53000 \text{ h}^{-1}$  and  $41000$  and at extremely low catalyst loadings of 0.01 and 0.005 mol-% relative to **S1**, respectively.<sup>109</sup> See Chart 1 for a list of some of the most active Mo/W Cp based epoxidation pre-catalysts.

The epoxidation mechanism of organometallic Mo/W complexes is not known. However, it has been shown that  $[\text{CpM}(\text{CO})_3\text{R}]$  (including **22** – **31**) type complexes are oxidized by *e.g.*, TBHP, forming high-valent dioxidometal(VI) complexes of the type  $[\text{CpMO}_2\text{R}]$ , species that are similar to **19**. DFT investigations show that, under catalytic conditions,  $[\text{CpMO}_2\text{R}]$  may further react with TBHP, generating an activated  $[\text{CpMO}(\text{OH})(\text{OOR})(\text{R})]$  species in a fashion similar to the Thiel mechanism (Reaction C Scheme 8).<sup>115–118,120,121,135</sup> However, Poli and co-workers

have shown that an organometallic Cp\*—Mo bond is not entirely hydrolytically stable,<sup>144</sup> and *ring-slippage* reactions in metallocenes, Cp and indenyl complexes of nearly all transition metals are well-documented,<sup>145</sup> raising some concerns with regard to the actual epoxidation mechanism in the case of **22** – **31**.<sup>67</sup> In fact, Colbran and Harper have shown using NMR spectroscopy that **32**, supported by a pentaaryl cyclopentadienyl ligand (CpAr<sub>5</sub>), undergoes partial loss of the CpAr<sub>5</sub> ligand in the presence of TBHP, leading to an *in-situ* formed non-Cp complex that is far more active in epoxidation.<sup>67</sup> In the report it is argued that the presumed stability of an alkylcyclopentadienyl (**22** – **31**) Mo complex under oxidative conditions during catalysis may be partially unfounded, and that *in-situ* formation of a “true” catalyst *via* partial loss of Cp ligand(s) should not be disregarded.<sup>67</sup>

### 2.3.5.2 [MO<sub>2</sub>X<sub>2</sub>L<sub>2</sub>] Systems

Octahedral [MO<sub>2</sub>X<sub>2</sub>(L)<sub>n</sub>]<sub>y</sub> type complexes, where M = Mo, W; X = singly anionic ligand such as halide (may also be organometallic); n = 1 or 2 for bi- or monodentate neutral (L) ligands; and y = 1 or 2 for monomeric and dimeric complexes, are by far the largest class of studied Mo/W complexes. Kühn and co-workers have extensively studied monomeric [MO<sub>2</sub>Cl<sub>2</sub>(L)] type and similar complexes where L = bidentate neutral bipyridine type ligand, having a generic structure as shown for **33'** in Figure 5, reaching TOFs ~ 8000 h<sup>-1</sup> at most in the epoxidation of **S1**.<sup>82,116,151,117,121,134,146–150</sup> However, a dimeric pyrazole-derived complex {[MoO<sub>2</sub>Cl(L)]<sub>2</sub>(μ-O)} (**34**), reported by Gonçalves in 2007, is one of the most active dimeric Mo complexes in this class, attaining TOF ~ 32000 h<sup>-1</sup> in the epoxidation of **S1**.<sup>152</sup> Moreover, **34** performed well with H<sub>2</sub>O<sub>2</sub> in a water/MeCN reaction medium, and could epoxidize **S4** with a moderate 67% selectivity.<sup>152</sup> Very similar (TOF ~ 31000 h<sup>-1</sup>) activity was reported for a monomeric pyridylimine based complex **35**.<sup>153</sup>

Recently, Mösch-Zanetti and co-workers introduced dinuclear Mo—Mo bonded thiophenolato-oxazoline supported oxidomolybdenum(V) complexes **36** and **37**.<sup>69</sup> These complexes are the most active epoxidation pre-catalysts ever reported, reaching nominal TOFs of *ca.* 62000 and 107000 h<sup>-1</sup> for **36** and **37**, respectively, in the epoxidation of **S1** performed at 0.001 mol-% loading in chloroform.<sup>69</sup> However, epoxidation performance was severely reduced with more challenging substrates **S2** – **S4**.<sup>69</sup> **36** and **37** significantly outperform some previous complexes with similar ligands, such as **38** and **39**, including the previous record holder complex having a Mo—Mo triple bond, **40**, that reach TOFs ~ 5000:5000:60000 h<sup>-1</sup> for **38:39:40**, respectively.<sup>154–156</sup> A feasible explanation for the extremely high activity of **36** and **37**, as suspected by the authors, might be the five-coordinate nature of the Mo centers, and the known hemilability of the ligands, possibly allowing for a low-energy approach of TBHP in order to activate the complexes.<sup>69</sup> However, the authors

also mention that upon treatment of **36** with 10 eqv. TBHP in chloroform, an immediate discoloration could be observed with simultaneous formation of a colorless, voluminous precipitate. Moreover, free proligand was observed in solution by  $^1\text{H}$  NMR spectroscopy afterwards. The colorless precipitate eventually turned blue, indicating the formation of mixed Mo-POMs (POM = polyoxometalate), *i.e.*, molybdenum blue, as suspected by the authors.<sup>69</sup>

Amino(bis)phenolato ligands complex virtually all transition metals, and typically form moisture and oxygen stable complexes that are easy to handle and can be stored almost indefinitely.<sup>157</sup> First presented in epoxidation by Finney and Mitchell in their groundbreaking work, it was shown that complexes **41** – **43** supported by a bulky monoanionic tridentate aminophenolato ligand rule out the Mimoun metallacycle mechanism by preventing the simultaneous coordination of an alkene and TBHP to the metal, thus favoring the Sharpless/Thiel mechanism as more probable (see step A1 in Scheme 8 section 2.3.4.1).<sup>158</sup> Since then, amino(bis)phenolato supported Mo/W complexes have found extensive use as epoxidation pre-catalysts.<sup>157,159–167</sup>

Representing some notable results within these types of complexes, quite recently, Mösch-Zanetti and co-workers were able to reach near unparalleled 99% epoxidation selectivities with most substrates presented in Figure 3, employing dinuclear  $\text{MoO}_2$  complexes **44** – **46**.<sup>113</sup> Further work involved mononuclear (**47** – **49**) and dinuclear (**50** – **53**) aminophenolato bearing dioxidomolybdenum(VI) complexes featuring amido pendant arms.<sup>168</sup> These pre-catalysts reach TONs of  $\sim 110000$  at an extremely low 0.0005 mol-% catalyst loading in the epoxidation of **S1**, highlighting the extraordinary stability of the active species.<sup>168</sup> The high activity of **47** – **53** at extremely low catalyst loadings was attributed to H-bonding interactions from the amido pendant arms, which may be able to stabilize oxidant and/or substrate molecules in the second coordination sphere of the complexes.<sup>168</sup> Moreover, **47** – **53** remain moderately active even if the epoxidations are performed using  $\text{H}_2\text{O}_2$ , or in alcohols, particularly in TBOH, reagents that are known to inhibit epoxidation by coordinative competition.<sup>116</sup> Interestingly, **44** – **53** surpass in activity a notable aminotrisphenolato supported  $\text{MoOCl}$  complex **54**, which reaches a TOF = 7500  $\text{h}^{-1}$  as reported by Licini and co-workers.<sup>169</sup>

Hydroxamic acid derived Mo and W complexes have been described to be very active epoxidation pre-catalysts capable of enantioselective induction, akin to the well-known Jacobsen-Katsuki Mn-salen complex.<sup>170</sup> Recently, interesting results were obtained by Bhattacharyya and co-workers in the epoxidation of various alkenes using complexes **55** and **56**.<sup>171,172</sup> While the epoxidation did not work in  $\text{H}_2\text{O}_2$ , or proceeded very slowly, adding  $\text{NH}_4\text{HCO}_3$  as co-catalyst ( $\text{H}_2\text{O}_2/\text{BAP}$  system) allowed epoxidation of even some of the most difficult substrates. For example, norbornene oxide was obtained in 26% yield and 100% selectivity in 15

minutes with an initial TOF  $\sim 38000 \text{ h}^{-1}$  using **55**.<sup>171</sup> Moreover, a TOF  $\sim 37600 \text{ h}^{-1}$  was obtained for **56** in the epoxidation of **11**, thus making it one of the most active W complexes ever reported in epoxidation.<sup>172</sup> The reactivity of **55** and **56** was readily expanded to the oxidation of other alkenes, as well as alkanes, alcohols, amines and sulfides.<sup>171,172</sup>

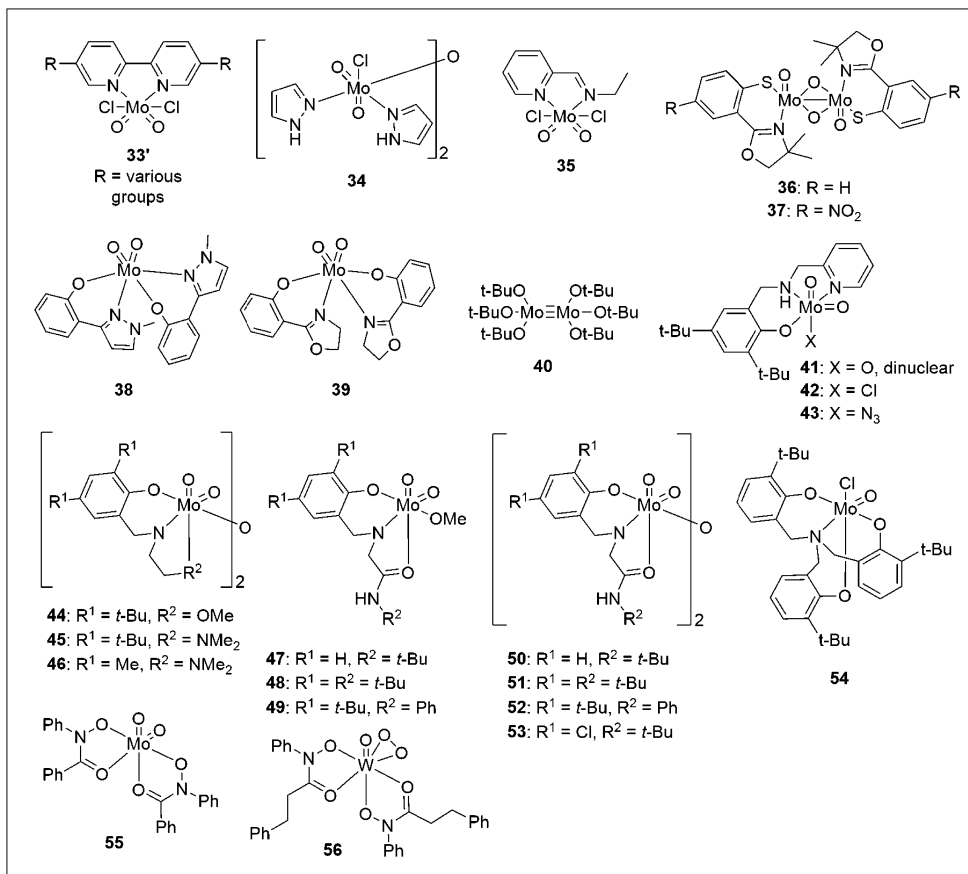


**Figure 5.** Some of the most active [MO<sub>2</sub>X<sub>2</sub>L<sub>2</sub>]-type and similar Mo and W pre-catalysts used in contemporary alkene epoxidation research.

### 2.3.5.3 Schiff-Base and Porphyrin Systems

Transition metal complexes based on multidentate Schiff-base ligands are renowned for their high catalytic activity in various reactions, ease of synthesis and high stability towards hydrolytic and oxidative conditions.<sup>173,174</sup> Several Schiff-base Mo complexes have been described as epoxidation catalysts (Figure 6).<sup>110,175–183</sup> Some prominent Schiff-base epoxidation systems also include V complexes, such as the recent porphyrin oxidovanadium(v) complexes **57** – **59** reported by Maurya and co-

workers.<sup>184,185</sup> **57** – **59** readily achieve selective epoxidation of even the most challenging substrates such as *trans*-**10**, **S2** and **S3**, showing near quantitative conversion and selectivity for the corresponding epoxides.<sup>184,185</sup> Strikingly, **57** – **59** display slightly higher activity for the epoxidation of **S2** compared to the benchmark substrate **S1**, reaching TOFs ~8900:2700:13800 h<sup>-1</sup> for **57**:**58**:**59**, respectively.<sup>184,185</sup> On the way to finding the “Holy grail” oxidation catalyst, Rao and co-workers report a rather rare<sup>186</sup> example of a Schiff-base complex [MoO<sub>2</sub>(κ<sup>3</sup>-L<sup>SAH</sup>)(H<sub>2</sub>O)]<sup>187</sup> (**60**) (SAH = salicylidenehydrazine) capable of aerobic oxidation of **9**, albeit with limited selectivity for the epoxide.<sup>188</sup>

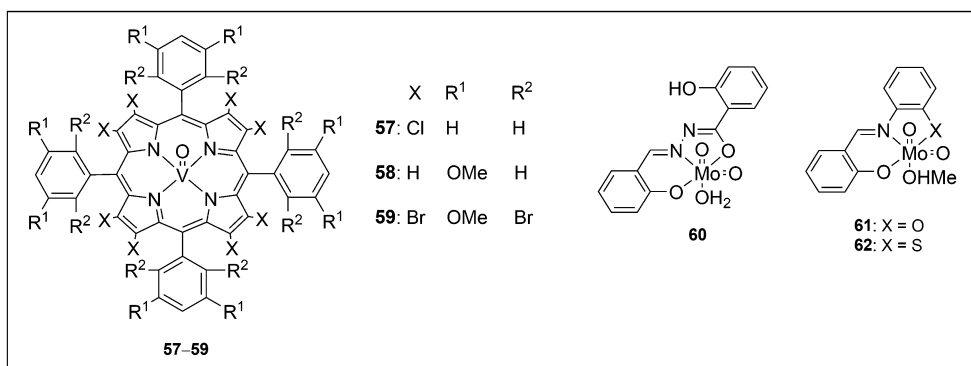
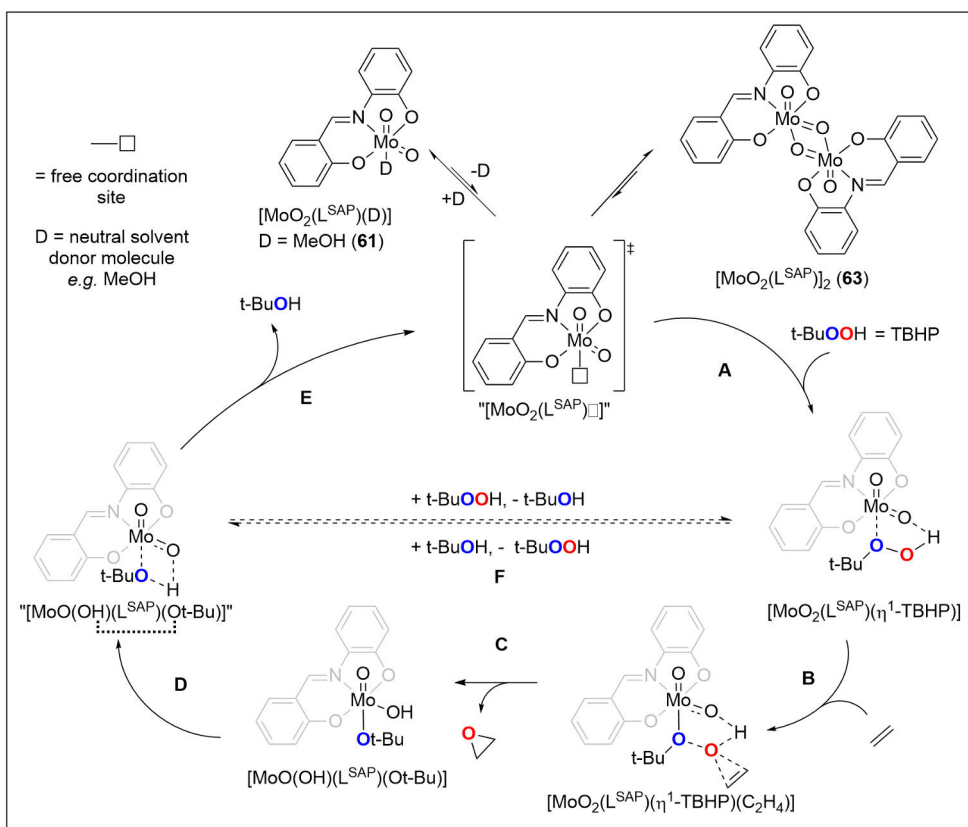


**Figure 6.** Some notable Schiff-base-type Mo and V complexes used in modern alkene epoxidation research.

Poli and co-workers have mechanistically investigated alkene epoxidation employing Schiff-base complexes [MoO<sub>2</sub>(κ<sup>3</sup>-L<sup>SAP</sup>)(MeOH)] (**61**) and [MoO<sub>2</sub>(κ<sup>3</sup>-L<sup>SATP</sup>)(MeOH)] (**62**), supported by tridentate dianionic κ<sup>3</sup>-L<sup>SA{T}P</sup> ligands (where SA{T}P = salicylideneamino{thio}phenolato).<sup>110,176,179</sup> Formally of the type [MoO<sub>2</sub>(κ<sup>3</sup>-L)(D)], **61** and **62** are examples of so-called “pseudo octahedral, pseudo six-coordinate” complexes, having one weakly coordinating donor molecule D, MeOH in the case of both **61** and **62**. Consequently, **61** and **62** readily interconvert between their monomeric and dimeric forms [MoO<sub>2</sub>(κ<sup>3</sup>-L<sup>SAP</sup>)]<sub>2</sub> (**63**) and [MoO<sub>2</sub>(κ<sup>3</sup>-L<sup>SATP</sup>)]<sub>2</sub> (**64**) via facile addition/removal of MeOH ligand through unsaturated formally 14-electron species [MoO<sub>2</sub>(κ<sup>3</sup>-L<sup>SA{T}P</sup>)□], respectively, where □ represents a free coordination site.<sup>110,176,179</sup>

It is proposed that the epoxidation power of **61** and **62**, possibly including other MoO<sub>2</sub> complexes supported by tridentate Schiff-base ligands, in fact arise from the relatively easily accessible transient five-coordinate 14-electron reactive species. Mechanistic investigations involving DFT show that [MoO<sub>2</sub>(κ<sup>3</sup>-L<sup>SAP</sup>)□] may coordinate TBHP as a neutral molecule, forming the neutral TBHP adduct [MoO<sub>2</sub>(κ<sup>3</sup>-L<sup>SAP</sup>)(η<sup>1</sup>-TBHP)] in the first step of the “Poli mechanism” (step A Scheme

9). This contrasts with the more common interpretations invoking  $M(OH)(OOR)$  species with anionic OOR ligands (*e.g.*, see Sharpless/Thiel mechanisms Scheme 8 section 2.3.4.1). The TBHP adduct, which is assumed to be catalytically activated, is stabilized by H-bonding to the equatorial oxido ligand. Upon introduction of an alkene substrate such as ethylene the transient ternary “catalyst-TBHP-alkene” adduct  $[MoO_2(\kappa^3-L^{SAP})(\eta^1-TBHP)(C_2H_4)]$  is formed in the step B, followed by intramolecular rearrangement, generating  $[MoO(OH)(\kappa^3-L^{SAP})(Ot-Bu)]$  as well as the epoxide (step C).  $[MoO(OH)(\kappa^3-L^{SAP})(Ot-Bu)]$  intramolecularly (and reversibly) rearranges in the presence of excess TBHP to regenerate  $[MoO_2(\kappa^3-L^{SAP})(\eta^1-TBHP)]$  species, restarting the catalytic cycle (step F). However, in principle  $[MoO(OH)(\kappa^3-L^{SAP})(Ot-Bu)]$  may also rearrange into  $[MoO_2(\kappa^3-L^{SAP})(TBOH)]$ , a neutral alcohol adduct analogous to **61**, which may be expected to release TBOH in a similar way **61** loses methanol, generating  $[MoO_2(\kappa^3-L^{SAP})\square]$  (step E).<sup>110</sup>



**Scheme 9.** Main features of the alkene epoxidation mechanism involving **61** and ethylene as the model substrate, as proposed by Poli and co-workers.

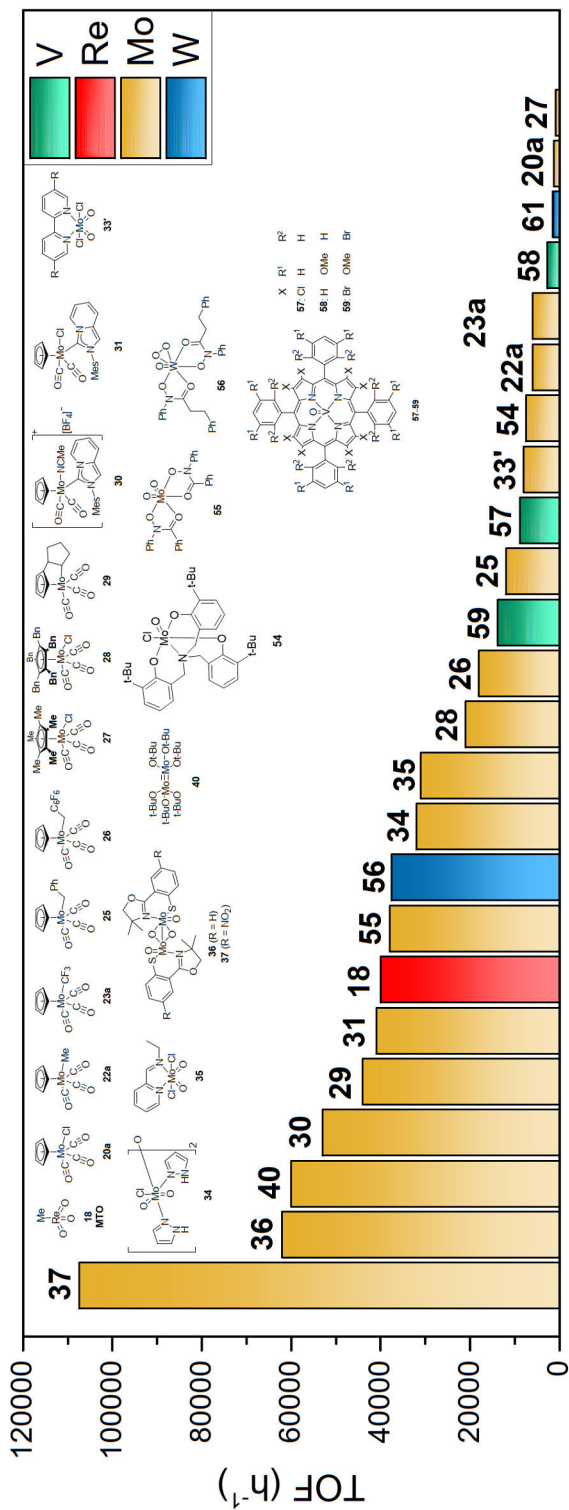


**Chart 1.** Comparison of the maximum reported TOFs obtained with some of the most notable molybdenum (orange), tungsten (blue) and vanadium (green) based complexes against the benchmark rhenium (red) MTO/H<sub>2</sub>O<sub>2</sub> system in the epoxidation of *cis*-cyclooctene (**11**) or cyclohexene (**8**) (norbornene (**11**) for **55** and **56**).



## 2.4 Catechol Oxidation

In light of the importance of metal catalyzed, O<sub>2</sub> mediated oxidation reactions in nature as well as in the industry (sections 2.1.2 and 2.1.3), these types of reactions have been extensively investigated. Specifically, oxidative dehydrogenation and (di)oxygenation of catechols have been successfully carried out with Cu and Fe based transition metal catalysts that structurally and/or functionally mimic the CO and CDOs, respectively.<sup>42,43,189,190</sup> In the context of both CO and CDO model chemistry, several catechol substrates are used as model compounds. The most frequently used model substrate is 3,5-di-*tert*-butylcatechol (**S6**, 3,5-DTBCH<sub>2</sub>, see Table 3) followed by other alkyl substituted catechols such as 4-*tert*-butylcatechol (**S7**, 4-TBCH<sub>2</sub>).<sup>191</sup> The use of (di)alkyl substituted catechols as model substrates is justified, since oxidation of the prototypical catechol, pyrocatechol (**S8**, benzene-1,2-diol), has been reported to lead to a mixture of unknown composition.<sup>192</sup> In the context of catechol dioxygenation, the unclear reaction of **S8** most likely emanates from the combined high reactivity of activated <sup>1</sup>O<sub>2</sub> (see section 2.2.3.3) and the unprotected nature of pyrocatechol, by virtue of lacking sterically demanding alkyl groups. On the other hand, in some cases **S7** or **S8** have also been reported to be much more unreactive than **S6**.<sup>191,193</sup> A drawback of **S6** is its relatively facile autoxidation, especially under basic conditions, however.<sup>194</sup>

### 2.4.1 Vanadium Catechol Dioxygenase Mimetics

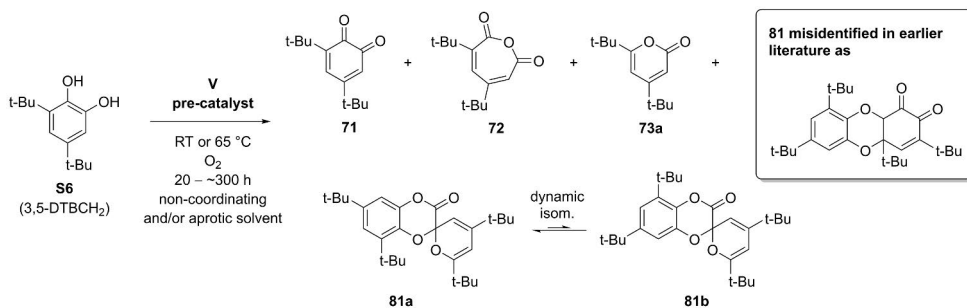
In addition to Fe, the catecholato chemistry of V (including Mo and W, to an extent), is well-developed thanks to the works of Pierpont and Sawyer, among others.<sup>195–201</sup> It is currently well-established that vanadium readily reacts with a variety of catechols and derivatives thereof, forming redox non-innocent complexes.<sup>202–207</sup> Furthermore, V-containing compounds have long been recognized to mediate catechol dioxygenase-like reactions.<sup>191,193,208,209</sup> V catalyzed CDO mimetic studies almost exclusively involve the use of **S6** as the model catechol substrate, with about 13 known (di)oxygenation products having been isolated and characterized.<sup>210,211</sup>

Simple vanadium compounds such as [VO(acac)<sub>2</sub>] (**65**) (acac = pentane-2,4-dionato, acetylacetonato), [VO(acac)(μ-OMe)<sub>2</sub>] (**66**), as well as other V complexes based on similar ligands, including [VO(tmh)(μ-OMe)<sub>2</sub>] (**67**), (tmh = 2,2,6,6-tetramethylheptane-3,5-dionato; [VO(aap)<sub>2</sub>] (**68**), (aap = 1-(2-hydroxyphenyl)-1,3-butanedionato); [VO(dmba)<sub>2</sub>] (**69**), (dmba = 1,5-bis(*p*-methoxyphenyl)pentane-1,3,5-trionato; [VO(dba)<sub>2</sub>] (**70**) (dba = 1,5-diphenylpentane-1,3,5-trionato), were found to afford the dehydrogenation product 3,5-di-*tert*-butyl-1,2-benzoquinone (3,5-DTBQ, **71**), the intradiol dioxygenase product 3,5-di-*tert*-butyl muconic acid anhydride (**72**), and the extradiol dioxygenase product 4,6-di-*tert*-butyl-2-pyrone

(**73a**) in the oxidation of **S6**, with a rather similar product distribution throughout (Table 3 entries 1 – 3).<sup>191,208</sup> Additionally, nearly identical results were obtained with salen-type complexes [VO(salen)] (**74**), [salen = ethylenebis(salicylideneaminato)]; [VCl(salen)] (**75**), and [VCl(saldpt)] (**76**), [saldpt = *N,N'*-(3,3'-dipropylamino)bis(salicylideneaminato)], and [VO(acac)(TCC)] (**77**), (TCC = 3,4,5,6-tetrachlorocatecholato) (Table 3 entry 4 – 5).<sup>208,209</sup>

The work of Tatsuno and co-workers later demonstrated the CDO mimetic activity of several V-based POMs (*n*-Bu<sub>4</sub>N)<sub>4</sub>H<sub>5</sub>[PV<sub>14</sub>O<sub>42</sub>] · H<sub>2</sub>O (**78**), (*n*-Bu<sub>4</sub>N)<sub>3,3</sub>Na<sub>3,7</sub>[MnV<sub>13</sub>O<sub>38</sub>] · 24 H<sub>2</sub>O (**79**), and (*n*-Bu<sub>4</sub>N)<sub>5</sub>Na<sub>2</sub>[NiV<sub>13</sub>O<sub>38</sub>] · 16 H<sub>2</sub>O (**80**) in the oxidation of **S6**.<sup>193</sup> However, in addition to the typical products (**71** – **73**), a then-misidentified “quinone dimer”, later characterized<sup>211</sup> by Finke and co-workers as the extradiol dioxygenase product spiro[1,4-benzodioxin-2(3H),2'-[2H]pyran]-3-one-4',6,6',8-tetra(*tert*-butyl) (**81a**), together with its dynamic (nonisolable) structural isomer (**81b**) were additionally obtained in *ca.* 7 – 11% yield (Table 3 entry 6).<sup>193</sup> It was found that monomeric oxidovanadium(V) complexes Na[VO(3,5-DTBC)<sub>2</sub>] (**82**) and Na<sub>2</sub>[VO(OMe)(3,5-DTBC)<sub>2</sub>] (**83**) did not display CDO mimetic activity, similarly to Mo and W based POMs H<sub>3</sub>[PMo<sub>12</sub>O<sub>40</sub>] · 30 H<sub>2</sub>O (**84**) and H<sub>3</sub>[PW<sub>12</sub>O<sub>40</sub>] · 30 H<sub>2</sub>O (**85**), as well as [MoO<sub>2</sub>(acac)<sub>2</sub>] (**86**) (Table 3 entries 7 – 11).<sup>193</sup>

Despite the activity of various V compounds in **S6** oxygenation, the mechanism was not known. Tatsuno and Fenton together with co-workers noted characteristic features in the dioxygenation reactions such as the inability to oxygenate **S7** or **S8**, and the importance of the chosen solvent.<sup>191,208</sup> Namely, performing the oxidation of **S6** in methanol, DMF or THF yields only the dehydrogenation product **71**, with no oxygenated products, whereas MeCN, CHCl<sub>3</sub>, benzene and 1,2-dichloroethane (1,2-DCE) give practically identical results.<sup>191,208</sup> The oxygenation also worked equally well under a reduced catalyst loading of 0.1 mol-% of **65** relative to **S6** (Table 3 entry 2), emphasizing the high activity and stability of the active vanadium species (TON ≥ 500 for dioxygenated products **72** and **73a**).<sup>208</sup> Although the catalytically active species, or intermediate species en route to the active catalyst, was not known, it was recognized that ligand substitution most likely played a significant role. For example, species such as [V(salen)(3,5-DTBC)] and [VO(acac)(3,5-DTBC)], obtained after oxo abstraction from **74** and replacement of TCC from **77**, respectively, were invoked to be part of the catalyst activation, akin to the accepted CDO mechanism (see Scheme 2 in section 2.1.2.1).<sup>208,209</sup>

**Table 3.** Aerobic oxidation of **S6** catalyzed by structurally diverse vanadium(IV/V) compounds.

Entry	Pre-catalyst	Conv. (%)	Product distribution (%)				Ref.
			71	72	73a	81	
1 [a]	(65) [VO(acac) <sub>2</sub> ] (1 mol-%)	100	27	41	15	0	208
2 [a]	65 (0.1 mol-%)	100	25	43	7	0	208
3 [a]	(66 – 70) [VO(acac)(μ-OMe) <sub>2</sub> ]; [VO(tmh)(μ-OMe) <sub>2</sub> ]; [VO(aap)] <sub>2</sub> ; [VO(dmbs)] <sub>2</sub> ; [VO(dba)] <sub>2</sub>	100	22 – 25	46 – 48	7 – 10	0	191
4 [a]	(74 – 76) [VO(salen)]; [VCl(salen)]; [VCl(saldpt)]	100	22 – 28	39 – 43	6 – 7	0	208
5 [a]	(77) [VO(acac)(TCC)]	nd	24	45	6	0	209
6 [a]	(78 – 80) PV <sub>14</sub> O <sub>42</sub> ; MnV <sub>13</sub> O <sub>38</sub> ; NiV <sub>13</sub> O <sub>38</sub>	nd	15 – 19	34 – 36	11 – 20	7 – 11	193
7 [a]	(82) Na[VO(3,5-DTBC) <sub>2</sub> ]	nd	14	0	0	0	193
8 [a]	(83) Na <sub>2</sub> [VO(OMe)(3,5-DTBC) <sub>2</sub> ]	nd	90	0	0	0	193
9 [a]	(84) PMO <sub>12</sub> O <sub>40</sub>	nd	0	0	0	0	193
10 [a]	(85) PW <sub>12</sub> O <sub>40</sub>	traces	Traces	0	0	0	193
11 [a]	(86) [MoO <sub>2</sub> (acac) <sub>2</sub> ]	nd	11	0	0	0	193
12 [b]	(87) SiW <sub>9</sub> V <sub>3</sub> O <sub>40</sub>	75 ± 4	16 ± 1	40 ± 3	6 ± 1	10 ± 1	211
13 [b]	(88) P <sub>2</sub> W <sub>15</sub> V <sub>3</sub> O <sub>62</sub>	95 ± 5	9 ± 1	57 ± 3	11 ± 1	17 ± 1	211
14 [b]	(89) (MeCN) <sub>x</sub> Fe · SiW <sub>9</sub> V <sub>3</sub> O <sub>40</sub>	95 ± 5	16 ± 1	46 ± 2	15 ± 1	17 ± 1	211
15 [b]	(90) (MeCN) <sub>x</sub> Fe · P <sub>2</sub> W <sub>15</sub> V <sub>3</sub> O <sub>62</sub>	95 ± 5	22 ± 1	42 ± 3	11 ± 1	18 ± 1	211
16 [b]	(91) SiW <sub>11</sub> VO <sub>40</sub>	~ 1	0	0	0	0	211
17 [b]	65	95 ± 5	20 ± 1	45 ± 2	11 ± 1	18 ± 1	211
18 [b]	none (control)	< 1	0	0	0	0	211

Reaction conditions: [a] [V]:[S6] = 1:100 unless specified otherwise, non-alcohol, DMF or THF solvent (MeCN, C<sub>6</sub>H<sub>6</sub>, 1,2-DCE, CHCl<sub>3</sub> afford similar results), RT, 20 h, O<sub>2</sub> atmosphere. nd = not determined. Formulas for the POMs (entries 6, 9, 10, 12 – 16) have been simplified for clarity (see text). [b] Finke Protocol: [V]:[S6] = ~ 1:3400, 1,2-DCE, 65 ± 0.1 °C, 20 ~ 300 h, O<sub>2</sub> atmosphere, **S6** re-crystallized three times prior to use under N<sub>2</sub>. Acac = acetylacetonato, tmh = 2,2,6,6-tetramethylheptane-3,5-dionato, aap = 1-(2-hydroxyphenyl)-1,3-butanedionato, dmbs = 1,5-bis(*p*-methoxyphenyl)pentane-1,3,5-trionato, dba = 1,5-diphenylpentane-1,3,5-trionato, salen = ethylenebis(salicylideneaminato), saldpt = *N,N'*-(3,3'-dipropylamino)bis(salicylideneaminato), TCC = 3,4,5,6-tetrachlorocatecholato.

### 2.4.1.1 Finke's "Common Catalyst Hypothesis"

In 1999 – 2005 several important discoveries that would lead to a breakthrough in V catalyzed CDO mimetic chemistry were made by Finke and co-workers.<sup>211–214</sup> The rather similar product selectivities obtained in the oxidation of **S6** catalyzed by various structurally diverse V-containing compounds in the earlier literature (Table 3 entries 1 – 6), particularly in the case of V-POMs, was noted by Finke, Pierpont having made similar observations earlier.<sup>195</sup> From insights gained from these reports, four V-POMs (*n*-Bu<sub>4</sub>N)<sub>7</sub>[SiW<sub>9</sub>V<sub>3</sub>O<sub>40</sub>] (**87**), (*n*-Bu<sub>4</sub>N)<sub>9</sub>[P<sub>2</sub>W<sub>15</sub>V<sub>3</sub>O<sub>62</sub>] (**88**), (*n*-Bu<sub>4</sub>N)<sub>5</sub>[(MeCN)<sub>x</sub>Fe · SiW<sub>9</sub>V<sub>3</sub>O<sub>40</sub>] (**89**) and (*n*-Bu<sub>4</sub>N)<sub>5</sub>Na<sub>2</sub>[(MeCN)<sub>x</sub>Fe · P<sub>2</sub>W<sub>15</sub>V<sub>3</sub>O<sub>62</sub>] (**90**) were designed and examined as V-based functional CDO mimics.<sup>211</sup> Not only did these pre-catalysts yield nearly exactly the same product distribution as obtained in all the other cases (Table 3 entries 12 – 15 vs. entries 1 – 6), but from these pre-catalysts **89** reached a TON ~ 127000, a value that is unmatched to date by other CDO models based on *any* transition metal, nor the native CDO metalloenzymes themselves.<sup>211</sup> However, a more fundamental finding was that the oxidation of **S6** catalyzed by **87** – **90** was preceded by an (A → B) type induction period followed by sigmoidal oxygen uptake curves, characteristic features for an *autocatalytic* (A + B → 2B) type reaction (Figure 7).<sup>211</sup>

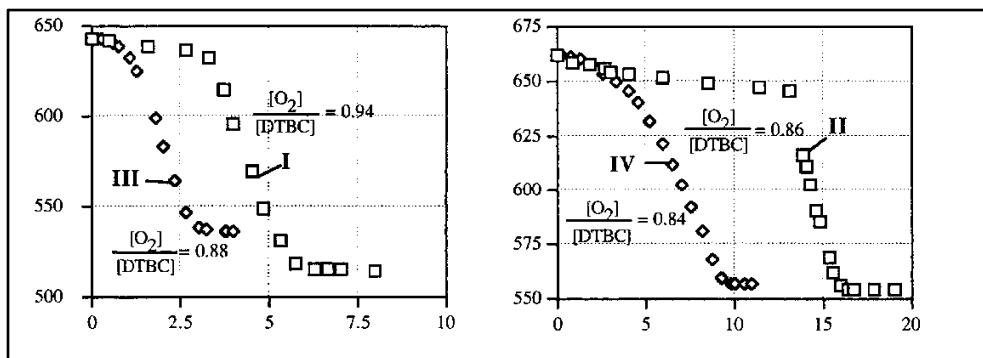


**Figure 7.** Oxygen pressure (Torr) vs. time (hours) plots obtained in oxygen uptake reactions involving compounds I – IV (corresponding to **87** – **90**, respectively) in the catalytic dioxygenation of **S6** performed in 1,2-DCE at 40 °C under O<sub>2</sub>. Reprinted with permission from "Weiner, H. & Finke, R. G., 'An All-Inorganic, Polyoxometalate-Based Catechol Dioxygenase That Exhibits > 100 000 Catalytic Turnovers', *J. Am. Chem. Soc.*, 1999, 121, 9831–9842". Copyright 1999 American Chemical Society.

Further work on V-POM based CDO mimetics with special emphasis in understanding the intricacies leading up to the observed product distribution revealed several key aspects about the reactions. Namely, it was found that the (A → B) induction period was linked to an initial, *non-catalytic* O<sub>2</sub>-mediated *autoxidation* of

**S6** into **71**, and the concurrent generation of  $\text{H}_2\text{O}_2$ .<sup>213</sup> Reactions performed using commercial **S6** (as-received, non-recrystallized, contains as much as 4% **71** by mass<sup>213</sup>) leads to a significant shortening of the induction periods, whereas treatment of the reactions with  $\text{H}_2\text{O}_2$  mid-induction period eliminates it altogether.<sup>213</sup>

Additional kinetic and mechanistic work involving oxygen uptake experiments pointed towards a scenario, whereby  $\text{H}_2\text{O}_2$  *leaches* vanadium from the catalyst precursors (V-POMs), generating the active catalyst.<sup>212,214</sup> More support for the  $\text{H}_2\text{O}_2$  leaching hypothesis was obtained in the case of the pre-catalyst (*n*-Bu<sub>4</sub>N)<sub>5</sub>[SiW<sub>11</sub>VO<sub>40</sub>] (**91**), a compound reportedly<sup>215,216</sup> resistant to the effects of  $\text{H}_2\text{O}_2$ , for which dioxygenase products could not be obtained (Table 3 entry 16).<sup>214</sup> A “common catalyst hypothesis” was coined, proposing that *any*  $\text{H}_2\text{O}_2$  sensitive V-POM based pre-catalyst would undergo transformation in the presence of excess **S6**,  $\text{H}_2\text{O}_2$  generated concomitant to **71**, and  $\text{O}_2$  into the “common catalyst”, which, once formed, then feeds into new catalytic cycles, generating the characteristic<sup>†</sup> dioxygenase product distribution in an “autoxidation-initiated-dioxygenase reaction” shown in nearly all cases in Table 3.<sup>213,214</sup>

#### 2.4.1.2 Common Catalyst Identification

Pierpont and co-workers have demonstrated that simple vanadium compounds such as **65** or  $[\text{V}(\text{CO})_6]$  react under an inert atmosphere with excess **S6** or **71**, forming the paramagnetic oxygen-sensitive complex  $[\text{V}(3,5\text{-DTBC})_2(3,5\text{-DTBSQ}^*)]$  (**92**, where 3,5-DTBSQ\* = 3,5-di-*tert*-butyl-1,2-semiquinonato) which at RT has a 10-line EPR spectrum having a  $\langle g \rangle \sim 2.004$  and a  $A(^{51}\text{V}) \sim 2.1$  G.<sup>202</sup> Upon exposure to  $\text{O}_2$ , **92** is slowly oxidized into  $[\text{VO}(3,5\text{-DTBC})(3,5\text{-DTBSQ}^*)]$  (**93**), which readily dimerizes into  $[\text{VO}(3,5\text{-DTBC})(3,5\text{-DTBSQ}^*)]_2$  [**93**]<sub>2</sub>, which has a characteristic nine-line EPR spectrum at RT with a  $\langle g \rangle \sim 2.004 - 2.006$  and a  $A(^{51}\text{V}) \sim 2.85$  G (see Figure 15 section 5.2.2.3), consistent with an organic radical (3,5-DTBSQ\*) coupling weakly to a diamagnetic vanadium center.<sup>202</sup> See Scheme 10 for reactions involving **92**, **93** and [**93**]<sub>2</sub>. Even further reaction with  $\text{O}_2$  in the absence of **S6** destroys **93**, leading to a loss of EPR signal and generation of free **71** as well as  $\text{V}_2\text{O}_5$ .<sup>202</sup>

The mixed (oxido)vanadium-catecholato-semiquinonato complexes **92** and **93** had been suspected as possible reaction intermediates in V-CDO mimetic reactions by Pierpont.<sup>195</sup> Decisive evidence of their involvement was found by Finke and co-

<sup>†</sup>  $[\text{V}]:[\text{S6}]$  stoichiometry strongly affects **S6** oxidation outcome. For example, performing a reaction with a  $[\text{V}]:[\text{S6}]:[\text{H}_2\text{O}_2]$  molar ratio of 1:4:1 *i.e.*, 25 mol-%  $\text{SiW}_9\text{V}_3\text{O}_{40}^{7-}$  relative to **S6**, yields  $56 \pm 6\%$  **71** and  $\leq 3\%$  dioxygenase products **72**, **73a** and **81**, highlighting the importance of performing the reactions with a *catalytic* amount of vanadium pre-catalysts.

workers, who demonstrated that an authentic sample of **[93]<sub>2</sub>** commenced the dioxygenation of **S6** immediately, with  $\text{Na}_2[\text{V}(\text{3,5-DTBC})_3]_2$  (**94**), a close analogue of **92**, showing an induction period of *ca.* 10 minutes (Figure 8).<sup>214</sup> Thus, **[93]<sub>2</sub>** and **94** acted as “kinetically competent” species on the way to the formation of the active catalyst.<sup>214</sup> However,  $[\text{VO}(\text{3,5-DTBC})_2]^{2-}$  (**95**), as a “kinetically incompetent” species, was not directly involved in the catalytic cycle, showing a *ca.* two-hour induction period (Figure 8).<sup>214</sup> Later on, the species **[93]<sub>2</sub>** and its half-fragment **93** have been explicitly detected during catalysis using EPR spectroscopy and ESI-MS when using *e.g.*, **65** and **78** as pre-catalysts. Invoking Halpern’s rules (see section 2.2) the species **[93]<sub>2</sub>** has been suggested by Finke and co-workers to be the catalytic resting-state, kinetically close to the presumed active species **93**.<sup>212,214</sup> By extension, due to the very similar product distribution obtained for nearly all V-containing pre-catalysts in Table 3, almost all pre-catalyst are strongly implied to transform into the same active form during catalysis, and thus follow the “common catalyst hypothesis”.<sup>211–214</sup>

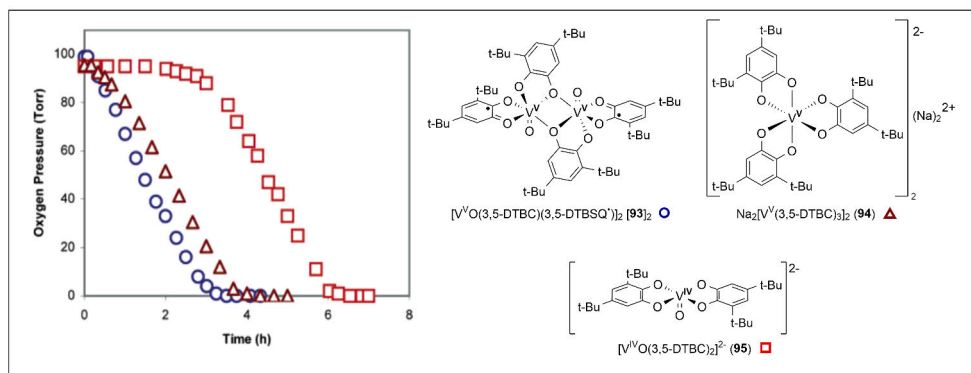
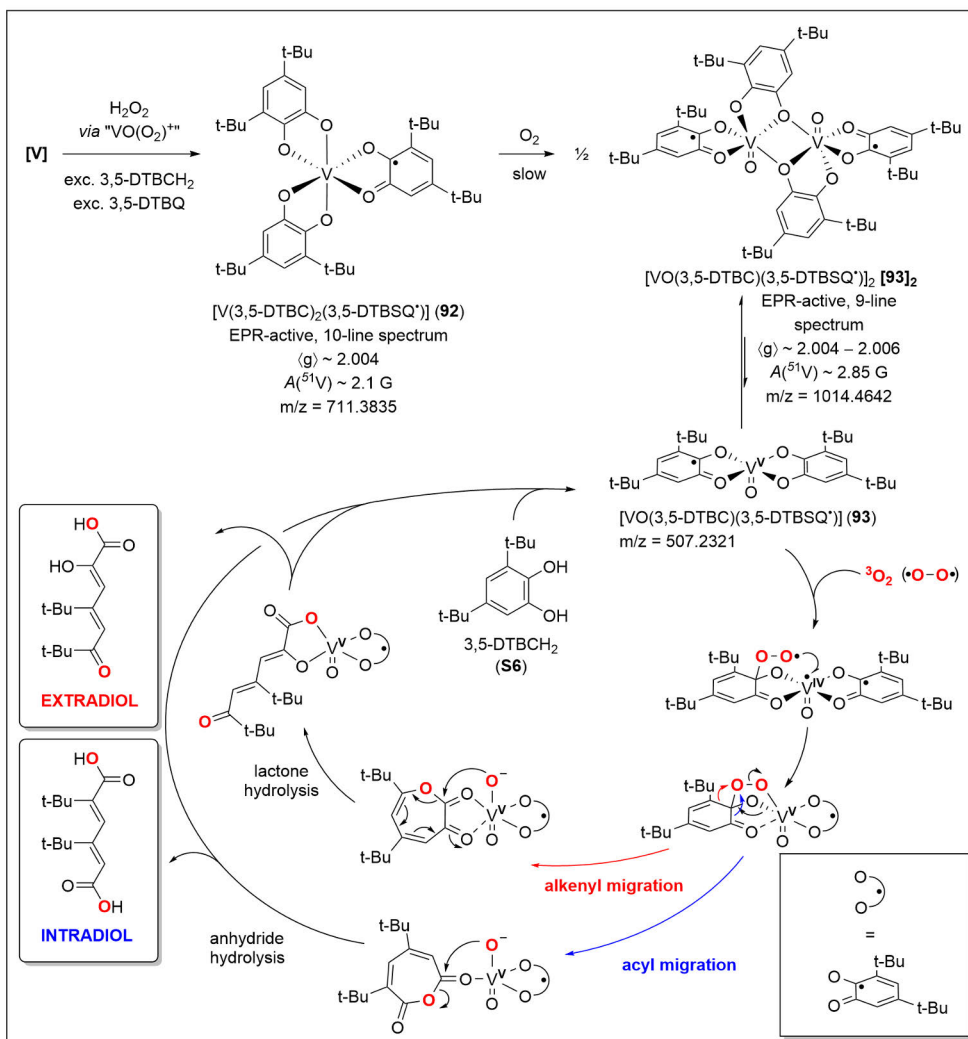


**Figure 8.** Oxygen pressure vs. time plots obtained in oxygen uptake reactions involving kinetically competent and incompetent vanadium(IV/V) catecholato complexes **93** – **95** en route to the catalytically active species in the catalytic dioxygenation of **S6** performed in 1,2-DCE at 40 °C under  $\text{O}_2$ . Reprinted with permission from “Yin, C. & Finke, R. G., ‘Vanadium-Based, Extended Catalytic Lifetime Catechol Dioxygenases: Evidence for a Common Catalyst’, *J. Am. Chem. Soc.*, 2005, *127*, 9003–9013”. Copyright 2005 American Chemical Society.

The results obtained by Finke and co-workers united the previously seemingly disparate literature on V catalyzed CDO mimetic chemistry: it was now understood that **S7** and **S8** fail to produce dioxygenase products because they are not autoxidized easily in comparison to **S6**, and thus unable to form the active catalysts. This was later further exemplified with another easily autoxidized substrate, 3,6-di-*tert*-butylcatechol (3,6-DTBCH<sub>2</sub>). Various vanadium precursors were shown to react similarly with 3,6-DTBCH<sub>2</sub> as they do with **S6**, generating analogous EPR-active



**Scheme 10.** General vanadium catalyzed **S6** dioxygenation mechanism as per the common catalyst hypothesis by Finke and co-workers. Adapted from <sup>212</sup>. The formation of the presumed active catalyst **93** from any  $\text{H}_2\text{O}_2$  sensitive initial V-precursor **[V]**, via **92** and **[93]<sub>2</sub>** as proposed by Pierpont and co-workers is also presented. For the individual reaction steps, see section 2.1.2.1.

vanadium-catecholato-semiquinonato species, as well as a characteristic CDO mimetic product distribution.<sup>217</sup> Moreover, strongly coordinating solvents including MeOH, THF and DMF lead to poor performance in **S6** dioxygenation due to competitive coordination at vanadium, hindering formation of the active catalyst(s). The formation of the active catalyst could additionally be inhibited by treatment of **[93]<sub>2</sub>** catalyzed **S6** oxygenation, mid-reaction, by excess multidentate ligand 1,4,7-triazacyclononane (TACN), dropping the yield of the major intradiol product **72** to

< 0.2% from ~ 40%, and promoting the yield of the autoxidation product **71** from ~21% to 41%.<sup>212</sup> The apparently high activity of **65**, even at 0.1 mol-% loadings, on the other hand, could now be rationalized by the extremely high activity of the presumed active catalyst **93** capable of at least 127000 turnovers. Based on all available information, a general V catalyzed CDO mimetic mechanism has been proposed by Finke and co-workers (Scheme 10), exemplified by the dioxygenation of **S6**, closely paralleling that proposed for iron (see Scheme 2 section 2.1.2.1).<sup>212</sup>

## 2.4.2 Vanadium Catechol Oxidase Mimetics

While most TYR and CO mimetic chemistry focus on Cu-based functional/structural models,<sup>43,218</sup> many other mono- and dinuclear complexes of metals including Co, Mn, Ni, Zn and Fe have been described to catalyze the oxidative dehydrogenation of catechols.<sup>42,219–221</sup> Similarly to V catalyzed CDO mimetic chemistry, the substrate of choice in V-CO mimetic chemistry is **S6**, followed by **S7** and **S8**.<sup>222–224</sup> There is also a single report by Maurya and co-workers demonstrating the oxidation of dopamine by oxidovanadium(V) complexes.<sup>225</sup> A typical V catalyzed CO mimetic study entails the monitoring of the substrate oxidation by *in-situ* UV-Vis absorption spectroscopy, as 1,2-benzoquinone, 4-TBQ (**96**, 4-TBQ = 4-*tert*-butyl-1,2-benzoquinone) and **71** have a characteristic strong absorption signal at *ca.* 400 nm (see Figure 13 section 5.2.1). The measurements are performed at variable [V]:[S] ([S] = substrate concentration) concentrations usually assuming the reactions follow Michaelis–Menten kinetics (see section 4.3.1 for more details).

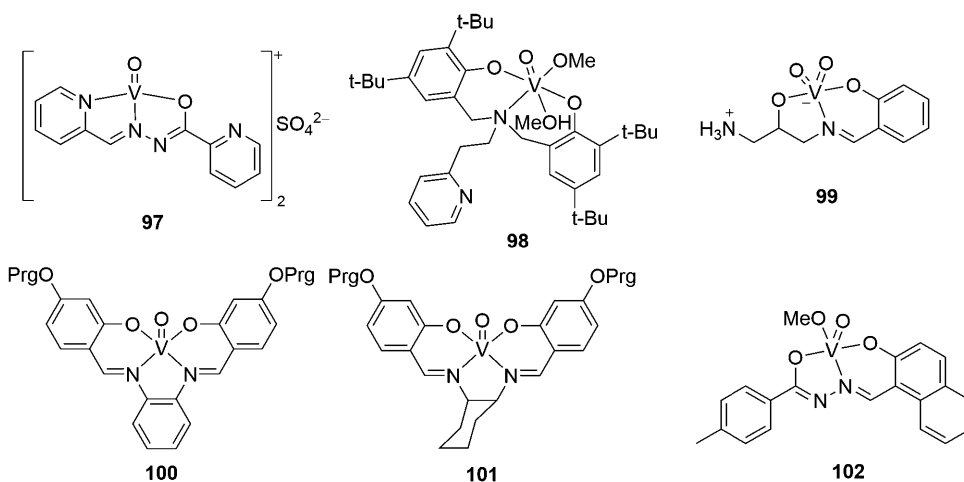
V catalyzed CO mimetic chemistry is a rather new area of research. While the very first reports of V-CO mimetic chemistry by Chakravorty and co-workers date back in the early 2000's,<sup>226–228</sup> the 2012 work of Ramadan, Hu, and co-workers, involving seven oxidovanadium(IV) picolyl hydrazone complexes such as **97** and V-POMs, respectively, were the first to address the kinetics involved in these reactions.<sup>229,230</sup> **97**, the most active complex from the study by Ramadan and co-workers, reportedly reaches an enzymatic turnover number ( $k_{cat}$ ) of 1439 h<sup>-1</sup> in the oxidative dehydrogenation of **S7** in DMF and the presence of one eqv. Et<sub>3</sub>N relative to **S7** (Table 4 entry 1).<sup>229</sup> Since these reports, several oxidovanadium(IV/V) complexes supported by multidentate aminobisphenolato (**98**), iminophenolato (**99**), salen (**100** and **101**) and aryl hydrazide (**102**) type ligands have been described (Table 4 entries 2 – 6).<sup>222–224,231</sup> From these reports, the dioxidovanadium(V) complex **99** is the most active V-CO mimic ever reported, reaching  $k_{cat} = 2063$  h<sup>-1</sup> in the oxidative dehydrogenation of **S6** in methanol (Table 4 entry 2).<sup>222</sup> Mechanistic investigations involving ESI-MS(+) and iodometric titration revealed that free ligand is released and H<sub>2</sub>O<sub>2</sub> is produced during the reaction.<sup>222</sup> Despite this **71** was reportedly obtained in 67% yield.<sup>222</sup> In the study by Maurya and co-workers **S6** failed



to react in the presence of **98** in methanol, supposedly due to steric factors, whereas **S8** was oxidized with a  $k_{\text{cat}} = 3.24 \text{ h}^{-1}$  (Table 4 entry 6).<sup>224</sup>

Despite the several reports of V-CO mimetic chemistry the mechanism of action is debatable as each report offers a drastically different proposal. However, a central feature in all proposals is an indirect participation of  $\text{O}_2$  as a proton acceptor as seen in the widely accepted Cu-mediated CO mechanism (Scheme 4 section 2.1.3.1).<sup>223,229,231</sup> Moreover, in the case of **100** and **101**, the proposed mechanism involves prior activation of **S6**, forming 3,5-DTBSQ<sup>•</sup>, akin to that seen in the CDO mechanism (Scheme 2 section 2.1.2.1).<sup>223</sup> However, this is suggested to occur *via* a ligand-assisted pathway that invokes a one-electron reduction of a ligand imine C=N bond, instead of a metal-centered one.<sup>223</sup>

**Table 4.** A near exhaustive list of vanadium pre-catalysts studied in contemporary CO mimetic research.



Entry	Substrate	Solvent	Cat.	$k_{\text{cat}} (\text{h}^{-1})$	Ref.
1	<b>S7</b>	DMF	<b>97</b>	1439	229
2	<b>S6</b>	MeOH	<b>99</b>	2063	222
3	<b>S6</b>	MeOH	<b>102</b>	1737	231
4	<b>S6</b>	MeCN	<b>100</b>	395.1	223
5	<b>S6</b>	MeCN	<b>101</b>	384.3	223
6	<b>S8</b>	MeOH	<b>98</b>	3.24	224

Prg = propargyl group ( $-\text{CH}_2\text{C}\equiv\text{CH}$ )

### 3 Aims of the Studies

The aims of this PhD thesis were to design, synthesize and characterize new Mo, W and V based complexes supported by multidentate amino(bis)phenolato and similar ligands, and explore their activity in catalytic alkene epoxidation and catechol oxidation chemistry mimicking the action of VHPOs and CO. The unexpected results from study II prompted studies pertaining to CDO mimetic chemistry as well.

The work can be summarized as follows:

- I. Investigation of oxidovanadium(V) complexes supported by L-proline derived amino acid phenolato ligands as biomimetic models of VHPOs. The complexes were found to catalytically oxidize catechols to *o*-quinones under aerobic conditions and were thus additionally investigated as functional CO mimics.
- II. Investigation of CO mimetic chemistry of Mo, W and V complexes based on a bioinspired, highly hydroxyl functionalized Schiff-base ligand. Although the aims of this study were set on CO mimetic chemistry, the CDO mimetic properties of the studied vanadium complex were serendipitously discovered.
- III. Upon discovery of the CDO mimetic properties of the vanadium complex in the study II, several vanadium complexes that display CO mimetic activity in our previous publications (incl. publication I) were (re)investigated as functional CDO mimics. Mechanistic investigations were able to draw connections to the work of Finke and co-workers.
- IV. Investigation of dioxidomolybdenum(VI) and -tungsten(VI) complexes supported by multidentate aminobisphenolato ligands in catalytic alkene epoxidation. Inspired by the work of Mösch-Zanetti and co-workers, the aim was to explore ligand centered H-bond donating effects and its possible effects on the alkene epoxidation activity of the complexes. Furthermore, an alkene epoxidation mechanism based on experimental results and support by DFT was proposed for these types of complexes for the first time.

## 4 Materials and Methods

### 4.1 General Instrumentation

All NMR spectra were recorded primarily on a Bruker AVANCE-III 500 MHz instrument equipped with a broad-band smart probe. Additionally, Bruker AVANCE-III 400 MHz and 600 MHz instruments equipped with a broad-band smart probe, and CryoProbe Prodigy triple resonance inverse probe, respectively, were used for  $^1\text{H}$  and  $^{13}\text{C}$  NMR measurements. Homo- and heteronuclear DQF-COSY, NOESY, HSQC and HMBC 2D NMR experiments were performed for selected compounds. All  $^1\text{H}$  and  $^{13}\text{C}$  NMR spectra are reported in parts per million (ppm) relative to tetramethylsilane (TMS,  $\delta$  0.00 ppm), but referenced to residual solvent signals, regardless whether TMS is present or not, according to published data.<sup>232</sup> The 0.00 ppm vanadium reference frequency was calculated from the TMS  $^1\text{H}$  frequency using the unified chemical shift scale by IUPAC ( $\Xi(^{51}\text{V}, \text{VOCl}_3) = 26.302948$ ) where  $\Xi$  = precise ratio of the resonance frequency of a nuclide, in %, vs. that of the primary reference, < 1 w-% TMS in  $\text{CDCl}_3$ .<sup>233</sup>

All infrared (IR) spectra were recorded on a Bruker VERTEX 70 FTIR spectrophotometer equipped with a RT-DLaTGS detector (RT-DLaTGS = room temperature deuterated lanthanum  $\alpha$ -alanine doped triglycine sulfate). For each individual measurement, 64 scans were performed using a Harrick VideoMVP™ Single Reflection ATR (Attenuated Total Reflection) Microsampler accessory. All IR spectra were recorded in transmittance mode. All ultraviolet-visible-near infrared (UV-Vis-NIR) spectra were recorded on an Agilent CARY60 UV-Vis spectrophotometer between 200–1000 nm using a  $\varnothing = 1$  cm quartz cuvette. Circular Dichroism (CD) spectra were recorded on a Chirascan qCD spectrophotometer. ESI-HRMS spectra were recorded on a Bruker Daltonics MicroTOF-Q II electrospray ionization time-of-flight (ESI TOF) mass spectrometer using both positive and negative polarizations. All MS results are given in cationic or anionic mass peaks as mass-to-charge (m/z) ratios.

Cyclic voltammetry (CV) electrochemical measurements were performed at RT for selected compounds using a standard three-electrode setup on an Autolab PGSTAT101 potentiostat. Platinum wire ( $\varnothing = 1$  mm) and glassy carbon working electrodes were polished and rinsed with quartz distilled water and technical EtOH

prior to use. The Ag/AgCl quasi-reference electrode was calibrated against the ferrocene/ferrocenium (Fc/Fc<sup>+</sup>) redox-couple ( $E_{1/2}(\text{Fc}/\text{Fc}^+) = 0.55 \text{ V}$ ).<sup>234</sup> A coiled Pt wire acted as the counter electrode. The electrochemical measurements were performed in dry electrochemical grade MeCN with 0.1 M *n*-Bu<sub>4</sub>NBF<sub>4</sub> as the supporting electrolyte. A variable scan-rate between 50 – 750 mV s<sup>-1</sup> was used. Electrochemical windows for measurements performed on Pt and glassy carbon working electrodes were –0.8 to +2.3 V and –2.5 to +2.5 V, respectively.

XRD data of all studied compounds were collected with four different diffractometer setups: i) Bruker-Nonius Kappa CCD equipped with APEXII detector using graphite-monochromated Mo-K $\alpha$  ( $\lambda = 0.71073 \text{ \AA}$ ) radiation, ii) Rigaku Oxford Diffraction SuperNova single-source diffractometer equipped with an Eos detector using multi-layer optics monochromated Mo-K $\alpha$  radiation, iii) Rigaku Oxford Diffraction SuperNova dual-source (Cu/Mo) equipped with an Atlas detector using multi-layer optics monochromated Cu-K $\alpha$  radiation ( $\lambda = 1.54184$ ) and iv) on a Bruker-AXS SMART APEX II equipped with a CCD detector using monochromatized Mo-K $\alpha$  radiation. For data obtained using Rigaku instruments collection and processing were carried by CrysAlisPro software.<sup>235</sup> Data collection and processing were done using COLLECT<sup>236</sup>, HKL Denzo<sup>237</sup> and Scalepack<sup>237</sup> whereas absorption correction was applied using SADABS<sup>238</sup>. Crystal structures were solved and refined within Olex<sup>239</sup> program package using SHELXS<sup>240</sup>/SHELXT<sup>241</sup> and SHELXL<sup>242</sup>, respectively.

## 4.2 Syntheses and Characterization

All syntheses and workups were performed under ambient conditions using as-received commercial technical/analytical grade solvents without extra purification or drying steps involved, unless explicitly stated. All reagents were either synthesized according to published procedures or obtained from commercial sources, in which case they were used as-received, unless stated otherwise. All new compounds were characterized by IR, <sup>1</sup>H and <sup>13</sup>C NMR spectroscopy, as well as ESI-MS for new complexes. Some compounds were additionally characterized by UV-Vis spectrophotometry, and all complexes except **V2** and **V3** were characterized by single crystal XRD.

### 4.2.1 Proligand Syntheses

For publication I the proligand **H<sub>2</sub>L1** was prepared in refluxing MeOH by Mannich condensation between 2,4-di-*tert*-butylphenol, formaldehyde, and L-proline according to the report of Safaei and Sheykhi, with some modifications.<sup>243</sup> Proligands **H<sub>2</sub>L2** – **H<sub>2</sub>L4** were synthesized analogously. The compounds were

purified by column chromatography on silica gel and isolated as slightly purple to pink colored solids. The proligand **H<sub>4</sub>L5** (publication II) was synthesized in refluxing EtOH using imine condensation between 3,5-di-*tert*-butylsalicylaldehyde and tris(hydroxymethyl)aminomethane, following the report by Mukherjee and Dey, with slight changes.<sup>219</sup> The pure compound was obtained as a brightly yellow microcrystalline solid after trituration in DCM. Proligands **H<sub>2</sub>L6–7** and **H<sub>2</sub>L9–10** (publication IV) were prepared in refluxing MeCN by S<sub>N</sub>2 substitution between bis(3,5-di-*tert*-butyl-2-hydroxybenzyl)amine<sup>244,245</sup> (**103**, see Figure 11). and appropriately *N*-substituted  $\alpha$ -bromo-*N*-(alkyl/aryl)acetamides<sup>246–249</sup>, synthesized and characterized separately. Proligand **H<sub>2</sub>L8** (publication IV) was synthesized *via* a modified *in-situ* Schotten-Baumann like reaction<sup>250</sup> involving acyl substitution between sodium bis(3,5-di-*tert*-butyl-2-hydroxybenzyl)glycinate<sup>251</sup> (**104**, see Figure 11) and benzylamine in the presence of thionyl chloride. **H<sub>2</sub>L6–9** were purified by column chromatography on silica gel followed by crystallization from MeOH, whereas crude **H<sub>2</sub>L10** crystallized from MeOH after the reaction. See publications I – IV for the most detailed descriptions of the syntheses and characterization.

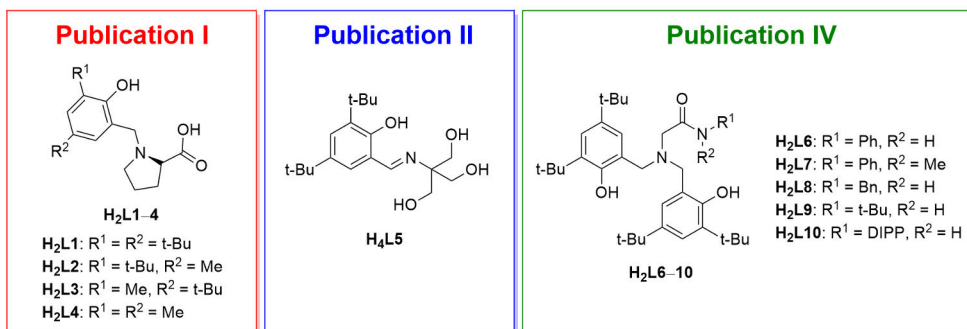


**Figure 9.** The structures of all proligands prepared and characterized in this PhD work. DIPP = 2,6-di-*iso*-propylphenyl.

## 4.2.2 Complex Syntheses

All complexes were synthesized *via* ligand exchange applying different conditions using various proligands (Figure 9) and equimolar amounts of vanadium precursors **65**, [VO(Oi-Pr)<sub>3</sub>] (*i*-Pr = *iso*-propyl) (**105**), or VOSO<sub>4</sub> · 5 H<sub>2</sub>O (**106**), molybdenum precursors **86** or Na<sub>2</sub>MoO<sub>4</sub> · 2 H<sub>2</sub>O (**107**), or tungsten precursors [W(eg)<sub>3</sub>] (**108**) or Na<sub>2</sub>WO<sub>4</sub> · 2 H<sub>2</sub>O (**109**). Metal precursors **65**, **105**, **106**, **107** and **109** were obtained from commercial sources, whereas **86**<sup>252</sup> and **108**<sup>253</sup> were synthesized according to known procedures.

For publication I the complexes **V1** – **V4** were obtained by gently warming **H<sub>2</sub>L1** – **H<sub>2</sub>L4** with one equivalent of **65**, or **105**, or **106** in MeOH. Two equivalents of Et<sub>3</sub>N

may additionally be added if **106** was used as the vanadium precursor. **V1** – **V4** were obtained as dark red-brown needle like crystals from MeOH at  $-26\text{ }^{\circ}\text{C}$  over a period of several days. They were isolated by Büchner filtration, washed with ice-cold *n*-hexane and air-dried. **Mo1** (publication II) was obtained as yellow crystals by reacting **H4L5** with one equivalent of **86** in MeOH at RT for three days. Additionally, **Mo1** can be synthesized using **107** and a small amount of glacial acetic acid. **W1** (publication II) was obtained as pale-yellow microcrystals in a reaction between equimolar amounts of **H4L5** and **108** in MeOH:CHCl<sub>3</sub> (1:1 V:V) at RT. Additionally, **109** can be used to synthesize **W1**, in analogy to **Mo1**. Complexes **Mo2** – **Mo6** and **W2** – **W5** (publication IV) are very easily obtained in MeOH as yellow and pale-yellow crystals by reaction between equimolar amounts of respective ligand precursor **H<sub>2</sub>L6–10** and **86** or **107**, and **108** or **109**, respectively. The complexes were isolated by Büchner filtration, washed with small amounts of ice-cold MeOH and air-dried. Additionally, previously reported vanadium and molybdenum complexes **V6** – **V9**<sup>254–259</sup> and **Mo7** – **11**<sup>260–263</sup> were synthesized and characterized according to published methods for use in catalytic catechol oxidation (publication III) as well as in alkene epoxidation (publication IV), respectively (see Tables 5 and 7 as well as Scheme 13).

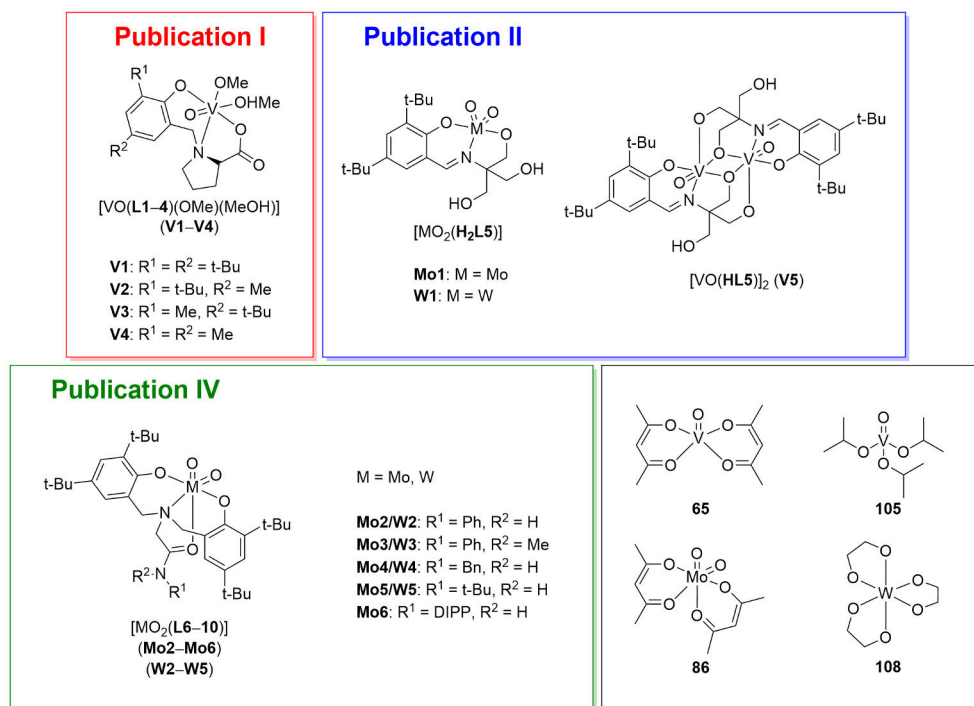


**Figure 10.** The structures of all new complexes designed, prepared, and characterized in this PhD work. Also presented are the structures of the various Mo, W and V precursor complexes used in synthetic work. DIPP = 2,6-di-*iso*-propylphenyl.

## 4.3 Catalysis

### 4.3.1 Catechol Oxidase Mimetics

Complexes **V1** – **V5**, **Mo1** and **W1** (publications I and II) were examined in CO mimetic chemistry with substrates **S6** – **S8**. The reactions were performed at RT in MeOH, MeCN and CHCl<sub>3</sub> and monitored by *in-situ* UV-Vis spectroscopy, following the formation of the respective *o*-quinones that have a characteristic absorption at *ca.* 400 nm (see Figure 13).<sup>264,265</sup> Reaction kinetics were assessed using the method of initial rates. For this purpose, in a typical catalytic reaction, solutions containing the pre-catalysts and **S6** – **S8** were combined in a quartz cuvette, with [V]:[S] varying between a factor of 1:10 to 1:17500. The initial reaction rates at every [V]:[S] molar ratio were determined from absorbance *vs.* time plots directly using the on-board Cary WinUV Kinetics software, and then fitted with Origin software to the Michaelis–Menten equation (6) using non-linear regression analysis. From the data analysis was obtained the maximum reaction rates  $V_{max}$  and the Michaelis constants (substrate concentration at  $\frac{1}{2} V_{max}$ ). The turnover frequency was calculated using equation (7), where  $[E_T]$  is the concentration of the pre-catalysts *i.e.*, number of catalyst active sites.

$$v = \frac{V_{max} \times [S]}{K_M + [S]} \quad (6)$$

$$k_{cat} = \frac{V_{max}}{[E_T]} \quad (7)$$

### 4.3.2 Catechol Dioxygenase Mimetics

Complexes **V1**, **V5**, **V6** – **V9** (publication III) were (re)examined as functional CDO mimics in the oxidation of **S6**. The reactions were performed with a slightly modified Finke protocol.<sup>211</sup> In a typical reaction, several mg of the complexes were reacted with *ca.* 1000 mg **S6** in 1,2-DCE under an O<sub>2</sub> atmosphere at 65 °C for 21 – 53 h with the [V]:[S6] molar ratio varying between 1:300 to 1:881. The progression of the reactions was monitored by thin-layer chromatography (TLC). Upon completion, all products were isolated by column chromatography on silica gel [3 cm × 45 cm (diameter × height) using *ca.* 250 mL Merck silica gel 60 (0.040–0.063 mm pore size)] and DCM, and identified by <sup>1</sup>H and <sup>13</sup>C NMR spectroscopy according to published data.<sup>211</sup> Conversion was estimated based on TLC, and product yields were determined directly by weighing or estimated by <sup>1</sup>H NMR spectroscopy (for mixtures). Control reactions were performed under a 100% O<sub>2</sub> or N<sub>2</sub> atmosphere with and without several additives such as **V5**, Et<sub>3</sub>N, H<sub>2</sub>O<sub>2</sub>. The reaction product distribution was additionally qualitatively assessed with GC using

FID and MS detectors. GC-FID is equipped with HP-1 column (30 m  $\times$  320  $\mu\text{m}$   $\times$  0.25  $\mu\text{m}$ ), and He as the carrier gas, using following temperature program:  $T_{\text{inlet}} = 250\text{ }^{\circ}\text{C}$ , oven  $T_{\text{initial}} = 80\text{ }^{\circ}\text{C}$  (8 min), rate  $10\text{ }^{\circ}\text{C min}^{-1}$ ,  $T_{\text{final}} = 300\text{ }^{\circ}\text{C}$ , hold 5 min. GC-MS is equipped with Triple-Axis Detector, HP-5MS column (30 m  $\times$  250  $\mu\text{m}$   $\times$  0.25  $\mu\text{m}$ ), and He as the carrier gas, using temperature program:  $T_{\text{inlet}} = 250\text{ }^{\circ}\text{C}$ , oven  $T_{\text{initial}} = 80\text{ }^{\circ}\text{C}$  (4 min), rate  $25\text{ }^{\circ}\text{C min}^{-1}$ ,  $T_{\text{final}} = 300\text{ }^{\circ}\text{C}$ , hold 10 min.

Vanadium speciation during the CDO mimetic reactions was monitored by EPR and  $^{51}\text{V}$  NMR spectroscopy, as well as by ESI-HRMS(-). The reactions were performed at RT under ambient conditions in  $\text{CDCl}_3$  ( $^{51}\text{V}$  NMR) and toluene (EPR) using a  $[\text{V}]:[\text{S6}]$  molar ratio of  $\sim 1:100$ .  $^{51}\text{V}$  NMR measurements were done on the Bruker AVANCE III instrument from +4000 ppm to -4000 ppm. EPR was measured on a Freiberg Instruments Miniscope X-band EPR spectrophotometer. Full scan EPR spectra were recorded from 25 to 650 mT (250 to 6500 G), and center-field scans were performed from 334 to 339.5 mT (3340 to 3395 G) with a sweep time of 60 s, 0.100 mT signal modulation and 100% microwave power, with a 0 dB attenuation. The  $^{51}\text{V}$  NMR samples in  $\text{CDCl}_3$  were diluted in MS grade MeCN for ESI-HRMS measurements.

### 4.3.3 Alkene Epoxidation

Complexes **Mo2** – **Mo5** and **W2** – **W5** were investigated as pre-catalysts in the epoxidation of **S1** – **S5** (publication IV). For mechanistic and comparison purposes, known dioxidomolybdenum(VI) complexes **Mo7** – **Mo11** were additionally synthesized, characterized and (re)examined in epoxidation. Preliminary epoxidation experiments were carried out by  $^1\text{H}$  NMR spectroscopy using the benchmark substrate **S1**. In a typical run, 0.500 mL  $\text{CDCl}_3$  stock solution of **S1** ( $c = 0.153\text{ M}$ ) and 0.500 mL  $\text{CHCl}_3$  stock solutions of the respective complexes at appropriate catalyst loading ( $c = 1.53 \times 10^{-4}$  to  $1.53 \times 10^{-6}\text{ M}$ ) were combined in sealable test tubes, thermostated to  $50\text{ }^{\circ}\text{C}$  and subsequently treated with appropriate amount of TBHPaq (19.2  $\mu\text{L}$  *ca.* 8.0 M aqueous TBHP). For 1 mol-% experiments several mg of the respective complexes were directly weighed in the reaction medium containing **S1**. Conversion, yield, and selectivity were determined by  $^1\text{H}$  NMR spectroscopy after reactions were run for a specific time (*e.g.*, for 24 h).

Kinetics reactions were performed analogously in  $\text{CDCl}_3:\text{CHCl}_3$  and monitored by *in-situ*  $^1\text{H}$  NMR on the Bruker AVANCE III 500 MHz instrument. In a typical run,  $\text{CHCl}_3$  stock solutions of the respective complexes at appropriate catalyst loading and **S1** in  $\text{CDCl}_3$  were combined in  $\varnothing = 5\text{ mm}$  NMR tubes. After the reaction mixtures were thermostatted at  $50 \pm 0.1\text{ }^{\circ}\text{C}$  they were treated with appropriate amount of TBHPaq, immediately zeroed and subsequently monitored at specific



intervals for several hours (see publication IV for details). Conversion, yield, and selectivity at given intervals were determined using 1,2-DCE as an internal standard.

For reactions involving **S2** – **S5** and **W2** – **W5**, a Heidolph Parallel Synthesizer was used. In a typical experiment, 2 – 3 mg (for 1 mol-% experiments) complex, appropriate amount of **S2** – **S5**, and mesitylene internal standard was suspended in 0.5 mL CHCl<sub>3</sub> in 5 mL glass reactor vessels equipped with a magnetic stir-bar. The reactions were thermostatted at 50 °C, treated with TBHPdec (*ca.* 5.5 M TBHP in *n*-decane) or H<sub>2</sub>O<sub>2</sub> to commence the reactions, then zeroed. Conversion, yield, and selectivity for the epoxides were determined by GC-MS on an Agilent Technologies 7890 GC system by periodically withdrawing aliquots for GC-MS analysis. Prior to analysis, the withdrawn samples were treated with MnO<sub>2</sub> to quench any remaining peroxides.

# 5 Results and Discussion

## 5.1 Syntheses and Characterization

### 5.1.1 Proligands

In publication I, the original synthesis for **H<sub>2</sub>L1** as reported by Safaei and Sheykhi involves mixing of 2,4-di-*tert*-butylphenol, aqueous formaldehyde and L-proline with a molar ratio of 1:4:2 in neat conditions under reflux temperatures for two days.<sup>243</sup> In our hands, this method led to unsatisfactory results. Instead, a 16-hour reflux in MeOH using equimolar (1:1:1) amounts of the reagents was necessary for successful synthesis. Purification of the target compound *via* column chromatography was needed, as crystallization was difficult. If crystals were obtained, it was found that unreacted 2,4-di-*tert*-butylphenol co-crystallizes with **H<sub>2</sub>L1**. The NMR-pure target compound was obtained, rather peculiarly, as a light purple solid after column chromatography on silica gel (DCM:MeOH eluent) with a very good 80% yield. **H<sub>2</sub>L2** – **H<sub>2</sub>L4**, similarly light purple to pink colored solids, were prepared and purified analogously, and obtained with a yield of 60 – 94%. Being chiral, the compounds displayed particularly complicated <sup>1</sup>H NMR spectra in the pyrrolidine moiety. Thus, adequate characterization required DQF-COSY, NOESY, HMBC and HSQC 2D NMR methods.

The proligand **H<sub>4</sub>L5** (publication II) was successfully synthesized with an excellent 91% yield following the report by Mukherjee and Dey,<sup>219</sup> with slight modification in the purification step. However, the <sup>1</sup>H NMR spectrum of **H<sub>4</sub>L5** obtained in DMSO-d<sub>6</sub> differed significantly from that reported.<sup>219</sup> Nevertheless, the <sup>1</sup>H NMR spectrum obtained by us is in very good agreement with the expected structure of **H<sub>4</sub>L5**.

Interesting features in the <sup>1</sup>H NMR spectrum of **H<sub>4</sub>L5** is the signal of the phenolic proton, found at 14.90 ppm in DMSO-d<sub>6</sub>, which is significantly downfield for what would generally be expected for phenols or salicylaldehyde derivatives, at *ca.* 10 ppm or below. The significant downfield shift can be ascribed to moderate deshielding effect caused by intramolecular H-bonding of the phenol proton to the imine nitrogen atom, similar effects having been described for other Schiff-base compounds.<sup>266</sup> It is ultimately caused by enolimine-ketoenamine tautomerization

frequently observed in Schiff-bases.<sup>267</sup> Attempts to synthesize the aminephenol **110** (Figure 11) *via* NaBH<sub>4</sub> reductive amination of **H<sub>4</sub>L5** failed. However, traces of **110** were obtained by Mannich condensation between 2,4-di-*tert*-butylphenol, formaldehyde and tris(hydroxymethyl)aminomethane. Aminebisphenol **111** and benzoxazine **112** were obtained as unwanted by-products (Figure 11).

Recently, a straightforward one-pot Schotten–Baumann like reaction of wide utility, involving the synthesis of secondary and tertiary amides *via* SOCl<sub>2</sub> mediated coupling of carboxylic acids and amines has been described by Leggio and co-workers.<sup>250</sup> The protocol was tested in the synthesis of **H<sub>2</sub>L6** – **H<sub>2</sub>L10** (publication IV). SOCl<sub>2</sub> activated coupling of **104** with weakly nucleophilic amines *i.e.*, aniline (for **H<sub>2</sub>L6**), *N*-methylaniline (**H<sub>2</sub>L7**) and *tert*-butylamine (**H<sub>2</sub>L9**) failed and only produced the corresponding ammonium carboxylate salts based on the lack of CONH or CONCH<sub>3</sub> HMBC correlations in the expected peptide moiety (see below). Following unsatisfactory results with aniline, the coupling of **104** with 2,6-di-*iso*-propylaniline (for **H<sub>2</sub>L10**) was not attempted. However, **H<sub>2</sub>L8** was successfully obtained in a fair 28% yield *via* SOCl<sub>2</sub> mediated coupling of **104** with benzylamine. However, **H<sub>2</sub>L8** was accompanied by the formation of a major side product **113** through intramolecular acyl substitution (Figure 11).

The synthesis of the proligands **H<sub>2</sub>L6–7** and **H<sub>2</sub>L9–10**, which were obtained in 25 – 67% yield, was accomplished *via* base-assisted S<sub>N</sub>2 substitution between **103** and 2-bromo-*N*-phenylacetamide **114** (for **H<sub>2</sub>L6**), 2-bromo-*N*-methyl-*N*-phenylacetamide **115** (**H<sub>2</sub>L7**), 2-bromo-*N*-(*tert*-butyl)acetamide **116** (**H<sub>2</sub>L9**), or 2-bromo-*N*-(2,6-di-*iso*-propylphenyl)acetamide **117** (**H<sub>2</sub>L10**). To distinguish successful coupling from the salt formation (see above), the peptide functional group was identified using HMBC (<sup>1</sup>H—<sup>13</sup>C connection CONH for **H<sub>2</sub>L6** and **H<sub>2</sub>L8–10**, CONCH<sub>3</sub> for **H<sub>2</sub>L7**). The compounds were isolated by column chromatography on silica gel and re-crystallized from hot MeOH prior to complexations. The proligand **H<sub>2</sub>L10** directly crystallized from the reaction mixture.

### 5.1.2 Complexes

Complexes **V1** – **V4** of the type [VO( $\kappa^3$ -**L1–4**)(OMe)(MeOH)] were obtained in 30 – 80% yield by performing the complexations in 60 °C methanol over a period of *ca.* two hours (Publication I). The reactions with **H<sub>2</sub>L1–4** were repeated using all available vanadium starting materials *i.e.*, **65**, or **105**, or **106**, and all were found to afford the respective complex **V1** – **V4**, regardless of used V-precursor. Reactions involving **105** were typically the highest yielding, and procedurally the simplest. If **106** was used, an added base (Et<sub>3</sub>N) was not necessary, but improved yields slightly. Lastly, reactions involving **65** were often incomplete in two hours, leading to lowered yields as well as co-crystallization of unreacted **65** as teal-colored crystals.

Thus, given the sensitivity of **105** towards atmospheric moisture and synthetic problems associated with the use of **65**, the **106**/ $\text{Et}_3\text{N}$  route is considered the most optimal synthetic procedure. **V1** – **V4** dissolve well in most laboratory solvents, and are benchtop stable in their solid, crystalline state over a period of at least four years. However, they are rapidly destroyed by water and oxidants such as  $\text{H}_2\text{O}_2$  or TBHP when dissolved.

The solution-state structures of **V1** – **V4** are complicated as determined by  $^1\text{H}$  NMR spectroscopy, similarly to the case of the proligands. Moreover,  $^{51}\text{V}$  NMR spectroscopy revealed several signals the number and intensity of which are highly dependent on the used NMR solvent, highlighting the rather dynamic behavior of **V1** – **V4** in solution, a phenomenon well known for related V complexes as well.<sup>162,224,225,268–270</sup> For example, in  $\text{CDCl}_3$  **V1** has three  $^{51}\text{V}$  NMR signals at  $\delta$  –499, –502 and –533 ppm with a ratio of *ca.* 1:0.8:0.6, respectively. In  $\text{DMSO-d}_6$  **V1** has at least five different broad and severely overlapped  $^{51}\text{V}$  NMR signals in the range of  $\delta$  –459 to –550 ppm. The chemical shift in  $^{51}\text{V}$  NMR in various V-containing compounds is known to be very sensitive to even slight electronic changes at the V center, and can cover shift ranges from +2600 to –2100 ppm vs.  $[\text{VOCl}_3]$ .<sup>206,271–273</sup>

In **V1** – **V4** the numerous signals most probably arise from structural isomers: because the ligands **L1**–**4** are tridentate only, the oxido, methoxido and methanol ligands may coordinate in three different axial and equatorial positions, leading to distinct isomers. Martins and others have shown in similar aminobisphenolato supported oxidoalkoxidovanadium(V) complexes that depending on the exact ligand *trans* relative to the ligand amino group, stable isomers with slightly different  $^{51}\text{V}$  NMR shifts arise.<sup>268,270</sup> In addition, Maurya and co-workers have demonstrated similar effects in related complexes such as **98** (see Table 4 section 2.4.2).<sup>224,225</sup> Vanadium complexes may often also adopt five-coordinate geometries, so it may be reasonably expected that the different isomers in **V1** – **V4** may interconvert *via* removal of the MeOH ligand. This is supported by the fact that in  $\text{MeOH-d}_4$  **V1** has one major  $^{51}\text{V}$  NMR signal at  $\delta$  –466 ppm, and two minor signals at –493 and –554 ppm with 1:0.04:0.02 relative population, respectively. The very high excess of  $\text{MeOH-d}_4$  potentially “locks” **V1** into its kinetically most stable form, presumably of type  $[\text{VO}(\text{L1})(\text{OMe})(\text{MeOH-d}_4)]$ , hindering interconversion between the other isomers.

In the publication II, **Mo1** was easily obtained in 73% yield by mixing equimolar amounts of **H4L5** and **86** at RT for 72 hours. Slightly lower yields (60%) are reached if **107** is used. Yellow crystals suitable for XRD were obtained upon storage of the reaction mixture at –26 °C for a week. **W1** was similarly obtained in 47% yield in reaction between equimolar amounts of **H4L5** and **108** or **109**, although crystals could be obtained upon storage for two weeks at +5 °C. Use of **108** as the W

precursor leads to very poor 9% yield of **W1**. If Mo/W salts **107** or **109** were used in the syntheses, a small amount of glacial acetic acid was added to prevent formation of POMs.<sup>274</sup> Compounds that have exchangeable hydrogen atoms typically show extremely slow  $^1\text{H}/^2\text{H}$  exchange rates in DMSO- $d_6$ .<sup>275</sup> Thus, the coordination mode of **H<sub>n</sub>L5** could be unequivocally determined in **Mo1** and **W1** by  $^1\text{H}$  NMR spectroscopy in DMSO- $d_6$ . Both complexes are coordinated in a tridentate dianionic manner, having structures of the type  $[\text{MO}_2(\kappa^3\text{-H}_2\text{L5})]$ , where M = Mo (**Mo1**) and W (**W1**). However, **Mo1** fills the sixth coordination site by forming an infinite polymer, whereas **W2** forms an aqua complex (see Figure 12 section 5.1.3). **Mo1** and **W1** are sparingly soluble in alcohols and chlorinated solvents, but well soluble in MeCN or DMSO. Additionally, they are benchtop stable in solid form and when dissolved.

The compound **V5** (publication II) is obtained in 89% yield by mixing equimolar amounts of **H<sub>4</sub>L5** and **65** at RT in MeOH. An amber-colored non-crystalline solid is quickly precipitated upon introduction of the reagents. Re-crystallization from hot MeCN affords dark XRD quality single crystals of **V5**.  $^1\text{H}$  NMR measurements for both the non-crystalline solid and the crystals, performed in acetone- $d_6$  which displays similar diminished  $^1\text{H}/^2\text{H}$  exchange rates as DMSO, reveals that the ligand is coordinated in a tetradentate trianionic fashion, giving a structure of the type  $[\text{VO}(\kappa^4\text{-HL5})]$ , in stark contrast to **Mo1** and **W1**.  $^{51}\text{V}$  NMR spectroscopy shows a single signal at  $\delta$   $-562$  ppm, underlining the high coordinative rigidity of **V5** in solution. Originally assumed to potentially adopt a stable five-coordinate geometry, ESI-HRMS measurements instead point towards a dinuclear structure of the type  $[\text{VO}(\kappa^4\text{-HL5})]_2$ , which was confirmed by XRD. **V5** dissolves very well in acetone, and sparingly in MeOH, MeCN,  $\text{CHCl}_3$  and DMSO. It is benchtop stable in solid state as well as in solution.

**Mo2** – **Mo6** and **W2** – **W5** (publication IV) were synthesized *via* a technique whereby small ( $< 0.2$  mmol) amounts of **H<sub>2</sub>L6–10** were reacted with equimolar amounts of **86** or **107**, and a small amount of glacial acetic acid, in *ca.* 3 – 5 mL of MeOH in air-tight screw-capped scintillation vials. The static, non-stirred reaction mixtures were maintained at 50 or 60 °C in a thermal oven overnight. An interesting and very convenient, repeatable feature in the syntheses is the facile crystallization of the complexes out of solution, affording XRD quality single crystals quickly after the introduction of the reagents. For example, XRD quality single crystals of **Mo4** were obtained in 30 minutes by maintaining a solution of 20 mg **H<sub>2</sub>L9** and 12 mg **86** in *ca.* 3 mL MeOH in a 50 °C thermal oven. The technique was repeatable, affording **Mo1** – **Mo6** and **W2** – **W5** in 26 – 89% and 33 – 47% yield, respectively. **Mo2** – **Mo5** are insoluble in alcohols, sparingly soluble in  $\text{CHCl}_3$  and MeCN, and well soluble in DMSO. **Mo3**, featuring a tertiary amide pendant arm, displays highest solubility across all Mo complexes, being readily soluble in most solvents except

alcohols. **Mo6**, on the other hand, is practically insoluble in any solvent other than DMSO, in which it is only sparingly soluble when heated; single crystals suitable for XRD deposited during  $^{13}\text{C}$  NMR measurements in DMSO- $d_6$ . **W2** – **W5** share similar solubility characteristics with **Mo2** – **Mo5**, although generally they are slightly less soluble than their respective Mo analogs.<sup>276</sup> **Mo2** – **Mo6** and **W2** – **W5** show very good stability in the solid state as well as in solution, with no visible reactions occurring with oxidants such as TBHP. However, **W1** shows signs of slight deterioration over time when dissolved in DMSO- $d_6$ .

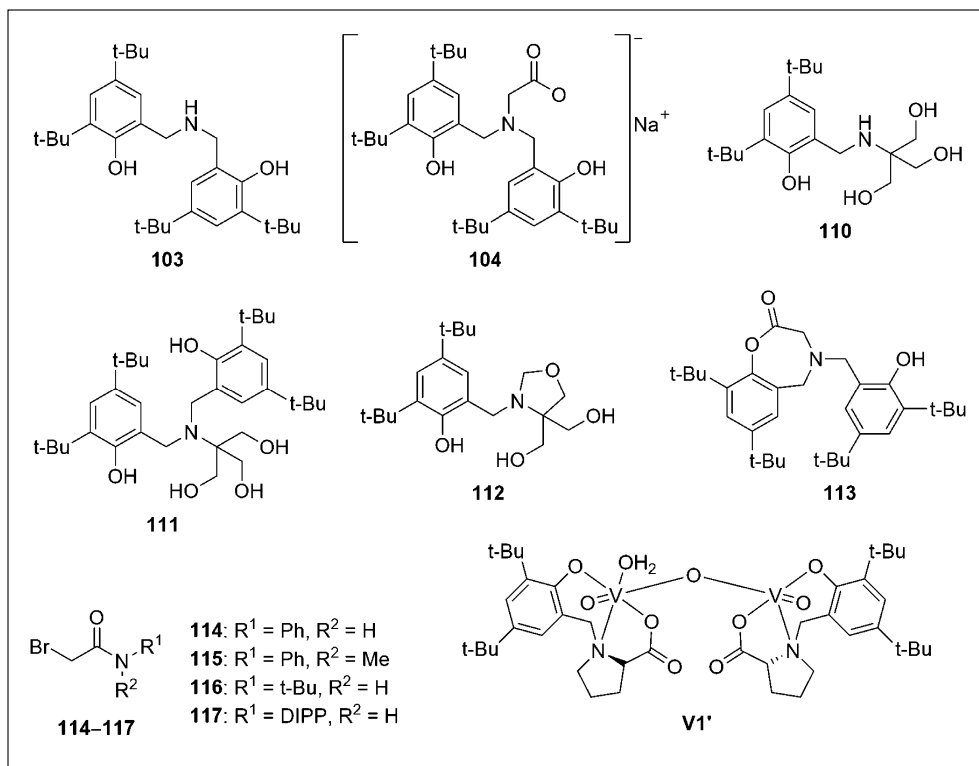


**Figure 11.** Notable compounds prepared throughout publications I–IV. DIPP = 2,6-di-*iso*-propylphenyl.

### 5.1.3 Description of Crystal and Molecular Structures

Single crystals suitable for XRD were obtained by re-crystallization of **V1** and **V4** from MeOH (publication I). **V1** and **V4** crystallize in monoclinic and orthorhombic crystal systems and in the space groups  $C2$  and  $P2_12_12$ , respectively. Owing to the chiral carbon atom in the pyrrolidine moiety, both compounds lack an inversion center. The asymmetric unit of **V1** contains two chemically identical but

crystallographically distinct molecules, whereas **V4** only contains one. Structurally **V1** and **V4** are very similar, adopting a distorted octahedral geometry. The equatorial plane of the complexes are occupied by **L1** and **L4** which coordinate to the oxidovanadium(V) centers in a meridional ONO' fashion, *via* a phenolato, amino and carboxylato groups. The phenolato and carboxylato donors are *trans* relative to each other. The fourth equatorial position *trans* to the amino ligand is occupied by the methoxido ligand. The octahedra are completed by the axial oxido and methanol ligands. See Figure 12 structure A for the crystal structure of **V1**.

Additionally, the dinuclear **V1'** (publication I) was obtained by re-crystallization of **V1** from wet MeCN (Figure 12 B). **V1'** crystallizes in a monoclinic space group  $P2_1$  and contains two crystallographically different molecules in the asymmetric unit. The molecular structure **V1'** consists of two different V-centered units bridged by an equatorial  $\mu$ -oxido ligand. The first unit adopts an approximate square pyramidal coordination sphere, in which the equatorial plane is occupied by **L1** as well as the bridging oxido ligand. The V=O oxido ligand occupies the fifth and only axial position. In contrast, the second unit adopts a distorted octahedral coordination sphere, being otherwise similar to the first unit, but coordinating an aqua ligand in the *trans* position relative to the V=O oxido group in the axial plane.

Both **Mo1** and **W1** (publication II) directly crystallized from their reaction mixtures as brilliant and pale, yellow-colored needle like crystals, respectively. Both complexes crystallize in the monoclinic  $P2_1/c$  space group and have a structurally very similar asymmetric unit (Figure 12 C). The tridentate dianionic **H<sub>2</sub>L5** occupies the equatorial plane in an ONO' fashion, coordinating *via* a phenolato, aldimino and alcoholato donors, with one of the M=O oxido ligands fulfilling the equatorial plane. The two neutral alcohol pendant arms are left "dangling", and do not coordinate. The axial positions are occupied by the oxido ligands (for both **Mo1** and **W1**), and an aqua ligand (for **W1** only). In **Mo1** an adjacent complex unit fills the sixth coordination site, and thus the overall crystal structure is polymeric (Figure 12 E), although the complex forms discrete monomeric units upon dissolution in *e.g.*, DMSO-*d*<sub>6</sub>. The structures and bonding parameters of **Mo1** and **W1** are well in line with those reported for similar Mo and W complexes<sup>180,277,278</sup>

XRD confirms the results of the ESI-MS investigations that hinted towards the dinuclear nature of **V5**. The crystal structure of **V5** is highly symmetric, consisting of two V=O centers that are coordinated by trianionic tetradentate **HL5** ligands, in stark contrast to **Mo1** and **W1** (Figure 12 D). The ligand coordinates in a meridional ONO' manner to a single V=O center *via* a phenolato, aldimino and alcoholato donors, leading to a structure that is in principle identical to those of **Mo1** and **W1**. However, in **V5** an additional bridging alcoholato ligand fulfills the sixth coordination site of the *other* V=O unit in the complex, leading to a highly rigid and centrosymmetric system, with both V centers having a distorted octahedral

configuration. The crystal system of **V5** is monoclinic with a space group  $P2_1/c$ . The structure of **V5** is very similar to some reported dinuclear vanadium complexes supported by analogous Schiff-base ligands.<sup>279–281</sup>

For the aminobisphenolato dioxidomolybdenum(VI) and -tungsten(VI) complexes **Mo2** – **Mo6** and **W2** – **W5** single crystals suitable for XRD are easily obtained in MeOH thanks to their limited solubility. The complexes crystallize either in the monoclinic (**Mo3** – **Mo6** and **W3** – **W5**) or triclinic (**Mo2** and **W2**) crystal system in  $P\bar{1}$ ,  $P2_1/n$  or  $P2_1/c$  space groups. From the complexes, **Mo2**, **Mo5**, **W2**, **W3** and **W4** crystallize as MeOH solvates, whereas **Mo6** crystallizes as a DMSO-d<sub>6</sub> solvate (Figure 12 F). The ligands coordinate to the MO<sub>2</sub> centers *via* two phenolato, neutral amino and carbonyl groups, yielding a dianionic tetradentate ONO'O'' type mode of coordination. The phenolato groups are *trans*, oxido groups *cis* and amino and carbonyl groups *cis* relative to one another, in an overall distorted octahedral geometry. The crystal structures of the complexes reveal extensive intermolecular H-bonding networking from the amide NH moieties to solvent molecules and adjacent complex units, except for **Mo3** and **W3**. The H-bond interactions may in part explain the low solubility of the complexes featuring secondary amides, as well as the collective tendency of the complexes to very easily crystallize. The molecular structures of **Mo2** – **Mo6** and **W2** – **W5** are very similar to other aminobisphenolato MoO<sub>2</sub>/WO<sub>2</sub> complexes prepared by our group and our collaborators, most notably **Mo7** – **Mo9** used as reference complexes in alkene epoxidation (see Scheme 13 section 5.3)<sup>164,165,260,261</sup>



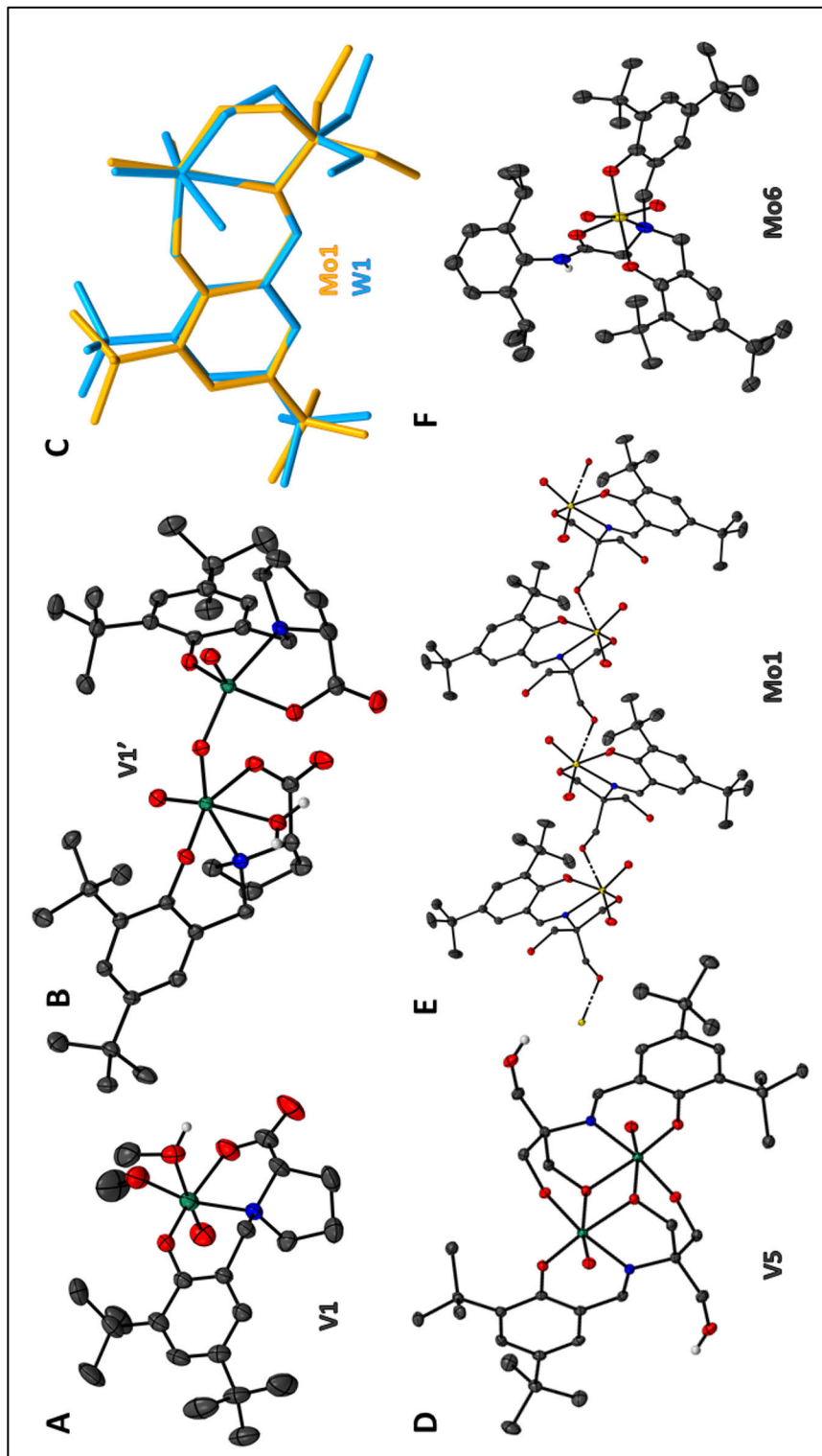
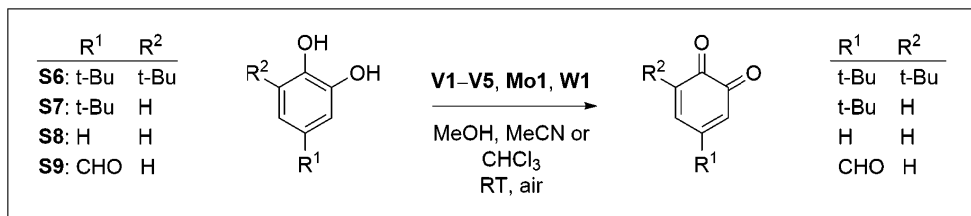


**Figure 12.** The XRD crystal structures of **V1** (A), **V1'** (B), **V5** (D), **Mo1** (E) and **Mo6** (F). Overlay of **Mo1** and **W1** shown in C. Key: carbon (black), oxygen (red), nitrogen (blue), Mo (yellow), W (sky blue), V (green). Most H atoms and solvents are omitted for clarity.

## 5.2 Catalysis – Catechol Oxidation

### 5.2.1 Catechol Oxidase Mimetics



**Scheme 11.** Different catechol substrates used in the Mo, W and V catalyzed CO mimetic investigations performed under ambient conditions.

Inspired by the reports by Maurya and co-workers showing the catechol oxidase mimetic properties of **98**, structurally related **V1** – **V4** were assessed in the oxidation of selected catechol substrates **S6** – **S8**.<sup>224</sup> Moreover, Mukherjee and Dey have demonstrated the rather high catecholase activity of a dicobalt(III) complex [Co(**H<sub>2</sub>L5**)(OAc)]<sub>2</sub> (**118**)<sup>219</sup> (see Table 5), warranting CO mimetic investigations for the structurally closely similar **V5**, but for **Mo1** and **W1** as well.

Preliminary screenings for CO mimetic properties involving **V1** – **V4** (publication I), **V5**, **Mo1** and **W1** (publication II) were performed by reacting **S6** – **S8** in the presence of 1 mol-% respective complex overnight in MeOH, MeCN and CHCl<sub>3</sub>, and analyzing the reaction mixture by UV-Vis-NIR spectroscopy thereafter (Scheme 11). 4-Formyl catechol (**S9**) was additionally evaluated in the case of **V1** – **V4**. The results show that **V1** – **V5** seemingly readily catalyze the oxidative dehydrogenation of **S6**, but the reaction is highly sensitive to the used solvent: **V1** – **V4** are only active in CHCl<sub>3</sub>, whereas **V5** remains active in all tested solvents. Additionally, **V5** can catalyze the oxidation of **S7**. On the other hand, no activity can be seen for any V complex for neither **S8** nor **S9**. The preliminary investigations also show that **Mo1** and **W1** are completely inactive in the oxidation of **S6** – **S8** in the studied time frame of *ca.* 24 hours. There are only limited reports on Mo/W catalyzed catechol oxidation, but Pierpont, Finke, and co-workers, have shown that Mo and W catalyzed reactions are slower by a factor of at least 100 when compared to respective reactions mediated by vanadium compounds.<sup>195,217</sup>

Reaction of **V1** – **V5** with 100 eqv. **S6** – **S8** leads to immediate changes in the UV-Vis-NIR spectra of the complexes. Specifically, characteristic blue solutions with intense LMCT (ligand to metal charge transfer) bands generally associated with vanadium catecholato species arise at *ca.* 650 and 830 nm,<sup>202,206,282</sup> as illustrated by **V5** reacting with **S7** (Figure 13). Moreover, the distinctive signal at *ca.* 400 nm corresponds to the formation of **96** (Figure 13). All bands progressively intensify,

after which the 650 and 830 nm bands start to diminish. The most probable explanation for this is the drop in concentration of the vanadium catecholato species, after sufficiently many turnovers.

The kinetics of **V1** – **V5** catalyzed oxidation of **S6** and/or **S7** was monitored by *in-situ* UV-Vis spectroscopy. The CO mimetic investigations with **V1** – **V4** were performed by varying the [**V1** – **V4**]:[**S6**] molar ratio by a factor of 1:10 to 1:160. For **V5**, [**V5**]:[**S6**] molar ratio was varied between 1:1000 to 1:17500, and for [**V5**]:[**S7**] 1:1000 to 1:10000, respectively. Using variable vanadium to catechol molar ratios the initial rates were obtained at respective concentrations. The initial rates were then plotted, and the reactions found to obey Michaelis–Menten like kinetics. From these data the turnover frequencies  $k_{\text{cat}} = 24, 17, 13, 11 \text{ h}^{-1}$ , and  $164 \pm 32 \text{ h}^{-1}$  for **V1** – **V5** in the oxidation of **S6** were obtained, respectively (Table 5 entries 1 – 5). Additionally, a  $k_{\text{cat}} = 94 \pm 4 \text{ h}^{-1}$  was obtained in the **V5** catalyzed oxidation of **S7** (Table 5 entry 6).

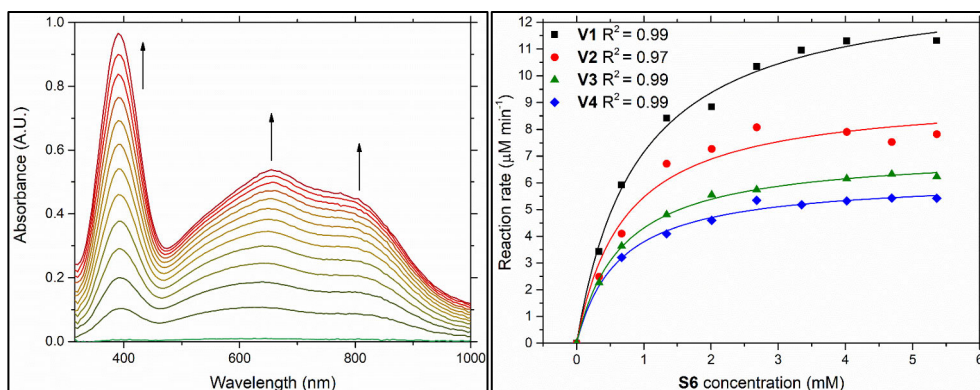


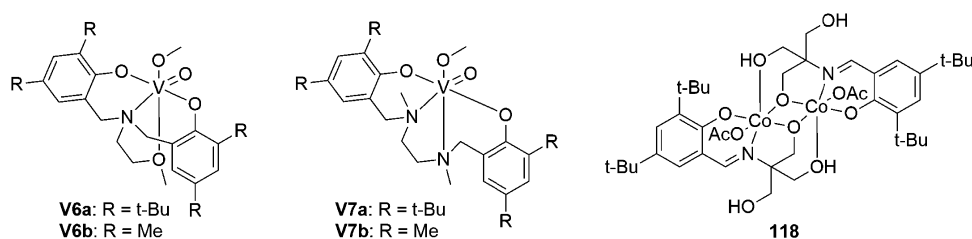
**Figure 13.** Formation of **96** as evidenced by the characteristic 400 nm band in the **V5** catalyzed aerobic oxidation of **S7** in  $\text{CHCl}_3$  (left). UV-Vis-NIR spectra recorded at five-minute intervals over a period of 60 min. The ca. 650 and 830 nm bands correspond to vanadium catecholato LMCT transitions. Michaelis–Menten plots of the oxidation of **S6** catalyzed by **V1** – **V4** in  $\text{CHCl}_3$ , with  $c(\text{V1} - \text{V4}) = 3.35 \times 10^{-5} \text{ M}$ ,  $c(\text{S6}) = 3.35 \times 10^{-4} - 5.36 \times 10^{-3} \text{ M}$  (right).

Barring any erroneous analysis or treatment of the kinetics data,<sup>283</sup> as can be seen from Table 5, all complexes based on aminophenolato ligands, including **V1** – **V4** as well as **V6** and **V7** based on linear diaminobisphenolato ligands, from an earlier report of ours,<sup>256</sup> display rather similar activity, with  $k_{\text{cat}}$  ranging from 10 to  $24 \text{ h}^{-1}$ . However, these results contradict the reports by Maurya and co-workers, who show that **98** catalyzes the oxidative dehydrogenation of **S8** in MeOH, but not **S6**, and hypothesize that substrate sterics are behind this behavior: since **S6** is sterically bulkier than **S8**, coordination of the former at vanadium is hindered, preventing oxidation.<sup>224</sup> However, it seems that the *t*-Bu substituted, sterically most demanding complexes such as **V1**,

**V2**, **V6a** as well as **V7a** are slightly more active relative to their methylated counterparts **V6b** and **V7b**, although barely so. In any case, the  $k_{\text{cat}} = 3.24 \text{ h}^{-1}$  (Table 4 section 2.4.2) obtained in the oxidation of **S8** by **98** is similarly very low, and in line with the activity shown by **V1** – **V4**, **V6** and **V8**. It should be emphasized, that the oxidation of **S8** is however not directly comparable to that of **S6**.

**V5** is about 10 times more active in the oxidation of **S6** relative to the rest of the studied complexes, and the only complex capable of catalyzing the oxidation of **S7** as well. **V5** reaches  $k_{\text{cat}}$  values of  $164 \pm 32 \text{ h}^{-1}$  and  $94 \pm 4 \text{ h}^{-1}$  in the oxidative dehydrogenation of **S6** and **S7**, respectively, and remains catalytically active in MeOH and MeCN, unlike **V1** – **V4**. Interestingly – although Co and V complexes are not directly comparable – **V5** shows similar activity relative to **118**, for which a  $k_{\text{cat}} = 79 \pm 1 \text{ h}^{-1}$  has been reported in the oxidation of **S6** in MeCN:DMF. It is notable that Schiff-base supported vanadium complexes including **97** and **99** – **102** are typically much more active than aminophenolato supported ones (Table 4 section 2.4.2). Whether this seemingly higher activity is attributable to *e.g.*, the coordinatively unsaturated nature of Schiff-base vanadium complexes (**97** and **99** – **102** are formally five-coordinate), allowing easier coordination of **S6** – **S8**, is debatable, however (see section 5.2.2).

**Table 5.** Data obtained in the oxidative dehydrogenation of catechols catalyzed by **V1** – **V7**. Structures of **V6**, **V7** and **118** are also shown.



Entry	Substrate	Solvent	Pre-catalyst	$k_{\text{cat}} (\text{h}^{-1})$	Reference
1	<b>S6</b>	$\text{CHCl}_3$	<b>V1</b>	24	publication I
2	<b>S6</b>	$\text{CHCl}_3$	<b>V2</b>	17	publication I
3	<b>S6</b>	$\text{CHCl}_3$	<b>V3</b>	13	publication I
4	<b>S6</b>	$\text{CHCl}_3$	<b>V4</b>	11	publication I
5	<b>S6</b>	$\text{CHCl}_3$	<b>V5</b>	$164 \pm 32$	publication II
6	<b>S7</b>	$\text{CHCl}_3$	<b>V5</b>	$94 \pm 4$	publication II
7	<b>S6</b>	$\text{CHCl}_3$	<b>V6a</b>	12	<sup>256</sup>
8	<b>S6</b>	$\text{CHCl}_3$	<b>V7a</b>	13	<sup>256</sup>
9	<b>S6</b>	$\text{CHCl}_3$	<b>V6b</b>	12	<sup>256</sup>
10	<b>S6</b>	$\text{CHCl}_3$	<b>V7b</b>	10	<sup>256</sup>
11	<b>S6</b>	MeCN:DMF 9:1 (V:V)	<b>118</b>	$79 \pm 1$	<sup>219</sup>

### 5.2.1.1 Detection and Role of H<sub>2</sub>O<sub>2</sub>

The natural enzymes TYR and CO produce water as a by-product in the oxidation of phenols and catechols, respectively. While some structural/functional CO models achieve this,<sup>45,50</sup> however, most functional CO models produce H<sub>2</sub>O<sub>2</sub> instead.<sup>46-49</sup> In the case of V-CO mimetic chemistry, there are only reports indicating that H<sub>2</sub>O<sub>2</sub> is generated from oxygen upon oxidation of catechols.<sup>222,223</sup> The detection of H<sub>2</sub>O<sub>2</sub> is significant in the sense that from the studied complexes **V1** – **V4** when dissolved are rapidly decomposed by H<sub>2</sub>O<sub>2</sub> or water, and TBHP to a lesser degree, as determined by UV-Vis and <sup>51</sup>V NMR spectroscopy.

An iodometric assay was performed after the reaction of **V5** with 100 eqv. **S7** in CHCl<sub>3</sub> maintained for several days at ambient conditions. After the reaction, H<sub>2</sub>O<sub>2</sub> was determined based on I<sub>3</sub><sup>-</sup>, which has a characteristic UV absorption signal at exactly 353 nm in water.<sup>46</sup> The reaction mixture was extracted with water to confine any generated H<sub>2</sub>O<sub>2</sub> and remove **96**, which can also oxidize I<sup>-</sup>.<sup>46</sup> The aqueous phase was adjusted to a pH ~ 2 with H<sub>2</sub>SO<sub>4</sub>, and a portion of the solution treated with KI (aq), and allowed to react overnight. The reaction was analyzed by UV-Vis spectroscopy thereafter, confirming the presence of I<sub>3</sub><sup>-</sup> and thus H<sub>2</sub>O<sub>2</sub>. As a control reaction, a portion of the prepared KI solution was allowed to react overnight with atmospheric oxygen, but no signal for I<sub>3</sub><sup>-</sup> could be detected afterwards. Moreover, a portion of the KI solution was treated with 30 w-% aqueous H<sub>2</sub>O<sub>2</sub> solution, again showing the characteristic signal for I<sub>3</sub><sup>-</sup>.

With H<sub>2</sub>O<sub>2</sub> having been detected as a co-product in the oxidation of **S7**, the effect of various amounts of H<sub>2</sub>O<sub>2</sub> on the initial oxidation rate of **S7** was evaluated with and without **V5** (1 × 10<sup>-4</sup> M; 0.1 mol-%) (Table 6 entries 1 – 5). In a control reaction **S7** reacts with 0.30 eqv. H<sub>2</sub>O<sub>2</sub> in the absence of **V5** with an initial rate of 3.04 ± 0.004 μM min<sup>-1</sup> (Table 6 entry 1). In the absence of H<sub>2</sub>O<sub>2</sub>, but with 0.1 mol-% **V5** the reaction rate increases to 9.9 ± 0.35 μM min<sup>-1</sup>, highlighting the significant beneficial role of **V5** (Table 6 entry 2). However, addition of both **V5** and H<sub>2</sub>O<sub>2</sub> has a synergistic effect in the **S7** initial oxidation rate (Table 6 entries 3 – 5). For example, addition of 0.1 mol-% **V5** and 0.30 eqv. H<sub>2</sub>O<sub>2</sub> relative to **S7** confers a higher effect than either of the reagents alone (Table 6 entry 5 vs. entries 1 and 2 combined). Based on these results and considering that the oxidation of **S7** generates H<sub>2</sub>O<sub>2</sub> from O<sub>2</sub>, the V catalyzed reaction can be inferred to be self-enhancing (*i.e.*, autocatalytic) unless the H<sub>2</sub>O<sub>2</sub> is immediately consumed upon formation. However, the iodometric assay demonstrates that not all H<sub>2</sub>O<sub>2</sub> is consumed during the reactions.

**Table 6.** Initial reaction rate of **S7** oxidation monitored over a period of 20 minutes by UV-Vis spectroscopy. All measurements were run in duplicate.

Entry	Pre-catalyst	Additive	Initial rate ( $\mu\text{M min}^{-1}$ )
1	none	0.030 M $\text{H}_2\text{O}_2$	$3.04 \pm 0.004$
2	<b>V5</b>	none	$9.9 \pm 0.35$
3	<b>V5</b>	0.010 M $\text{H}_2\text{O}_2$	$10 \pm 3$
4	<b>V5</b>	0.020 M $\text{H}_2\text{O}_2$	$16 \pm 3$
5	<b>V5</b>	0.030 M $\text{H}_2\text{O}_2$	$19 \pm 2$

Reaction conditions:  $\text{CHCl}_3$ , RT.  $[\text{V5}] = 1 \times 10^{-4}$  M,  $[\text{S7}] = 0.1$  M.

### 5.2.1.2 Mechanistic Considerations – ESI-MS and $^{51}\text{V}$ NMR

The mechanism of aerobic V catalyzed catechol dehydrogenation is debatable, as most proposals are rather different. However, Mukherjee and Dey have analyzed the **118** catalyzed oxidation of **S6** by ESI-HRMS(+), revealing the formation of 1:1 and 1:2 catechol adducts of the type  $[\text{Co}_2(\text{H}_2\text{L5})_2(3,5\text{-DTBCH})]^+$  and  $[\text{Co}_2(\text{H}_2\text{L5})(\text{HL5})(3,5\text{-DTBCH})_2]^+$ .<sup>219</sup> The authors conclude that such bi-adduct formation is unlike that proposed for the native CO enzyme (see Scheme 4 section 2.1.3.1). There are only very limited mechanistic studies of V catalyzed catechol oxidation involving ESI-MS, and available studies only include measurements performed in the positive ionization mode.<sup>222,223</sup> The study by Mukherjee and Dey allowed an apt opportunity to compare mechanisms between Co (**118**) and V (**V5**), complexes of striking structural similarity.

ESI-MS is a soft ionization method capable of giving reliable, semi-quantitative information about speciation in solution.<sup>284,285</sup> The Mo, W and V speciation was monitored by ESI-MS(+) during the reaction of **Mo1**, **W1** and **V5** with 100 eqv. **S6** and **S7** in  $\text{CHCl}_3$ . For **Mo1** and **W1**, mono catecholato sodium adducts of the type  $\text{Na}[\text{MO}(\text{H}_2\text{L5})(3,5\text{-DTBC})]^+$  and  $\text{Na}[\text{MO}(\text{H}_2\text{L5})(4\text{-TBC})]^+$  (M = Mo, W) are detected with low intensity. The removal of an oxido ligand by coordination of catechols, often leading to reduction at the metal center, is well-documented.<sup>198,203,204,206</sup> However, no intact **Mo1** or **W1** can be detected. Due to a lack of a characteristic isotope pattern for vanadium, no species assignable to intact **V5** or catecholato adducts could be reliably done using ESI-MS(+) in the case of **V5** + **S6/S7**.

The negative mode ESI-MS(–) proved to be far more informative than ESI-MS(+). For **Mo1**, the most intensive species in the presence of excess **S6** is  $[\text{MoO}(3,5\text{-DTBC})_2(3,5\text{-DTBCH})]^-$ , followed by low-intensity species  $[\text{MoO}_2(3,5\text{-DTBC})(3,5\text{-DTBCH})]^-$ , and a species best described as a reduced oxidomolybdenum(v) complex  $[\text{MoO}(3,5\text{-DTBC})_2]^-$ .<sup>197</sup> The mono-adduct  $[\text{MoO}(\text{HL5})(3,5\text{-DTBC})]^-$  was detected with a < 3 % intensity. Similar speciation is observed in the case of **S7**, with the most intensive signals being assignable to species

$[\text{MoO}(4\text{-TBC})_2]^-$  and  $[\text{MoO}(4\text{-TBC})_2(4\text{-TBCH})]^-$ . Low-intensity signals were observed for chloride adducts of the type  $[\text{MoO}(\text{H}_2\text{L5})(4\text{-TBC})]\text{Cl}^-$  and  $[\text{MoO}(\text{H}_2\text{L5})(4\text{-TBC})]_2\text{Cl}^-$ , as well as for the mono-adduct  $[\text{MoO}(\text{HL5})(4\text{-TBC})]^-$ . Interestingly, **W1** seemed more resistant to dissociation, with only species still supported by **HL5**, such as  $[\text{WO}(\text{HL5})(3,5\text{-DTBC})]^-$ ,  $[\text{WO}_2(\text{HL5})(3,5\text{-DTBQ})]^-$  and  $[\text{WO}(\text{H}_2\text{L5})(3,5\text{-DTBC})]\text{Cl}^-$  being detected in low intensity with **S6**, and species  $[\text{WO}(\text{HL5})(4\text{-TBC})]^-$  and  $[\text{WO}(\text{H}_2\text{L5})(4\text{-TBC})]\text{Cl}^-$  correspondingly with **S7**.

Most profoundly, the reaction of **V5** with 100 eqv. **S6** leads to the formation two new signals at  $m/z = 711.3884$  and  $m/z = 507.2336$ , with 100% and 23% intensity, respectively. These species correspond to  $[\text{V}(3,5\text{-DTBC})_2(3,5\text{-DTBSQ}')]^-$  (observed as  $[\text{V}(3,5\text{-DTBC})_3]^-$ ) and  $[\text{VO}(3,5\text{-DTBC})(3,5\text{-DTBSQ}')]^-$  (obs. as  $[\text{VO}(3,5\text{-DTBC})_2]^-$ ), namely **92** and **93**, which have simulated  $m/z = 711.3835$  and  $507.2321$ , respectively. These complexes are central in V catalyzed CDO mimetic chemistry in relation to the “common catalyst hypothesis” proposed by Finke and co-workers (see Scheme 10 section 2.4.1.2). A signal for a monomeric species  $[\text{VO}(\text{H}_2\text{L5})(3,5\text{-DTBC})]^-$  or  $[\text{VO}(\text{HL5})(3,5\text{-DTBCH})]^-$  is detected at *ca.* 9% intensity. In the case of **S7** the most intensive assignable species corresponds to  $[\text{VO}(\text{H}_2\text{L5})(4\text{-TBC})]^-$  or  $[\text{VO}(\text{HL5})(4\text{-TBCH})]^-$ , with  $[\text{V}(4\text{-TBC})_2(4\text{-TBSQ}')]^-$  (where  $4\text{-TBSQ}^- = 4\text{-tert-butylsemiquinonato anion}$ ), the **S7** equivalent of **92**, also detectable in  $\sim 30\%$  level as  $[\text{V}(4\text{-TBC})_3]^-$ . However, no intact **V5** can be detected in either case using **S6** or **S7**.

The reaction of **V5** with 100 eqv. **S6** and **S7** was additionally monitored by  $^{51}\text{V}$  NMR spectroscopy. Upon treatment of **V5** with 100 eqv. **S6/S7**, the signal corresponding to **V5** at *ca.*  $\delta -562$  ppm vanishes completely, a clear indication of dynamic and very rapid changes to the first coordination sphere of **V5**. New, broadened signals arise at *ca.*  $\delta +1391$  ppm in the case of **S6**, and at *ca.*  $+1185$  as well as  $-438$  ppm in the case of **S7**. These significant changes in the  $^{51}\text{V}$  NMR spectra, as well as the absence of any signals at *ca.*  $-400$  to  $-600$  ppm (in the case of **S6**), the  $^{51}\text{V}$  NMR shift region typically associated with oxidovanadium(V) complexes supported by redox-innocent  $\text{NO}_5$  type ligand set,<sup>206,273</sup> hints that **V5** probably reacts rather completely. This is also supported by the ESI-MS measurements. The  $-438$  ppm  $^{51}\text{V}$  NMR signal observed in the reaction with **S7** has been tentatively assigned to  $[\text{VO}(\text{HL5})(4\text{-TBCH})]^-$  (or  $[\text{VO}(\text{H}_2\text{L5})(4\text{-TBC})]^-$ ), the most intensive V-containing species detected in ESI-MS(-). This designation is in line with spectroscopic assignments done for similar mono catecholato  $\text{V}=\text{O}$  complexes by the groups of Rehder and Pecoraro.<sup>206,273</sup>

The results obtained in the ESI-MS and  $^{51}\text{V}$  NMR investigations, particularly in the case of **V5**, strongly imply that neither **V5**, nor a close structural derivative thereof, can reasonably be proposed to be the active catalyst in the CO mimetic reactions. Consequently, a catalytic cycle resembling the one presented for the

structurally closely related **118** cannot be credibly suggested. Moreover, the investigations reveal that **Mo1** and **W1** are also extensively transformed into a mix of mono/bis/tris catecholato species, although **W1** seems to be more resistant to the total dissociation of **H<sub>2</sub>L5**.

## 5.2.2 Catechol Dioxygenase Mimetics

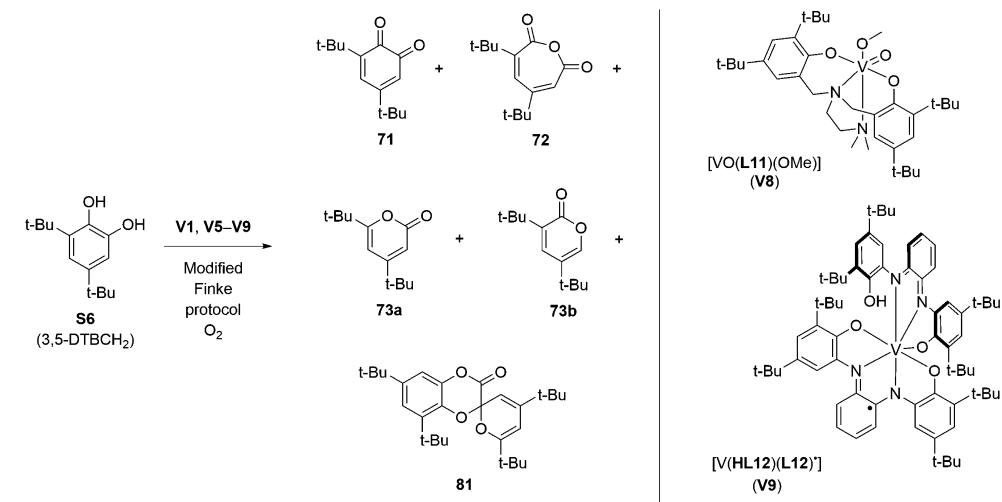
The compounds **92** and **93**, earlier characterized by Pierpont and Finke, were rather serendipitously discovered by ESI-MS in the reaction medium containing **V5** and 100 eqv. **S6** in the CO mimetic investigations. As it followed, additional screening of the **V5** catalyzed **S6** oxidation reaction was warranted, with subsequent investigations involving TLC and <sup>1</sup>H NMR spectroscopy leading to a realization that several products other than **71** are also formed. Subsequently, the catechol oxidation reactions mediated by **V1** – **V7**, compounds earlier claimed by us to display catecholase activity, were systematically and more rigorously (re)analyzed in terms of product distribution as well as vanadium speciation by means of column and gas chromatography, EPR spectroscopy and ESI-MS.

### 5.2.2.1 Product Distribution – Column and Gas Chromatography

As indicated by TLC and <sup>1</sup>H NMR spectroscopy, several products were initially detected in the **V5** catalyzed **S6** oxidation reaction and later isolated by column chromatography on silica gel. Using a slightly modified Finke protocol, the **V5** catalyzed oxidation of **S6** yielded 16% of the *o*-quinone **71**, 30% of the intradiol product **72**, as well as 17% of the extradiol products **73a** and 4% **81**, respectively (Table 7 entry 3). Interestingly, a structural isomer of the extradiol product **73a**, namely 3,5-di-*tert*-butyl-2-pyrone (**73b**), was obtained in 9% isolated yield, leading to total isolated yield of 76% (Table 7 entry 3). While **73b** has been documented before in **S6** dioxygenation reactions mediated by metal complexes based on Fe<sup>210,286</sup>, Mn<sup>287</sup>, Ni<sup>288</sup>, as well as Rh<sup>289</sup>, apparently this is, to the best of our knowledge, the first report concerning the finding of **73b** in the context of V-CDO mimetic chemistry.<sup>191,193,208,209,211–214</sup> After these results, a structurally diverse set of pre-catalysts **V1**, **V6a**, **V7a** as well as two other V complexes not previously assessed in CO/CDO mimetic chemistry, namely **V8** and **V9** (see Table 7), were evaluated in **S6** oxidation following an identical procedure. The *o*-quinone **71** and anhydride **72** were reliably obtained with an isolated yield of 16 – 21% and 33 – 39%, respectively, in the reactions catalyzed by the other V complexes as well, making these compounds major products in all reactions (Table 7 entries 4 – 8). Moreover, **73** and **81** were obtained with variable success rate in almost all cases.



**Table 7.** The characteristic product distribution obtained in the catalytic aerobic oxidation of **S6** by structurally diverse V complexes **V1** and **V5 – V9** using a slightly modified Finke protocol. The products were isolated by column chromatography on silica gel. Conversion and yields were estimated by TLC or <sup>1</sup>H NMR spectroscopy.



Entry	Pre-catalyst	Reaction time (h)	Conv. (%)	Total isol. yield (%)	Product isolated yield (%)				
					71	72	73a	73b	81
1	<b>65 – 70, 74 – 80</b>	16 – 24	≤ 100	Varies	15 – 28	34 – 48	6 – 20	N/A	7 – 11
2	<b>87 – 90</b>	20 – ~300	75 – 95	Varies	9 – 22	40 – 57	6 – 15	N/A	10 – 18
3	<b>V5</b>	21	≥ 95	76	16	30	17	9	4
4	<b>V1</b>	52	≥ 95	65	21	35	4	5	0
5	<b>V6a</b>	21	≥ 95	79	19	33	17	5	5
6	<b>V7a</b>	44	≥ 95	57	19	38	0	0	0
7	<b>V8</b>	53	≥ 95	62	16	39	0	0	7
8	<b>V9</b>	44	≥ 95	56	18	38	0	0	0
9	<b>Control 1</b>	48	5 <sup>[a]</sup>	5 <sup>[a]</sup>	5	0	0	0	0
10	<b>Control 2</b>	48	7 <sup>[a]</sup>	7 <sup>[a]</sup>	7	0	0	0	0
11	<b>Control 3</b>	48	25 <sup>[a]</sup>	25 <sup>[a]</sup>	24	1	0	0	0
12	<b>Control 4</b>	48	0 <sup>[a]</sup>	0 <sup>[a]</sup>	0	0	0	0	0
13	<b>Control 5</b>	49	100 <sup>[a]</sup>	100 <sup>[a]</sup>	94	6	0	0	0
14	<b>Control 6</b>	48	45 <sup>[a]</sup>	45 <sup>[a]</sup>	44	1	0	0	0

**Modified Finke protocol reaction conditions:** 4.50 mmol **S6**, 5 – 15 × 10<sup>-3</sup> mmol (<< 1 mol-% rel. **S6**) **V1**, **V5 – V9** in 60 mL 1,2-DCE under 100% O<sub>2</sub>, *t* = 21 – 53 h, *T* = 65 °C. <sup>[a]</sup> Conversion and non-isolated yield determined by <sup>1</sup>H NMR spectroscopy. Control reactions were performed under 100% O<sub>2</sub>/N<sub>2</sub> atmosphere at *T* = 65 °C with the following conditions: **Control 1**: 0.45 mmol **S6**, 6 mL 1,2-DCE, O<sub>2</sub>. **Control 2**: 0.45 mmol **S6**, 4.57 × 10<sup>-3</sup> mmol proligand **H<sub>2</sub>L11**, 6 mL 1,2-DCE, O<sub>2</sub>. **Control 3**: 0.91 mmol **S6**, 9.0 × 10<sup>-3</sup> mmol Et<sub>3</sub>N, 30 mL 1,2-DCE, O<sub>2</sub>. **Control 4**: 0.90 mmol **S6**, 9.0 × 10<sup>-3</sup> mmol **V5**, 30 mL 1,2-DCE, N<sub>2</sub>. **Control 5**: 0.90 mmol **S6**, 9.0 × 10<sup>-3</sup> mmol **V5**, 1.80 mmol 30 w-% H<sub>2</sub>O<sub>2</sub>, 30 mL 1,2-DCE, N<sub>2</sub>. **Control 6**: 0.90 mmol **S6**, 1.80 mmol 30 w-% H<sub>2</sub>O<sub>2</sub>, 30 mL 1,2-DCE, N<sub>2</sub>.

The results obtained in the oxidation of **S6** catalyzed by **V1**, **V5** – **V9** are similar if not identical to those acquired for other vanadium compounds **65** – **70** and **74** – **80** of the earlier literature (Table 7 entry 1, collated data from Table 3)<sup>191,193,208,209</sup>, and V-POMs **87** – **90** reported by Finke and co-workers in particular (Table 7 entry 2 collated data from Table 3).<sup>211</sup> The yields obtained for the major products **71** and **72** are well within or near the expected limits, *i.e.*, 16 – 21% *vs.* 9 – 28% for **71** and 30 – 39% *vs.* 34 – 57% for **72**, respectively, although generally the isolated yields for **72** are lower in comparison to that reported by Finke and co-workers. The extradiol products **73** and **81** represent minor products, whose isolation *via* column chromatography is more challenging than that of **71** and **72**. Especially, **81** was only isolated in a very low 4 – 7% yield for **V5**, **V6a** and **V8** (Table 7 entries 3, 5 and 7), generally falling short of the literature reports (7 – 18%). The TLC signal for **81** is very faint, only becoming visible after I<sub>2</sub> development, leading to easy inadvertent loss of product due to failure in detection and recovery. It should be noted, that in the older literature **81** is often not detected at all, possibly for the same reason (*cf.* Table 3 entries 1 – 5). For **V1**, **V5** and **V6a** the pyrone **73a** is obtained in 4 – 17% isolated yield (Table 7 entries 3 – 5), well reflecting that shown in the literature (6 – 20%), although for **V7** – **V9** the isolation was unsuccessful. However, to our best knowledge, the identification of **73b**, obtained in 5 – 9% yield (Table 7 entries 3 – 5) marks the first successful isolation in the context of V catalyzed CDO mimetic chemistry.

Due to the partly inadequate recovery of some of the **S6** oxidation products by means of column chromatography, a question remained whether or not the extradiol dioxygenase products **73** and **81** are formed in all studied V catalyzed reactions, notably those involving **V7** – **V9** as well. All reactions were thus additionally screened using GC-FID/MS. The results conclusively show that a nearly identical product distribution comprising of the dehydrogenation product **71**, intradiol dioxygenase product **72** as well as extradiol dioxygenase products **73** and **81** are obtained for each pre-catalyst (Figure 14). Not only are all the same products formed in each reaction, but the relative intensities of the products are very similar, hinting towards a rather homogeneous product distribution across all reactions, although quantification was never attempted. Moreover, the GC results are in line with the column chromatographic observations.

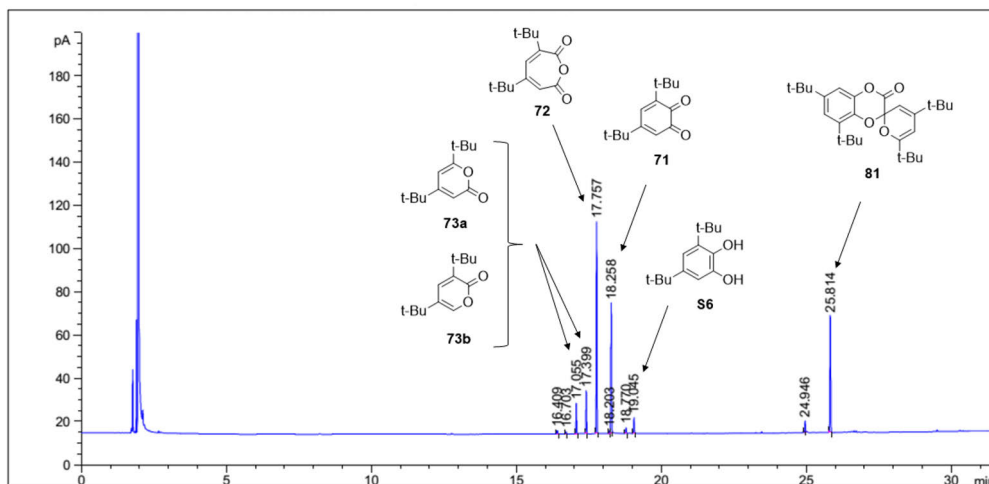


**Figure 14.** Gas chromatogram showing the product distribution in the **V9** catalyzed aerobic oxidation of **S6**. Nearly identical gas chromatograms are obtained for **V1** and **V5** – **V8** catalyzed oxidation of **S6** (Publication III Supporting Information).

### 5.2.2.2 Product Distribution – Control Reactions

Control reactions were performed in the presence or absence of V pre-catalysts and several additives to gain more insight with regards to the product distribution obtained in the oxidation of **S6** (Table 7 entries 9 – 14). In the V-CDO mimetic studies by Finke and co-workers, **71** is regarded as an “autoxidation” product. This was indeed revealed by the control experiment 1, run without catalysts, which shows that **71** is exclusively obtained in ~5% NMR yield by simply reacting **S6** with excess O<sub>2</sub> over a period of 48 hours (Table 7, control 1, entry 9). While 5% yield is low, it is non-negligible, and indicates that **71** may in fact be obtained *via* a non-catalytic, autoxidative pathway.

However, the yield for **71** obtained non-catalytically is noticeably less than what is observed in the presence of the V pre-catalysts (~5% vs. 16 – 21%; Table 7 entries 3 – 8 vs. 9). It has been shown that H<sub>2</sub>O<sub>2</sub> + **V5** in combination exert a synergistic effect on the initial rate of oxidation of **S7**, more so than either of the reagents alone (see Table 6 section 5.2.1.1). Moreover, the **V5** catalyzed reaction was explicitly shown to liberate H<sub>2</sub>O<sub>2</sub> based on the iodometric test. Judging from the yields of **71** shown in Table 7 across all V complexes, which point towards a rather identical outcome in the reactions overall, generation of H<sub>2</sub>O<sub>2</sub> is strongly implied in the case of the rest of the V pre-catalysts as well.

In addition, however, the autoxidation of **S6** is well documented under (stoichiometric) basic conditions,<sup>194</sup> warranting analysis on the impact of base catalysis as well. Considering the free ligands in **V1**, **V5** – **V9** are basic to some

extent, it was found that the oxidation of **S6** in the presence of ~ 1 mol-% **H<sub>2</sub>L11** derived from **V8** yielded 7% **71** (Table 7, control 2, entry 10). This value is well within experimental error when compared to control 1, and hardly indicative of base catalysis by the proligand, although the other proligands were not evaluated. Ramadan and co-workers have obtained a rather high  $k_{\text{cat}} = 1439 \text{ h}^{-1}$  in the **97** catalyzed oxidation of **S7** under a molar stoichiometry of 1:100:100 for **97**:**S7**:Et<sub>3</sub>N, respectively.<sup>229</sup> However, performing the oxidation of **S6** in the presence of even 1 mol-% Et<sub>3</sub>N, in the *absence* of V pre-catalysts yielded a total NMR conversion of 25% with the yield for **71** being about 24% (Table 7, control 3, entry 11). Interestingly, and quite surprisingly, the anhydride **72** was also obtained with a modest 1% yield. The control 3 clearly demonstrates the strong catalytic effect of 1 mol-% Et<sub>3</sub>N in the oxidation of **S6**.

The fact that **72** was obtained in the Et<sub>3</sub>N catalyzed oxidation of **S6**, even if only in 1% yield, is unexpected. One conceivable explanation would be the over oxidation of **71**. However, the groups of Tatsuno and Fenton have demonstrated earlier the inability of **71** to be further aerobically oxidized, even in the presence of 1 mol-% **66** – **70** and **74** – **77**, making the previous statement rather speculative at best.<sup>191,208</sup> Notwithstanding, there are reports indicating that the stoichiometric Baeyer-Villiger like oxidation of **71** into **72** using peracids such as *m*-CPBA is possible.<sup>290,291</sup> These reactions are very facile, with near quantitative yields of **72** obtained in just 5 – 10 minutes at 0 °C.<sup>290</sup> The 1% **72** obtained at 65 °C over a period of two days, in the reaction with a catalytic amount of Et<sub>3</sub>N may possibly be ascribed to similar reactions mediated by H<sub>2</sub>O<sub>2</sub>, instead of peracids, which are known to be very slow without transition metal catalysis.<sup>292</sup>

While the “dioxygenase-pathway” products **72**, **73** and **81** require O<sub>2</sub> as per the definition of “dioxygenation,” apart from **72**, which may possibly be obtained *via* other routes as well, the role of H<sub>2</sub>O<sub>2</sub> in the reactions was additionally studied under anaerobic conditions (Table 7, controls 4 – 6, entries 12 – 14). As predicted, **S6** is not oxidized under N<sub>2</sub> in the presence of 1 mol-% **V5** without added H<sub>2</sub>O<sub>2</sub> (Table 7, control 4, entry 12). However, full conversion with 94% and 6% selectivity for **71** and **72**, respectively, was obtained if **S6** is reacted with two eqv. H<sub>2</sub>O<sub>2</sub> in the presence of 1 mol-% **V5** (Table 7, control 5, entry 13). Likewise, a moderate 45% conversion with 44% selectivity for **71** and 1% for **72** is obtained solely by the effects of two eqv. H<sub>2</sub>O<sub>2</sub> relative to **S6**, without added catalysts (Table 7, control 6, entry 14).

These results reveal that **S6** may be moderately oxidized into **71** by H<sub>2</sub>O<sub>2</sub> in addition to O<sub>2</sub>. Since H<sub>2</sub>O<sub>2</sub> is produced from O<sub>2</sub> in the autoxidation of **S6**, an autocatalytic feedback loop is thus created. Moreover, the non-dioxygenase Baeyer-Villiger like pathway yielding 6% **72** from **71** (presumably) is enhanced in the presence of a Lewis acid catalyst *i.e.*, vanadium(V), a reaction that is well-documented for other substrates.<sup>293</sup> However, especially in the context of the control

reaction 5, the possible accidental inclusion of small amounts of O<sub>2</sub> through leaks or *via* disproportionation of H<sub>2</sub>O<sub>2</sub>, a reaction well-known to be transition metal catalyzed,<sup>88</sup> cannot be completely out ruled. In addition, the somewhat speculative catalytic/ non-catalytic Baeyer-Villiger like **71** oxidation pathway (controls 4 and 6) was not tested with genuine **71**.

### 5.2.2.3 Vanadium Speciation: EPR and ESI-MS

According to Finke's common catalyst hypothesis, the suggested catalyst resting state **[93]<sub>2</sub>** and catalytically active V species **93**, respectively, are generated from virtually any H<sub>2</sub>O<sub>2</sub> sensitive V containing compound by the effects of metal leaching.<sup>214</sup> The chemistry of vanadium peroxide compounds is a particularly well studied area, in most part due to the high relevance of these compounds to the VHPOs.<sup>88,294</sup> For instance, oxidoalkoxidovanadium(V) compounds such as **105** are known to react with H<sub>2</sub>O<sub>2</sub> in ethanol, generating oxidomonoperoxido species of the type [VO(O<sub>2</sub>)(OEt)<sub>2</sub>], with the oxidobisperoxido compounds [VO(O<sub>2</sub>)<sub>2</sub>]<sup>-</sup> becoming prominent at higher H<sub>2</sub>O<sub>2</sub> concentrations.<sup>294</sup> In the leaching process, according to Finke and co-workers, V-POMs such as **87** react with H<sub>2</sub>O<sub>2</sub>, generating mixed oxidoperoxido vanadium(V) species including [VO(O<sub>2</sub>)<sup>+</sup> which then readily react with strong σ and π donors **S6** and **71**, forming **92** en route to the CDO active species **93** (see Scheme 10 section 2.4.1.1).<sup>213</sup> The catalyst resting state **[93]<sub>2</sub>**, which has a characteristic nine-line EPR spectrum<sup>202</sup> as shown in Figure 15, has been detected in reactions involving **S6** and **65**, **85**, or **95**.<sup>214</sup>

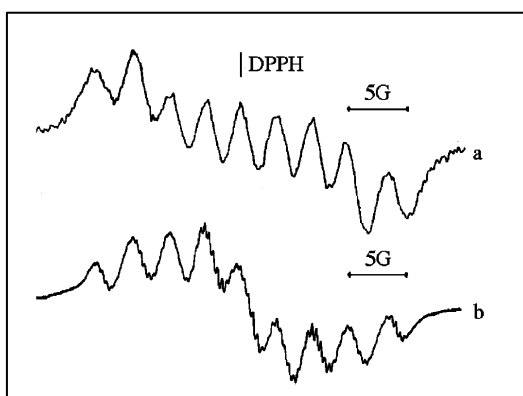


**Figure 15.** The center-field EPR spectrum of a reaction mixture containing **S6** and **65** (a) is identical within experimental error to the nine-line EPR spectrum obtained for an authentic sample of **[93]<sub>2</sub>** recorded in toluene (b). Reprinted with permission from "Yin, C. & Finke, R. G., 'Vanadium-Based, Extended Catalytic Lifetime Catechol Dioxygenases: Evidence for a Common Catalyst', *J. Am. Chem. Soc.*, 2005, 127, 9003–9013". Copyright 2005 American Chemical Society. DPPH = 2,2-diphenyl-1-picrylhydrazyl "g-marker" internal EPR standard.

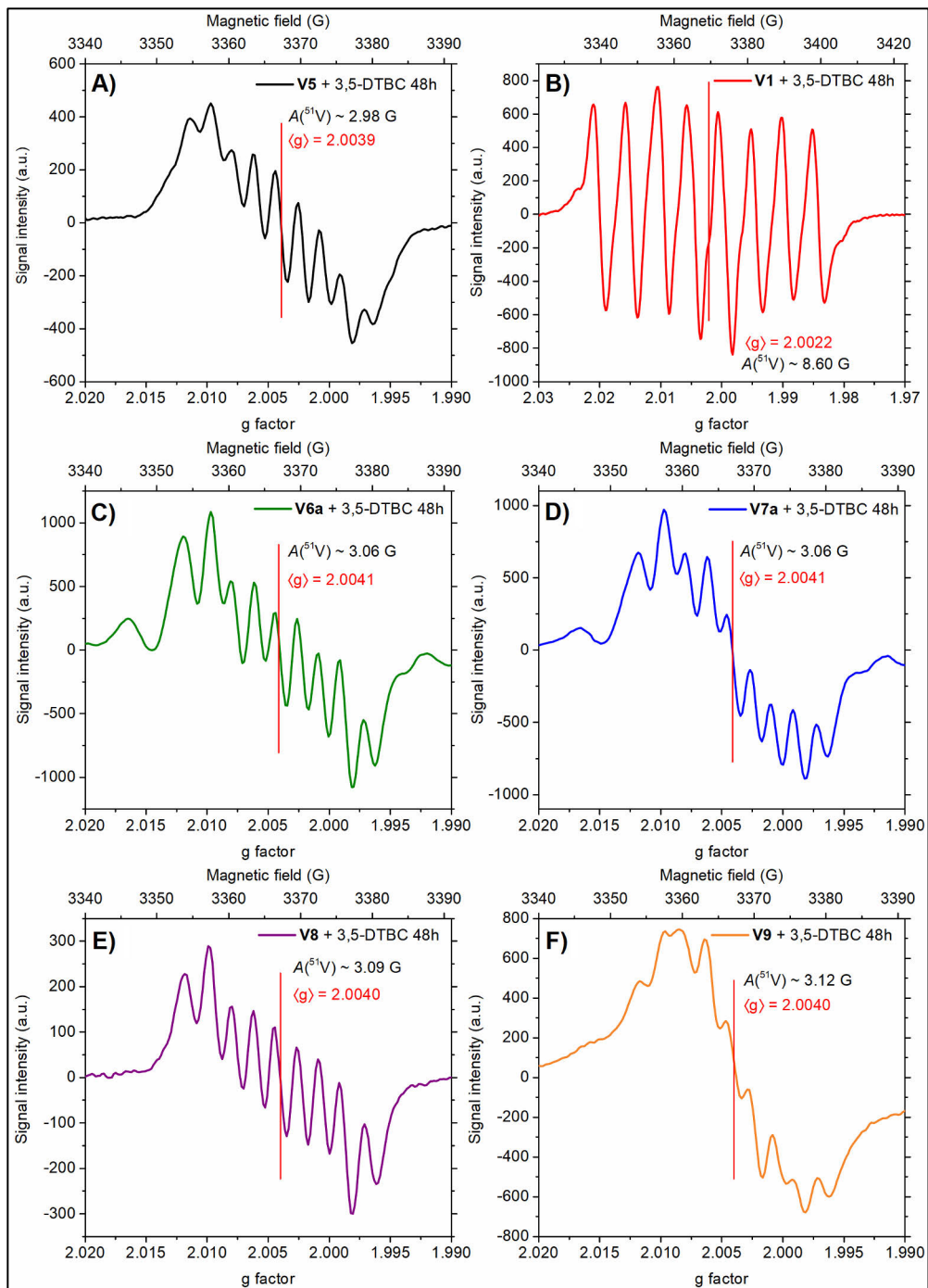


**Figure 16.** Ambient atmosphere 48-hour center-field EPR spectra of reactions A – F containing V1, V5 – V9 and 100 eq. S6 recorded in toluene at RT.

The product distribution analyses provide reasonable evidence to suggest that **V1** and **V5 – V9** most likely operate according to Finke's established common catalyst hypothesis. The reaction between **S6** and 1 mol-% **V1** and **V5 – V9** in toluene under ambient conditions at RT was monitored by EPR spectroscopy at given time intervals  $t = 30$  min, 6 h, 24 h, 48 h and 72 h. Except for **V1**, which immediately begins to show interesting EPR signals containing eight to 10 lines at  $t = 30$  min and 6 h, the EPR spectra from reactions containing **V5 – V9** are unremarkable until  $t = 48$  h. At 48 hours, all reactions except B containing **V1** display nine-line EPR signals having  $\langle g \rangle = 2.0039 - 2.0041$  and average  $A(^{51}\text{V}) = 2.98 - 3.12$  G (Figure 16 spectra A and C – F). These results are very similar to the reports by Finke and co-workers, who obtained EPR spectra centered at  $\langle g \rangle = 2.004 - 2.006 (\pm 0.002)$  having average  $A(^{51}\text{V}) = 3.04 - 3.08$  G ( $\pm 0.1$  G) in reactions involving **S6** and **65**, **85**, and **95**, as shown in Figure 15.<sup>214</sup> Moreover, the EPR spectra shown in Figure 16 A and C – F are in very good agreement with the EPR spectrum for **[93]<sub>2</sub>**, for which a  $\langle g \rangle \sim 2.004$  and  $A(^{51}\text{V}) = 2.85$  G have been obtained by simulation.<sup>202</sup> These EPR experiments thus provide compelling evidence of the involvement of **[93]<sub>2</sub>** in the reactions containing **V5 – V9** and **S6**.

Quite curiously, the EPR behavior of **V1** differs significantly from the other studied V pre-catalysts in the presence of **S6**. For **V1**, a 10-line EPR spectrum with  $\langle g \rangle \sim 2.0036$  and  $A(^{51}\text{V}) \sim 2.05$  is obtained at  $t = 30$  min, with little changes being observed at  $t = 24$  hours. This spectrum agrees well with **92**, for which  $\langle g \rangle \sim 2.004$  and  $A(^{51}\text{V}) \sim 2.1$  G has been reported.<sup>202</sup> At  $t = 24$  h, **V1 + S6** shows a mixture of two EPR spectra, for which a  $\langle g \rangle = 2.0040$  and  $2.0021$ , and a  $A(^{51}\text{V}) \sim 2.05$  G and  $8.91$  G can be obtained, respectively. Upon further progression of the reaction, at  $t = 48$  h, only a single eight-line EPR signal characteristic for a vanadium(IV) species having a  $\langle g \rangle \sim 2.0022$  and  $A(^{51}\text{V}) \sim 8.60$  G can be seen (Figure 16 spectrum B). Although no attempts were made to isolate the species affording this EPR signal, ESI-MS(–) analysis of the reaction mixture during which time the EPR signal was visible revealed a 100% intensity signal at  $m/z = 618.2806$ . Interestingly, this signal agrees well with a species of the type  $[\text{V}^{\text{IV}}\text{O}(\text{L1})(3,5\text{-DTBSQ}^*)]^-$  having a simulated  $m/z = 618.3000$ . The  $\langle g \rangle$  and  $A(^{51}\text{V})$  values, and the eight-line spectrum are representative of a 3,5-DTBSQ\* ligand weakly bound to a vanadium(IV) center.<sup>193</sup> It should be noted, that similar  $\langle g \rangle$  and  $A(^{51}\text{V})$  values have been reported for  $[\text{V}(\text{TCSQ}^*)_3]$  (**119**), where  $\text{TCSQ}^* = 3,4,5,6\text{-tetrachlorosemiquinonato}$ .<sup>205</sup> The different EPR behavior of **V1** may be qualitatively explained simply by considering **V1** is supported by a tridentate ligand **L1**, which leaves the vanadium center susceptible to ligand exchange, readily observed by  $^{51}\text{V}$  NMR spectroscopy. Thus, **V1** undergoes more rapid changes upon reaction with excess **S6** compared to the rest of the studied V pre-catalysts, manifesting as faster changes in the EPR spectra as a function of time.

In addition to EPR spectroscopy, the reaction of **V1** and **V5 – V9** with 100 eqv. **S6** was monitored by ESI-HRMS(+/-) in MeCN at the start of the reaction ( $t = 30$  min) as well as post-reaction ( $t = 48$  h). However, there are no drastic changes in the ESI-HRMS(-) spectra across the monitoring period, in contrast to the EPR experiments. Rather, immediately upon treatment of **V1**, **V5 – V9** with 100 eqv. **S6** signals corresponding to **92** and **93** are almost invariably visible, representing the highest-intensity species throughout the 48-hour observation period (Figure 17). Mono catecholato adducts of the type  $[\text{VO}(\text{L})(3,5\text{-DTBC})]^-$  can be detected for **V1**, **V5** and **V8** in very low intensity at  $t = 30$  min, highlighting that all V pre-catalyst react rather fully with **S6**. Additionally, **V9** is the only complex showing a signal for the intact pre-catalyst, albeit with very low intensity (*ca.* 5%). With ESI-MS(+) no species attributable to V containing compounds can be reliably assigned.

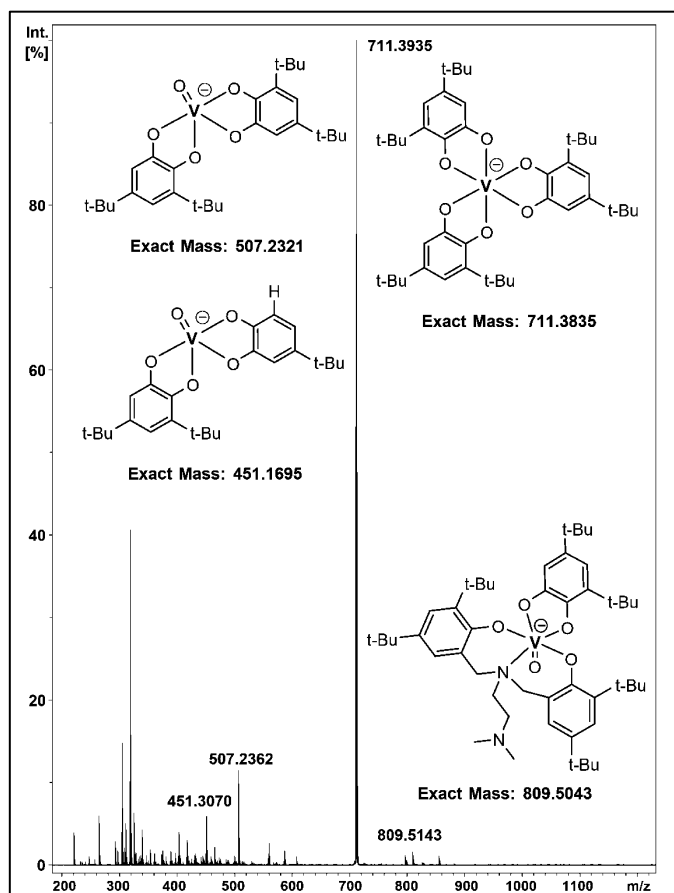


**Figure 17.** Negative mode ESI-MS spectrum showing speciation between  $m/z \sim 200$  to  $1200$  about 30 min after treatment of **V8** with 100 eqv. **S6**. A very similar ESI-MS(-) spectrum is obtained with **V1**, **V5 – V7** and **V9**.



The ESI-MS samples were additionally screened with  $^{51}\text{V}$  NMR spectroscopy at  $t = 30$  min. These measurements show the initial signal(s) corresponding to **V1** and **V5** – **V8** (**V9** being paramagnetic) vanish completely, again corroborating with the ESI-MS observations that the pre-catalyst react completely. Of course, a detrimental impact of paramagnetic species on the  $^{51}\text{V}$  NMR spectra may partly contribute to lack of visible signals.

### 5.2.3 Vanadium Catalyzed Catechol Oxidase vs. Dioxygenase Mimeticism?

It has been demonstrated throughout this PhD work that **V1** and **V5** – **V9** primarily show CDO mimetic behavior in the catalytic oxidation of **S6**. Overall, the oxidation of **S6** and the reactivity of all studied V pre-catalysts closely parallel that seen in the common catalyst hypothesis proposed by Finke and co-workers. Although catechols including **S6** are strongly coordinating  $\sigma$  and  $\pi$  donating ligands, Finke and co-workers have with reasonable support shown that vanadium leaching by the effects of  $\text{H}_2\text{O}_2$  is the key cause of this reactivity. Prior to this work, the common catalyst hypothesis has only ever been explicitly shown to be true for V-POMs such as **87** – **91**, and simple V complexes supported by bidentate acac type ligands **65** – **70** and **77**, or salen type ligands, including **74** – **76**. Moreover, at the time **65** – **70** and **74** – **77** have been evaluated in catechol oxidation, the mechanism has been unknown. Even V complexes based on multidentate aminobisphenolato or similar ligands, frequently used as pre-catalysts<sup>295–297</sup> in various oxidation reactions involving  $\text{H}_2\text{O}_2$  and organic hydroperoxides are seemingly not exempt from the effects of V leaching, as demonstrated herein. Particularly the non-oxido V complex **V9** recently described by Salojärvi<sup>259</sup> and co-workers lacking any terminal M—O bonds typically regarded<sup>70</sup> as susceptible to solvolysis by oxidants does not seem any more resistant to leaching than the other studied V complexes. This is made more problematic considering **V9** is a rather coordinatively saturated complex featuring two catecholato type multidentate ligands derived from **S6**.

Although only **V1**, **V5** – **V9** have been explicitly shown to obey Finke's common catalyst hypothesis thus far, based on the available data it can with reasonable confidence be implied that **V2** – **V4** do as well. A question, then, remains whether *any* V complex, most critically **97** – **102** (Table 4 section 2.4.2), truly show catecholase activity? While optimally this should be determined experimentally for **97** – **102** and other reported V-CO mimics, which is out of the scope of this PhD thesis, there are multiple indicators throughout the combined V-CO and V-CDO mimetic literature suggesting the answer to the question can be, and most likely is a “no”. In fact, it may be argued that V complexes seem to *only* display “genuine” CDO mimetic activity, the formation of *o*-quinones such as **71** having demonstrably

been shown to occur *via* autoxidation. The formation of **71** is thus truly achieved only by suppressing the CDO mimetic activity, which may be accomplished in several ways.

Firstly, the detrimental effect of added excess multidentate ligands such as TACN on the CDO activity of V compounds has been noted quite long ago.<sup>212</sup> Secondly, and quite similarly to the first point, the used solvent is instrumental in determining whether a complex has CDO mimetic activity or not: alcohols and other strongly coordinating solvents such as THF and DMF inhibit CDO mimetic activity. Both added ligands and coordinating solvents hinder or prevent the formation of **92** and **93** (if **S6** is used as substrate) which requires coordination of catechols and oxidant molecules. Most contemporary V-CO research involve solvents such as MeOH and DMF and multidentate ligands that intrinsically suppress CDO mimetic activity, leaving only the autoxidation pathway viable. Thirdly, Lewis bases such as Et<sub>3</sub>N has been shown to completely extinguish CDO mimetic activity when used in stoichiometric or even catalytic amounts.<sup>230</sup> While base mediated autoxidation of catechols is well known, we show here that even a catalytic amount of Et<sub>3</sub>N significantly promotes autoxidation of **S6**, even in the absence of V pre-catalysts.

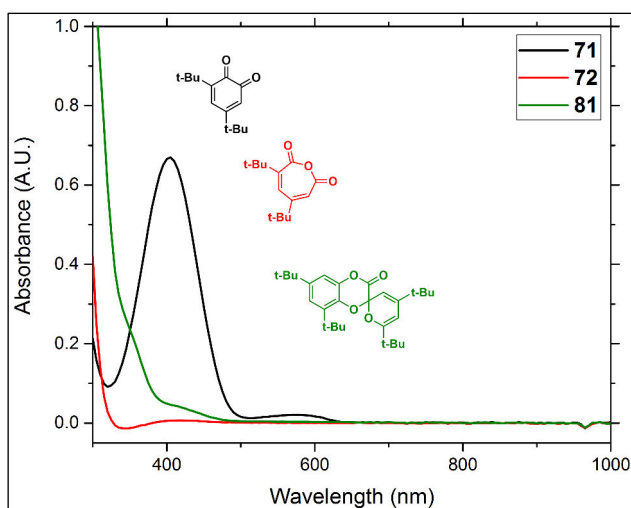
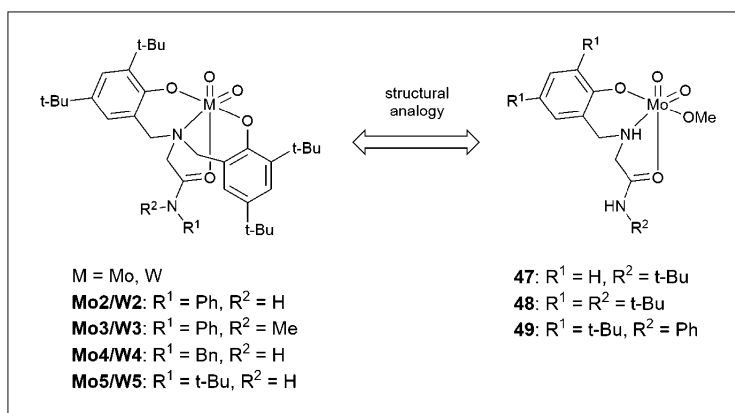


**Figure 18.** The UV-Vis-NIR spectra of **71**, **72** and **81** ( $c \sim 1$  mM) in CHCl<sub>3</sub>, respectively. The compounds **72** and **81** lack any distinctive spectral features above ca. 345 nm, the UV cutoff point of CHCl<sub>3</sub>.

Other problems related to V-CO (and CDO) mimetic chemistry research lie in applied methods and techniques. Most V based catechol oxidation research involve the use of **S6**, a substrate with somewhat special reactivity relative to the other commonly studied catechols **S7** – **S9**, except for 3,6-DTBCH<sub>2</sub>. Most V-CO mimetic studies, including our own, have involved only **S6** since **S7** – **S9** are not easily

oxidized. These reactivity trends have long been recognized in the V-CDO mimetic research community as well. Techniques such as UV-Vis spectroscopy and ESI-MS(+), which are frequently solely relied upon in V-CO mechanism elucidation, are unsuitable in detecting the tell-tale signs of CDO mimetic chemistry. For instance, the commonly encountered **S6** derived catechol dioxygenase products **72** and **81** do not have remarkable UV-Vis spectral features such as the strong  $\sim 400$  nm absorption shown by **71** (Figure 18). Moreover, vanadium species such as **92**, **93** and **[93]<sub>2</sub>** are only visible in the negative mode ESI-MS conditions, and their formation is strongly affected by **[V]:[S6]** stoichiometry, to the point they are not formed at all, and all CDO mimetic activity is thus quenched (see footnote on page 51). While EPR and <sup>51</sup>V NMR spectroscopy are powerful tools to determine the fate of used V pre-catalyst, depending on the used V pre-catalyst, the formation of EPR active species such as **[93]<sub>2</sub>** may take as long as 48 hours from reaction onset, making mechanistic investigations with EPR potentially problematic if reaction monitoring periods are kept short.<sup>223</sup>

### 5.3 Catalysis – Alkene Epoxidation

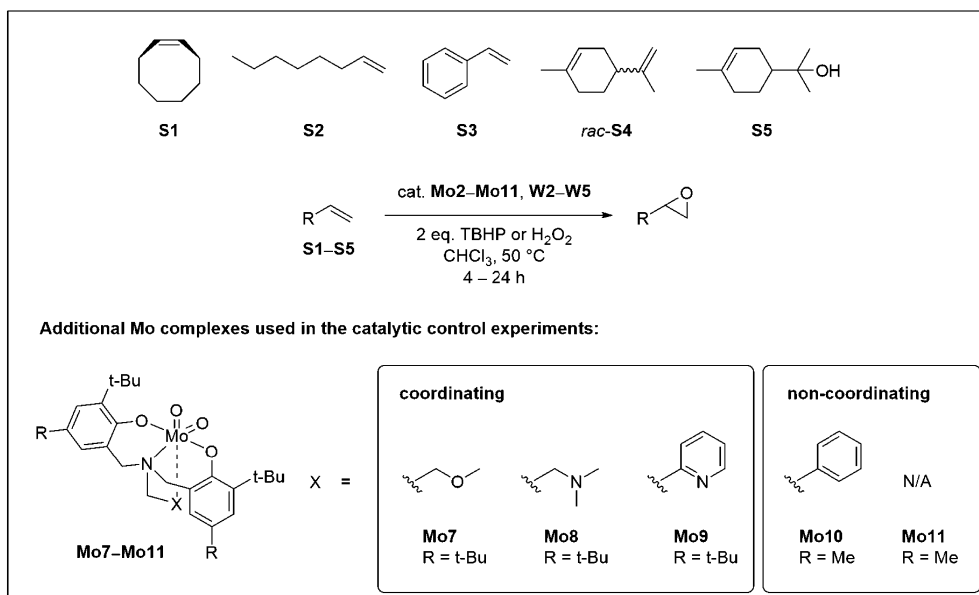


**Scheme 12.** Structural comparison of Mo and W complexes **Mo2 – Mo5** and **W2 – W5** between monomeric **47 – 49** reported by Möschi-Zanetti and co-workers.

Möschi-Zanetti and co-workers recently reported very high activities of aminomono-phenolato dioxidomolybdenum(VI) complexes **47 – 53** in the epoxidation of **S1**, reaching TONs up to 110000 at catalyst loadings as low as 0.0005 mol-% in CHCl<sub>3</sub> using TBHPdec.<sup>168</sup> Moreover, the complexes retained their high epoxidation activity even at 0.1 mol-% catalyst loadings when the reactions were performed in MeOH, EtOH, i-PrOH and TBOH, green solvents which typically inhibit epoxidation.<sup>113,116</sup> Additionally, some of the complexes remained active at sub 1 mol-% loadings in the epoxidation of challenging substrates **S2 – S5**, and when H<sub>2</sub>O<sub>2</sub> was used as the

oxidant instead of TBHP. The very high epoxidation activity and selectivity of the complexes has been ascribed to H-bond donating effects from the ligand amido pendant arm, whereby the expected catalytically active (alkyl)peroxido species are intramolecularly stabilized during epoxidation.<sup>168</sup> Inspired by these results, we studied whether similar H-bond donating amido functionalization would enhance the epoxidation activity of structurally similar aminobisphenolato complexes **Mo2** – **Mo6** and **W2** – **W5** as well (Scheme 12).

The complexes **47** – **53** feature either *N*-phenylacetamido or *N*-*tert*-butylacetamido functionalities which coordinate to the Mo centers *via* the amido carbonyl donor oxygen.<sup>168</sup> Thus, a similar pendant arm was opted for **Mo2** – **Mo6** and **W2** – **W5**. As a “baseline” H-bond donating pendant arm **Mo2/W2** contain an *N*-phenylacetamide moiety. In contrast, **Mo3/W3** feature an *N*-methyl-*N*-phenylacetamido pendant arm, with a blocked H-bond donating capability. The compounds **Mo3/W3** acted as controls to verify any enhancing effects from the H-bond donor capable complexes. Lastly, **Mo4/W4** and **Mo5/W5** were designed as steric controls against **Mo2/W2**, as it was envisioned the *N*-benzylacetamido and *N*-*tert*-butylacetamido moieties would be sterically demanding enough to interfere with any H-bond donating effects. In addition, **Mo6**, having a severely sterically hindered *N*-(2,6-di-*iso*-propylphenyl)-acetamido pendant arm was prepared but could not be used in catalysis due to poor solubility in common laboratory solvents, including DMSO.



**Scheme 13.** A general reaction scheme of epoxidations catalyzed by **Mo2** – **Mo11** and **W2** – **W5** using substrates **S1** – **S5**. Standard reaction conditions: 2 eqv. TBHP, chloroform,  $T = 50\text{ }^{\circ}\text{C}$ ,  $t = 4 - 24\text{ h}$ . Due to very poor solubility characteristics **Mo6** could not be tested in catalysis.

Preliminary investigations in the epoxidation of benchmark **S1** at 1 mol-% revealed a rather similar epoxidation behavior as a group for **Mo2** – **Mo5** and **W2** – **W5**, respectively (Figure 19). For Mo complexes, **S1** was epoxidized completely under 16 hours with quantitative selectivity, although a rather sharp rise of initial activity was observed for all pre-catalysts: a half-life ( $t_{1/2}$ ) of one to two hours after reaction onset was observed. Rather interestingly, an induction period lasting for about two hours was noted for **Mo2** and **Mo5**, followed by a sudden and very rapid increase in the yield of cyclooctene oxide (1,2-epoxycyclooctane). In contrast, **W2** – **W5** show markedly poorer performance compared to **Mo2** – **Mo5**, in line with literature reports,<sup>120,121,139,276,298</sup> reaching *ca.* 35% conversion in about two hours, after which the yield of cyclooctene epoxide begins to decline, presumably due to over oxidation or hydrolysis. For these reasons, the Mo analogs were only considered in subsequent epoxidation experiments. The activity of **Mo2** – **Mo5** in the epoxidation of **S1** was completely extinguished in polar and/or protic solvents such as in MeOH, EtOH, TBOH and MeCN, unlike **47** – **53**.<sup>168</sup> Modest activity was observed in non-polar aprotic solvents toluene, *n*-hexane, whereas slightly polar 1,2-DCE and DCM yielded good to moderate results, with DCM affording yields only slightly inferior to CHCl<sub>3</sub>/CDCl<sub>3</sub>, the most optimal solvent for **Mo2** – **Mo5** catalyzed epoxidation reactions. Moreover, reactions performed using H<sub>2</sub>O<sub>2</sub> did not yield any epoxide for any Mo or W complex. These results represent major deviations from the performance of the structurally related **47** – **53**.<sup>168</sup>

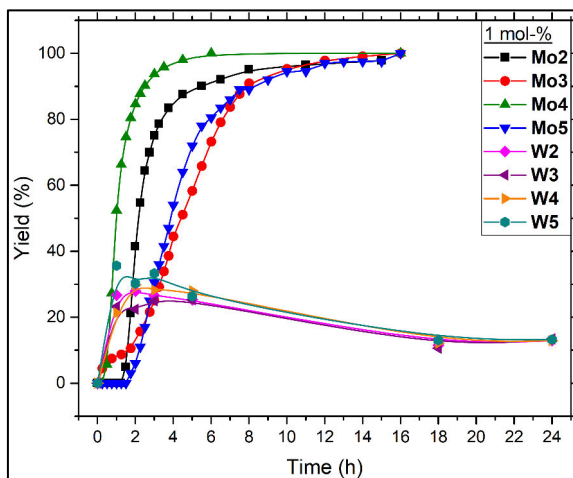


**Figure 19.** The yield of cyclooctene oxide vs. time profiles of **S1** epoxidation catalyzed by **Mo2** – **Mo5** and **W2** – **W5** at 1 mol-% catalyst loading, as monitored by *in-situ* <sup>1</sup>H NMR spectroscopy (Mo complexes) or GC-MS (W complexes). The reactions were performed in CDCl<sub>3</sub>/CHCl<sub>3</sub> at *T* = 50 °C.

The complexes **Mo2** – **Mo5** however remained very active at sub 1 mol-% loadings, in analogy to **47** – **53**.<sup>168</sup> Namely, no significant loss of activity could be

detected at 0.1 mol-% vs. that of 1 mol-% (Figure 20A vs. Figure 19), and fair activity was still present at 0.01 mol-% loadings (Figure 20B). All reactions progressed with full selectivity for cyclooctene oxide. **Mo2** especially remains nominally the most active, reaching practically full conversion still at 0.1 mol-%, and about 50% conversion at 0.01 mol-% respectively, although collectively the activities of **Mo2** – **Mo5** are rather similar. In terms of maximal TON (in a single run) **Mo2** – **Mo5** reach values of *ca.* 5300, 1500, 3500 and 3700, respectively, while maximal TOF values are correspondingly 920 h<sup>-1</sup>, 210 h<sup>-1</sup>, 600 h<sup>-1</sup> and 240 h<sup>-1</sup>, at 0.01 mol-% loadings (Table 8). These values are at least an order of magnitude higher than typically reported for aminobisphenolato dioxidomolybdenum(VI) complexes.<sup>164,165,260,261,263,299</sup>

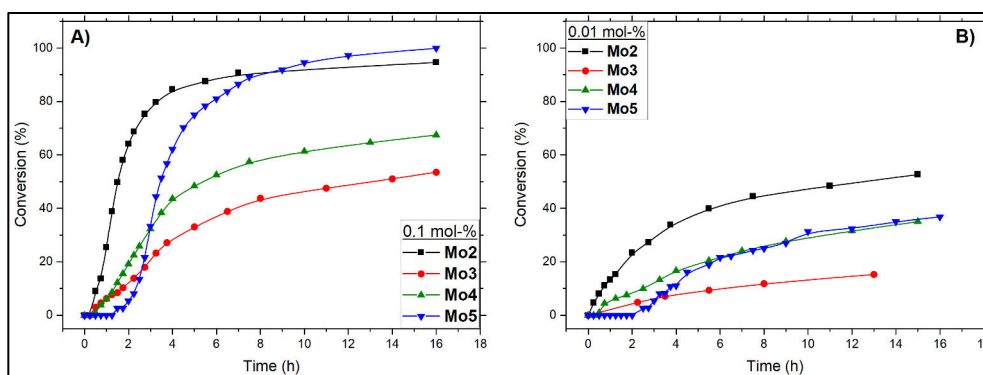


**Figure 20.** The conversion vs. time plots in the epoxidation of **S1** catalyzed by **Mo2** – **Mo5** at 0.1 (A) and 0.01 (B) mol-% catalyst loadings, respectively, as monitored by *in-situ* <sup>1</sup>H NMR spectroscopy. The reactions were performed in *ca.* 1 mL CHCl<sub>3</sub>:CDCl<sub>3</sub> (1:1 V:V) at *T* = 50 °C.

In most literature concerning Mo/W catalyzed epoxidation, the catalytic activity of any complex is by far most typically evaluated at a single catalyst loading, most often at 1 mol-% relative to an alkene substrate. The complexes **Mo2** – **Mo5** were found to be more active at 0.1 and 0.01 mol-% than at the widely used standard 1 mol-% conditions, in both relative and absolute terms. While this behavior might be interpreted as a beneficial effect from the amido moiety, similar to **47** – **53**, it was necessary to evaluate known complexes at sub 1 mol-% catalyst loadings to be certain. To this end, dioxidomolybdenum(VI) complexes supported by tetradentate aminobisphenolato ligands featuring 2-methoxyethyl (**Mo7**), *N,N*-dimethylethylamine (**Mo8**) and 2-pyridylmethyl (**Mo9**) pendant arms from earlier studies of ours were additionally synthesized and re-evaluated in epoxidation (Scheme 13).<sup>261</sup> Moreover, to adequately evaluate the effect of a coordinating pendant arm in epoxidation, the complexes **Mo10** and **Mo11** featuring tridentate aminobisphenolato ligands were also investigated (Scheme 13).<sup>262,263,300</sup> The complexes **Mo7** – **Mo9** do not feature H-bond donating capable pendant arms, whereas **Mo10** and **Mo11** lack a coordinating pendant arm entirely.

Quite remarkably, **Mo7** – **Mo11** show not only comparable, but partly even superior activity compared to **Mo2** – **Mo5** in the epoxidation of **S1**, especially at sub 1 mol-% catalyst loadings. At 1.0 mol-% catalyst loadings, **Mo7** – **Mo11** show slightly inferior overall activity relative to **Mo2** – **Mo5**: while **Mo2** – **Mo5** all reach full conversion at  $t \ll 16$  h and have reaction half-lives ( $t_{1/2}$ ) of one to two hours (not considering induction periods), **Mo7** – **Mo11** generally do not reach full conversion in 16 hours and have  $t_{1/2} \sim$  three to eight hours (Figure 21A). Curiously, **Mo7** – **Mo9** display an induction period lasting between 15 minutes to four hours, similarly to **Mo2** – **Mo5**, whereas no induction can be observed for **Mo10** and **Mo11**. The rather long *ca.* four-hour induction period displayed by **Mo9** is in accordance with previous reports.<sup>261</sup> However, at below 1 mol-% catalyst loadings **Mo7** – **Mo11** varyingly show superior epoxidation performance than **Mo2** – **Mo5** (Figure 21B and C). While **Mo9** and **Mo11** lose all activity at 0.1 mol-% loadings and below, **Mo7**, **Mo8** and **Mo10** have higher nominal TON and TOF values compared to **Mo2** – **Mo5**: at 0.01 mol-% loading, **Mo7**, **Mo8** and **Mo10** reach TONs of 5800, 9500 and 8200, and maximal TOFs of 360, 1000 and 2700 h<sup>-1</sup>, respectively, not considering induction times (Table 8).

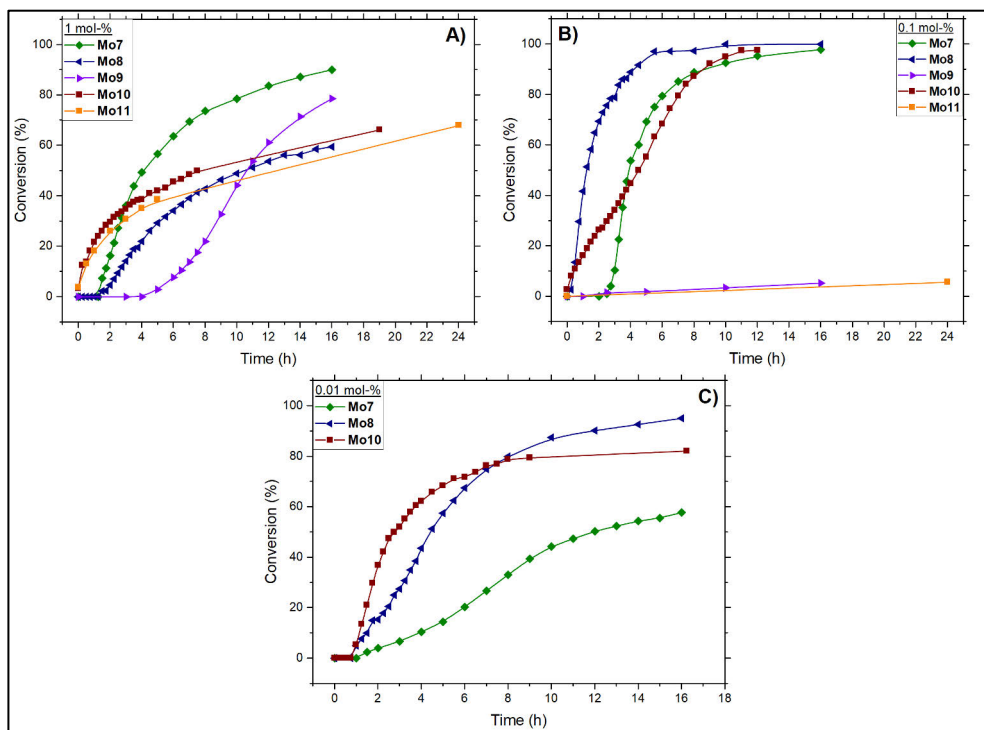


**Figure 21.** The conversion vs. time plots obtained in the epoxidation of **S1** catalyzed by **Mo7** – **Mo11** at 1.0 (A) 0.1 (B) and 0.01 (C) mol-% catalyst loadings, respectively, as monitored by *in-situ* <sup>1</sup>H NMR spectroscopy. The reactions were performed in *ca.* 1 mL CDCl<sub>3</sub> or CHCl<sub>3</sub>:CDCl<sub>3</sub> (1:1 V:V) at  $T = 50$  °C.

Among all Mo-based epoxidizing pre-catalysts, **86** is known to be capable of quantitative and very selective epoxidation of even the most challenging substrates such as terpenoids **S4**, **S5**, **11** – **13**, and long-chained terminal alkenes including **S2** and **9**, at 0.01 mol-% catalyst loadings.<sup>301</sup> Moreover, several groups have also reported their epoxidation results involving **S1** – **S5** using **86** in a control purpose.<sup>302–304</sup> However, to the best of our knowledge, epoxidation of **S1** with **86** have not been performed with catalyst loadings well below 1 mol-%. Thus, the epoxidation of **S1** was tested with **86** using 5, 1, 0.1, 0.01, 0.001 and 0.0001 mol-% catalyst loadings. The epoxidations were performed both on a Heidolph Parallel Synthesizer and *in-situ* <sup>1</sup>H NMR spectroscopy. Although superb performance was expected for **86**, astonishingly, a TOF ~ 62500 h<sup>-1</sup> was reached at 0.1 mol-% catalyst loading on the Synthesizer setup (Figure 22B), whereas a lower, but still very high TOF ~ 10800 h<sup>-1</sup> was obtained with the <sup>1</sup>H NMR setup (Figure 22A). These rather noticeable differences may be explained by diffusion: the reactions performed using the synthesizer are actively stirred, whereas the NMR reactions are limited by convection. Regardless of the used method, these TOF values are competitive with respect to the state-of-the-art (*cf.* Chart 1 section 2.3.5.3). Notably, no induction periods were observed using **86**, except at very dilute catalyst loadings.

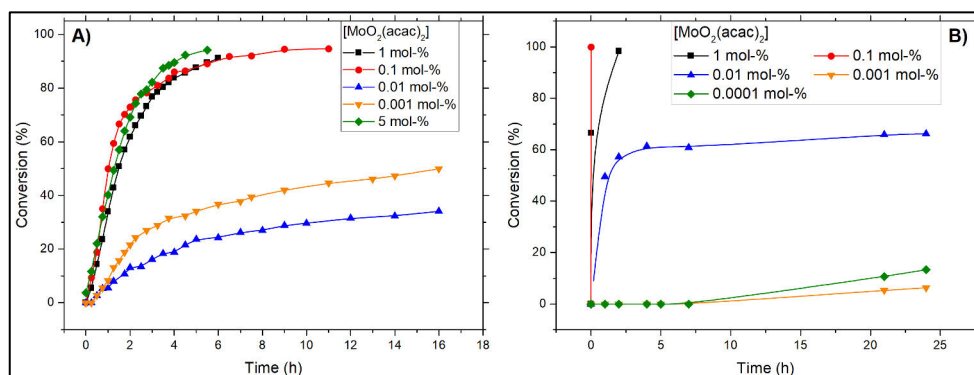


**Figure 22.** The conversion vs. time plots obtained in the epoxidation of **S1** catalyzed by **86** at various catalyst loadings, as monitored by *in-situ* <sup>1</sup>H NMR spectroscopy (**A**) or by GC-MS using a Heidolph Parallel Synthesizer (**B**). The reactions were performed in chloroform at  $T = 50\text{ }^{\circ}\text{C}$ .

In the catalytic reactions, it was noted that upon treatment of a CDCl<sub>3</sub> solution containing fully dissolved **86** with *ca.* 200 eqv. TBHP (rel. **86**), an off-white solid almost immediately precipitated out of solution. No attempts were made to characterize the solid but judging from the conversion vs. time plots (Figure 22A), the catalytically active component(s) most likely remain in solution. Strikingly, this behavior exactly matches that reported for **36** and **37** by Möscher-Zanetti and co-workers.<sup>69</sup> Moreover, the TOF yielded by **86** (62500 h<sup>-1</sup>), closely matches those



obtained for **36** and **37** ( $\sim 62000$  and  $107000 \text{ h}^{-1}$ , respectively) using similar reaction setup, hinting that the epoxidation chemistries of **36**, **37** and **86** might be similar. At the end of the reaction monitoring period, a brilliantly orange-colored homogeneous solution was recovered, but upon standing for a day under benchtop conditions, the orange color subsided, resulting in a blue precipitate, very similar to the reports involving **36** and **37**.<sup>69</sup>

The very high epoxidation activity of **86** has long been recognized to be result of the high hemilability of the acac ligand,<sup>68</sup> with modern consensus being that these type of ligands are rapidly dissociated from metal centers under oxidative conditions.<sup>26</sup> In a study by Zamaraev and co-workers, <sup>51</sup>V, <sup>1</sup>H NMR and EPR spectroscopy were used to study **65** catalyzed epoxidation of **8**.<sup>305</sup> According to this report, **65** reacts with equimolar amounts of TBHP to form oxidovanadium(V) species [VO(acac)<sub>2</sub>(OOt-Bu)] (**120**) and [VO(acac)<sub>2</sub>(Ot-Bu)] (**121**), from which neither are directly active in epoxidation. Rather, **120** decomposes into **65**, producing <sup>•</sup>OOt-Bu radicals which effected the epoxidation. Vanadium catalyzed epoxidation involving ROO<sup>•</sup> radicals is well documented.<sup>306</sup> Under a more “catalytically realistic” stoichiometry of [65]:[TBHP] = 1:>200, at least three other species **122** – **124** all lacking acac ligands are detected after rapid decomposition of both **120** and **121**. From the available data, it has been determined that **122** and **123** contain an OOt-Bu and O-tBu ligands, and may have structures of the type [VO<sub>2</sub>(OOt-Bu)] or [VO(O<sub>2</sub>)(OOt-Bu)], and [VO<sub>2</sub>(Ot-Bu)] or [VO(O<sub>2</sub>)(Ot-Bu)], respectively. However, only **122** epoxidizes **8** *via* a radical mechanism (see above). **124** was successfully characterized as [VO(Ot-Bu)<sub>3</sub>]. Both **123** and **124** equilibrate with the catalytically active **122**. By extending these results and considering **86** seemingly decomposes in the presence of excess TBHP, it may be unsubstantiated to assume a single catalytically active species, let alone one still supported by acac ligands, in the catalytic reaction between **86** and **S1**.

**Mo2** – **Mo5**, **Mo10** and **Mo11** were evaluated in the epoxidation of the more challenging substrates **S2** – **S5**, with **Mo7** – **Mo9** having been assessed earlier (Table 9).<sup>261</sup> Full selectivity for 1,2-epoxyoctane is observed for **Mo2** – **Mo4**, with conversions ranging between 34 – 43% in 24 h at 1 mol-%. However, **Mo5** was completely inactive in the epoxidation of **S2**. Lowering of the catalyst loading to 0.1 mol-% leads to slight drop in conversion (18 – 27%), although selectivity is full. Curiously enough, **Mo3** is deactivated at 0.1 mol-%, whereas **Mo5**, for which no reaction was observed for **S2** at 1 mol-%, reaches 20% and > 95% selectivity at 0.1 mol-%. With **S2**, **Mo2** – **Mo5** are deactivated at 0.01 mol-% loadings, however. For **Mo7** – **Mo11** conversions of 27 – 70% and rather similar selectivities (83 – 95%) are observed at 1 mol-% loadings.<sup>261</sup> In the case of **S3**, benzaldehyde was solely obtained with full conversion for **Mo2** – **Mo5**. Lower conversions (12 – 18%) but a selectivity of 19 – 32% have been reported for **Mo7** – **Mo9**.<sup>261</sup> Additionally, 76% and 48% conversions and 0% and 6% selectivity are obtained for **Mo10** and **Mo11**,

respectively. While all complexes are inactive in the epoxidation of **S5**, however, there is a stark dichotomy in the epoxidation of **S4** between MoO<sub>2</sub> complexes supported by tetra- and tridentate ligands. Complexes **Mo2** – **Mo9**, excluding **Mo5** and **Mo6**, progressively reach a 35 – 89% conversion and 36 – 70% selectivity in a 24-hour period, whereas **Mo10** and **Mo11** reach high 60 – 78% conversion and 69 – 78% selectivity in just one to three hours, respectively.

In summary, generally the epoxidations involving **Mo2** – **Mo11** followed the trends reported in the literature well,<sup>110,113,154,164–166,168,261</sup> namely that **S1** highly selectively affords the oxide in high yield, whereas the oxidation of terminal alkenes such as **S2** is selective but slow (poor conversion), and **S3** gives a good conversion with poor selectivity for the epoxide. However, the oxidation of **S4** was achieved with moderate conversion and selectivity, whereas **S5** did not react with any of the pre-catalysts, indicating that the OH group of the substrate may deactivate the complexes. All reactions worked equally well with TBHPaq and TBHPdec, indicating that the small water content in TBHPaq, which however becomes significant at very low catalyst loadings, did not seem to have a detrimental effect on catalysis. In contrast, H<sub>2</sub>O<sub>2</sub> and polar and/or protic solvents extinguished all epoxidation activity. From the data shown in Table 9 it is difficult to draw any meaningful structure-activity relationships between the tested complexes and substrates. However, importantly it can be seen that **Mo10** and **Mo11**, complexes supported by tridentate ligands, are as active if not slightly more active than **Mo2** – **Mo9** bearing tetradentate ligands. Moreover, any hypothetical beneficial H-bond donating effects in the ligands in **Mo2** – **Mo5** cannot realistically be proposed on account of the similar activity of **Mo7** – **Mo11**.

### 5.3.1 Epoxidation Mechanism – Role of the Pendant Arm

The complexes **Mo10** and **Mo11** missing a coordinating pendant arm were found to be equally active if not slightly superior to **Mo2** – **Mo9** in the epoxidation of **S1** – **S5** overall. This leads to a dilemma: what is/are the epoxidation mechanism(s) of **Mo2** – **Mo11**, and specifically, in what manner does the presence or absence of a coordinating pendant arm affect the epoxidation activity of the complexes? In the context of other reactions such as alkene polymerization, the impact of ligand sterics/electronics in aminobisphenolato supported metal complexes has been well established.<sup>307</sup> More recently, the coordinative nature of a pendant arm was found to be crucial in determining the activity of several aminobisphenolato MoO<sub>2</sub> complexes closely similar in structure to **Mo7** – **Mo9** in deoxydehydration of styrene glycol.<sup>262</sup> However, to date, similar structure-activity relationships have remained obscure in the context of alkene epoxidation catalyzed by MoO<sub>2</sub>/WO<sub>2</sub> aminobisphenolato complexes, as yet again demonstrated herein by **Mo2** – **Mo11** and **W2** – **W5**.

**Table 8.** Full catalytic data in the epoxidation of **S1** for **Mo2** – **Mo11**, excluding **Mo6**.

Loading (mol-%)	Conversion %, selectivity for the corresponding epoxide in parentheses for W complexes										
	Mo2	Mo3	Mo4	Mo5	Mo7	Mo8	Mo9	Mo10	Mo11	W2 – W5	86
5	90	14	21	75	33	36	78	40	59	–	100
1	98	100	100	100	90	60	79	66	68	13 – 15 (39 – 79)	>95
0.1	95	54	67	100	98	100	5	100	6	10 ( <b>W5</b> only)	>95
0.01	53	15	35	37	58	95	2	82	0	–	34
0.001	–	–	–	–	–	–	–	–	–	–	6*
0.0001	–	–	–	–	–	–	–	–	–	–	13*
N/A (control)	4 ± 1	3.5 ± 0.5	3.5 ± 0.5	3.5 ± 0.5	5.5 ± 2	4.5 ± 1	3.5 ± 0	–	–	< 5	–
TON											
1	98	100	100	100	90	60	79	66	68	5 – 10	100
0.1	950	540	670	1000	980	100	50	100	60	100 ( <b>W5</b> only)	1000
0.01	5300	1500	3500	3700	5800	<b>9500</b>	200	8200	0	–	6630
0.001	–	–	–	–	–	–	–	–	–	–	6400*
0.0001	–	–	–	–	–	–	–	–	–	–	133000*
Maximum TOF (h <sup>-1</sup> )											
1	59	8	25	8	6	4	5	7	10	< 1	1920
0.1	165	37	55	80	80	420	3	73	< 1	< 10	62500
0.01	920	210	600	240	360	1000	–	<b>2700</b>	0	–	4960
0.001	–	–	–	–	–	–	–	–	–	–	270*
0.0001	–	–	–	–	–	–	–	–	–	–	5570*

Reaction conditions: *t* = 16 h for Mo complexes, 24 h for W complexes, *T* = 50 °C, chloroform. \* Yield, TON and TOF values at 0.001 and 0.0001 mol-% catalyst loadings for **86** are nominal only; serious reproducibility problems start to occur at these loadings.

**Table 9.** Catalytic data in the epoxidation of **S2** – **S5** for **Mo2** – **Mo11**, excluding **Mo6**.

Substrate	Catalyst loading (mol-%)	Conversion % (selectivity for epoxide)										
		Mo2	Mo3	Mo4	Mo5	Mo7	Mo8	Mo9	Mo10	Mo11		
<b>S2</b> <sup>[a]</sup>	1	–	–	–	–	39 (88) <sup>[261]</sup>	32 (83) <sup>[261]</sup>	27 (79) <sup>[261]</sup>	–	–	–	–
<b>S2</b> <sup>[b]</sup>	1	43 (>95) <sup>[e]</sup>	34 (>95) <sup>[e]</sup>	42 (>95) <sup>[e]</sup>	0 (0)	–	–	–	–	–	–	–
<b>S2</b> <sup>[c]</sup>	1	61 (>95) <sup>[e]</sup>	61 (>95) <sup>[e]</sup>	59 (>95) <sup>[e]</sup>	0 (0)	–	–	–	–	–	–	–
<b>S2</b> <sup>[a]</sup>	0.1	18 (>95) <sup>[e]</sup>	0 (0)	27 (>95) <sup>[e]</sup>	20 (>95) <sup>[e]</sup>	–	–	–	–	–	–	–
<b>S2</b> <sup>[a]</sup>	0.01	0 (0)	0 (0)	0 (0)	0 (0)	–	–	–	–	–	–	–
<b>S3</b> <sup>[a]</sup>	1	100 (0) <sup>[d]</sup>	100 (0) <sup>[d]</sup>	100 (0) <sup>[d]</sup>	100 (0) <sup>[d]</sup>	12 (19) <sup>[261]</sup>	18 (32) <sup>[261]</sup>	16 (28) <sup>[261]</sup>	76 (0)	–	–	48 (6)
<b>S4</b> <sup>[a]</sup>	1	89 (70) <sup>[f]</sup>	73 (70) <sup>[f]</sup>	66 (70) <sup>[f]</sup>	0 (0)	49 (54) <sup>[261]</sup>	35 (36) <sup>[261]</sup>	39 (55) <sup>[261]</sup>	78 (78)	–	–	60 (69)
<b>S5</b> <sup>[a]</sup>	1	0 (0)	0 (0)	0 (0)	0 (0)	0 (0)	0 (0)	0 (0)	0 (0)	0 (0)	0 (0)	0 (0)

Reaction conditions: *t* = 24 h for **S2** – **S5** unless otherwise mentioned. *T* = 50 °C, chloroform; <sup>[a]</sup> 2 eqv. TBHP, 24 h; <sup>[b]</sup> 3 eqv. TBHP, 24 h; <sup>[c]</sup> 2 eqv. TBHP, 48 h; <sup>[d]</sup> **S3** is oxidized to benzaldehyde. <sup>[e]</sup> Trace amounts of 2- or 3-octanone is obtained. <sup>[f]</sup> Corresponding cyclohexanone is obtained as a major side-product.

### 5.3.1.1 Induction Period

In the epoxidations involving **S1**, an induction period lasting between *ca.* 15 min to four hours was noted prior to onset of some of the reactions. Significantly, the induction periods were exclusively associated with **Mo2** – **Mo9**, complexes based on tetradentate ligands, and particularly so with **Mo9** featuring a 2-pyridylmethyl pendant arm (Figures 19 – 21). Conversely, reactions catalyzed by **Mo10** and **Mo11** based on tridentate ligands, in addition to **86**, commenced almost immediately, except at very dilute catalyst loadings (Figures 21 and 22). Similar induction periods, which have been reported to be temperature dependent, have been observed *e.g.*, for **14** – **16**, and they are typically interpreted to be related to the formation of the presumed catalytically active M—OOR species (Thiel mechanism Scheme 8 section 2.3.4.1).<sup>133,183</sup> However, in some cases the presence of induction periods have been interpreted as indications of a radical nature of the epoxidation reactions.<sup>186</sup> No attempts were made to evaluate the possible radical nature of the tested epoxidations *e.g.*, by using known alkyl-radical scavengers such as **S7**, however.<sup>308</sup>

It was found that the induction period could be largely eliminated for the tested **Mo2**, **Mo5**, **Mo7** and **Mo8** by incubating the complexes in CDCl<sub>3</sub> in the presence of 200 eqv. TBHP for several hours prior to addition of 100 eqv. **S1** (Figure 23 pre-activated). If, on the other hand, the complexes were incubated in the presence of 100 eqv. **S1** for several hours prior to treatment with 200 eqv. TBHP, the induction period remained (Figure 23 no pre-activation). However, for **Mo9**, the induction period lasted for about four hours regardless of whether TBHP incubation was performed or not, whereas **Mo3** and **Mo4** were not evaluated. The <sup>1</sup>H NMR spectra of **Mo2**, **Mo5**, **Mo7**, **Mo8** and **Mo9** are unaffected by the excess TBHP, even during the whole course of the epoxidations, indicating that a type of “encounter complex” may be formed by pre-equilibration with TBHP, rather than a reaction outright (see Scheme 14 reaction A). Similar results were found with strongly coordinating solvents such as MeOH, MeCN, DMSO and pyridine. This is further substantiated by the fact the <sup>1</sup>H NMR spectra of **Mo10** and **Mo11** are immediately altered upon treatment with 200 eqv. TBHP. **Mo10** and **Mo11**, having a weakly bound MeOH ligand, readily react with TBHP to form the catalytically active species, manifesting as immediate conversion in the epoxidation of **S1**, whereas **Mo2** – **Mo9** may require pre-equilibration with TBHP prior to the onset of the reactions. For **Mo2** – **Mo9**, a partial ligand dissociation (of the pendant arm) may be envisioned.<sup>309</sup> Finney and Mitchell have already shown the rather robust nature of the 2-pyridylmethyl pendant arm in **41** – **43**, which may partly explain the unreactive nature of **Mo9**.<sup>158</sup> In fact, aminobisphenolato MoO<sub>2</sub> complexes featuring a 2-pyridylmethyl pendant arm have earlier been reported by Lei and Chelamalla to be inactive in the epoxidation of **S3**.<sup>161</sup> Rather interestingly, the activity can be reinvigorated by opting a longer 2-pyridylethyl pendant arm instead.<sup>161</sup> Such longer pendant arms show a reduced

coordinative ability to the extent they may be displaced by neutral solvent molecules such as MeOH, as determined by XRD for **98** (Table 4 section 2.4.2).<sup>224</sup>

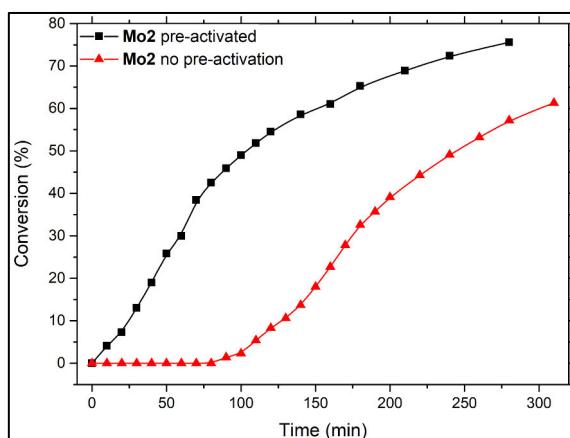


**Figure 23.** Epoxidation induction period can be removed by incubation of the complex in the presence of excess TBHP for several hours prior to treatment with **S1** as demonstrated by **Mo2** (pre-activation). If **Mo2** is similarly incubated for several hours in the presence of excess **S1** prior to addition of TBHP, the induction period persists (no pre-activation).

### 5.3.1.2 “Dilution Effect”

In all **S1** epoxidation experiments except those involving **Mo9** and **Mo11** the epoxidation performance increases in terms of higher TONs and TOFs with the lowering of the catalyst loading, a phenomenon dubbed as the “dilution effect”. For example, as shown by **Mo8**, the epoxidation performance is highest at 0.1 and 0.01 mol-% catalyst loadings, while increasing the amount of catalyst to 1 or 5 mol-% leads to poor epoxidation performance (Figure 24A). Kühn, Poli, and co-workers have encountered similar phenomena in **S1** epoxidation performed with **29**, **61** and **62**, respectively.<sup>110,140,176</sup> Kühn and co-workers have postulated that by reducing the catalyst loading, more catalytic centers will be involved and a more realistic TOF is obtained.<sup>140</sup> Poli and co-workers have similarly deduced that only a minor proportion of the complexes must be active at high catalyst loadings.<sup>110</sup> For **61** and **62** the dilution effect has been attributed to an equilibrium dissociation between the dimeric and monomeric forms (see Scheme 9 section 2.3.5.3).<sup>176</sup> Since the monomer such as **61** more readily interacts with TBHP compared to **63**, generating the active catalyst, it may be anticipated that the rate of deactivating dimerization is reduced under a lower catalyst loading relative to higher loads solely based on concentration effects.<sup>176</sup>

Considering the widely accepted Mo catalyzed epoxidation mechanism is believed to entail the formation of catalytically active Mo—OOR or similar species,

attention was directed towards the molar ratio between Mo pre-catalysts and TBHP, a reaction parameter often overlooked in the literature. At standard reaction conditions, for example at 1 mol-% catalyst loading, the molar ratio between [Mo]:[S1]:[TBHP] is 1:100:200, with the [Mo]:[TBHP] molar ratio difference progressively increasing with lower loads (*e.g.*, at 0.01 mol-% loading this ratio is 1:20000). Quite simply, the poor performance of all complexes except **Mo9** and **Mo11** at 5 mol-% catalyst loading can be explained by considering the molar ratio between [Mo]:[S1]:[TBHP] is 1:20:40, with a mere 1:40 ratio between Mo and TBHP, if TBHP stoichiometry is unaltered. Accordingly, by increasing the [Mo]:[TBHP] molar ratio to the standard factor of 1:200, the 5 mol-% epoxidation behaves closely similar to the 1 mol-% experiment, since the [Mo]:[TBHP] molar ratio will be identical (Figure 24B). Control reactions showed that the increased [S1]:[TBHP] ratio of 1:10 with respect to the standard 1:2 ratio has only very minor effects on the non-catalytic oxidation of S1 (Figure 24B).

It is likely that the “dilution effect” has been encountered before. Namely, Lei and Chelamalla report no benefits in increasing the catalyst loading from 2.5 to 5.0 mol-% in the epoxidation of **S3** using complexes structurally similar to **Mo9**.<sup>161</sup> In these experiments the [Mo]:[TBHP] molar ratio never exceeds 1:100, a ratio that was found suboptimal for **Mo2** – **Mo11**. Lacking a sterically demanding Bn pendant arm, deactivation by dimerization at low loadings may be envisioned for **Mo11**,<sup>300</sup> potentially explaining the poor performance of this pre-catalyst at sub 1 mol-% loadings.

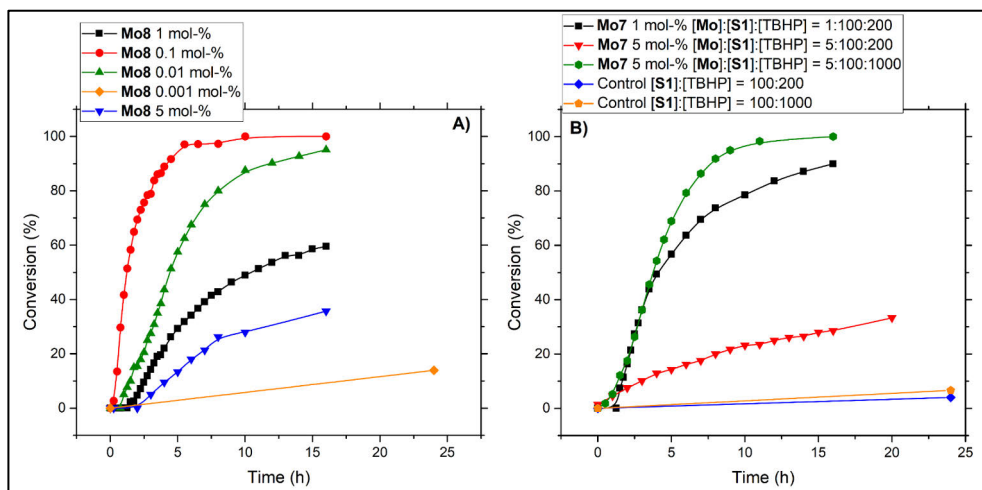


**Figure 24.** The **Mo8** catalyzed **S1** epoxidation conversion vs. time profiles at various catalyst loadings, demonstrating the “dilution effect” (A). Effect of [Mo]:[TBHP] in the epoxidation of **S1** as demonstrated by **Mo7** (B). Reactions were monitored by *in-situ* <sup>1</sup>H NMR spectroscopy and performed in chloroform.

### 5.3.1.3 Epoxidation Mechanism – DFT

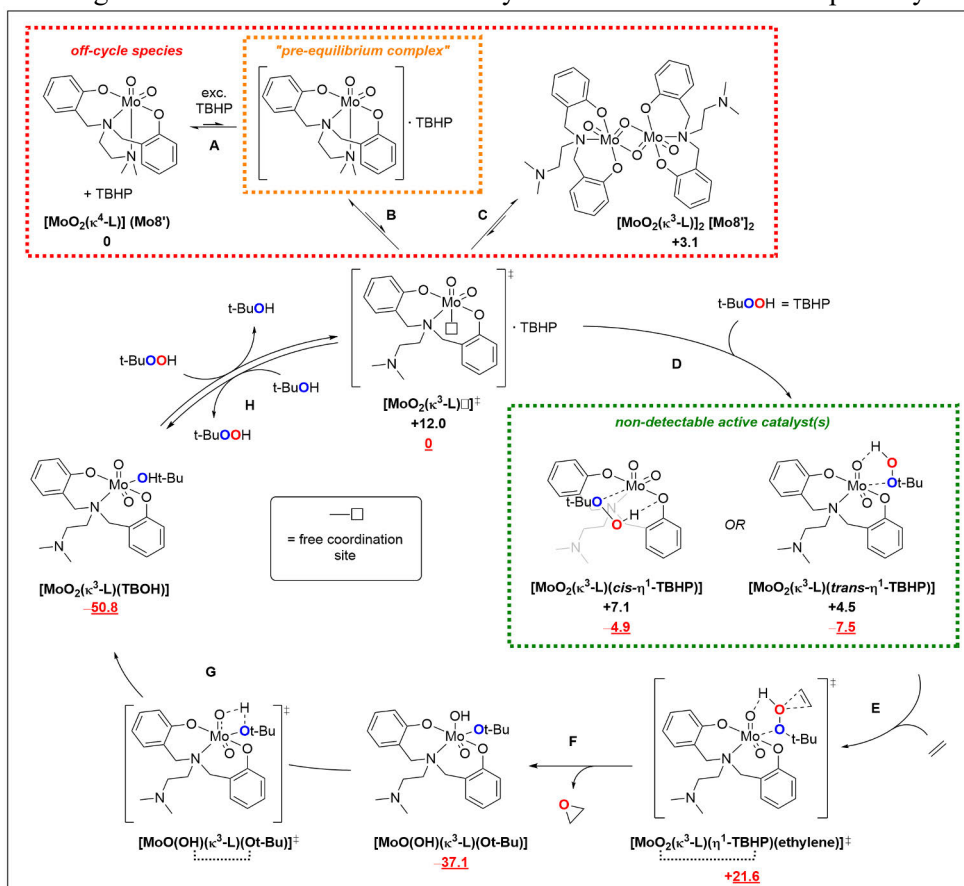
The [Mo]:[TBHP] molar ratio is one of the most important factors in determining the catalytic activity of the studied Mo complexes. Generally, the complexes show rather similar activities in terms of selectivity in the epoxidation of **S1** – **S5** overall, with significant structure-activity relationships arising only in the epoxidation of **S1** at sub 1 mol-% catalyst loadings, predominantly in the form of the “dilution effect”. A key feature in the studied epoxidations is that **Mo10** and **Mo11** show comparable if not slightly better activity relative to the other complexes overall, with respect to TON and TOF values. This implies that a coordinating pendant arm most likely does not play a crucial role in the overall epoxidation mechanism.

Finney and Mitchell have argued that the complexes **41** – **43**, by virtue of being supported by bulky tridentate ligands, rule out the Mimoun metallacycle epoxidation mechanism by preventing the simultaneous coordination of TBHP and alkene at the metal center, a prerequisite in the Mimoun mechanism.<sup>158</sup> By extending this same intuition, it follows that **Mo2** – **Mo9**, bearing bulky *tetradentate* ligands, should be inactive in epoxidation by disallowing (bidentate) coordination of the similarly bulky TBHP molecule. A partial dissociation of the pendant arm in **Mo2** – **Mo9** has been considered as a potential solution to this problem and was investigated computationally using density functional theory (DFT). The mechanistic insights from the works of Finney and Poli involving complexes **41** – **43**, **61** and **62** have been considered intuitively applicable for **Mo2** – **Mo11** due to structural similarities between these compounds.

DFT calculations using the nominally most active “tetradentate complex” **Mo8** having a simplified ligand structure (t-Bu groups omitted in the aromatic rings), denoted as **Mo8'**, were conducted adopting elements from the “Poli mechanism” with changes in relative energies  $\Delta H_{298}$  (in kcal mol<sup>-1</sup>) calculated in the gas phase to allow comparison between results.<sup>110,179</sup> The structures of **Mo8'** (+ TBHP) and some derivatives shown were optimized in the B3LYP/def2-TZVP level of theory (in Scheme 14 energies in kcal mol<sup>-1</sup> shown in black numbers under studied structures). According to the computations, the enthalpies associated with the de-coordination of the *N,N*-dimethylethylamine pendant arm from **Mo8'**, forming a formally five-coordinate complex, is endergonic by +12.0 kcal mol<sup>-1</sup>. In accordance with the Poli mechanism,<sup>110</sup> self-association of **Mo8'** into the dimeric [**Mo8'**]<sub>2</sub> via the five-coordinate intermediate species is possible, with [**Mo8'**]<sub>2</sub> being mere +3.1 kcal mol<sup>-1</sup> higher in energy relative to **Mo8'** (Scheme 14 reactions B and C). Although not observed directly during catalysis by <sup>1</sup>H NMR spectroscopy in the case of **Mo2** – **Mo9**, aminobisphenolato complexes structurally similar to [**Mo8'**]<sub>2</sub> have a precedent in the literature. For example, **Mo11** readily dimerizes in MeCN or non-coordinating solvents, due to being supported by a tridentate ligand.<sup>300</sup> Thus, partial ligand dissociation of the pendant arm may be reasonably conceived to effect dimerization.



Two modes of TBHP coordination emerged in the reaction mechanism. Namely, the five-coordinate intermediate from **Mo8'** has an approximate trigonal bipyramidal coordination geometry, allowing TBHP coordination “*cis*” or “*trans*” relative to the loose pendant arm (Scheme 14 reaction D). It is worth noting that the formation of the neutral TBHP adduct is likely to occur *via* an associative S<sub>N</sub>2 like reaction. Such a pathway should yield an energetically more favorable intermediate with respect to the “bare” five-coordinate species presented herein. The *cis*- and *trans*-TBHP adducts lie  $-4.5$  and  $-7.1$  kcal mol<sup>-1</sup> lower in energy relative to the five-coordinate species, set to 0 energy (Scheme 14 energies associated with the epoxidation cycle shown in red underlined values in kcal mol<sup>-1</sup> under studied structures). The [Mo8'(trans-TBHP)] is structurally analogous to the TBHP adduct in the Poli mechanism, being stabilized by H-bonding with the axial oxido ligand.<sup>110</sup> In contrast, the *cis*-TBHP adduct is stabilized by H-bonding with one of the phenolato O donors. We have considered the pathway involving the *trans*-TBHP adduct chemically more sensible than the *cis*-pathway.



**Scheme 14.** Main features of the alkene epoxidation mechanism involving **Mo8'**. Optimized geometries in the gas phase in relative energies shown in black, whereas energy profile of the epoxidation is shown in underlined red. The unit of energy = kcal mol<sup>-1</sup>.

The actual epoxidation step, modeled with ethylene, closely parallels that proposed for **62**. Alkene attack directs towards the O<sup>α</sup> atom (closest to H atom in TBHP) in the TBHP adduct which results in transition state that is endergonic by +21.6 kcal mol<sup>-1</sup> (Scheme 14 reaction E). The oxygen transfer step is characterized by elongation of the O<sup>α</sup>—O<sup>β</sup> bond in the TBHP ligand, as well as shortening of the Mo=O---HO<sup>α</sup> H-bonding contact in anticipation of proton shuttling. The catalytic conversion of ethylene to ethylene oxide produces t-BuO and OH ligands, and the process is exothermic by -37.1 kcal mol<sup>-1</sup> (Scheme 14 reaction F).

The active catalyst is regenerated after an intramolecular rearrangement generating TBOH and the original MoO<sub>2</sub> center, a process that is in line with the computational results by Poli and co-workers (Scheme 14 reactions G and H). The [MoO<sub>2</sub>(κ<sup>3</sup>-L)(TBOH)] species obtained from [MoO(OH)(κ<sup>3</sup>-L)(Ot-Bu)] *via* proton shuttling (reaction G) represents the global minimum (resting state) for the depicted reaction. However, proton transfer processes of this type are sometimes found to proceed with very high barriers in the gas phase (> +40 kcal mol<sup>-1</sup>).<sup>110</sup> These barriers have been shown to decrease dramatically in the presence of proton shuttling molecules, such as water or TBOH, however.<sup>110</sup> It is worth noting that stability difference between species [Mo**8'**(*trans*-TBHP)] + TBOH and [Mo**8'**(*trans*-TBOH)] + TBHP is only -1.9 kcal mol<sup>-1</sup> in favor for the latter species. Thus, the reaction H may proceed, in principle, in either direction. The regeneration of the active catalyst should be favorable given the very high excess of TBHP. Indeed, the “dilution effect”, an effect governed by the [Mo]:[TBHP] molar ratio, may be a manifestation of the facility of the forward H reaction. On the other hand, the reverse H reaction may become dominant in the presence of excess strongly coordinating solvents, well observed with **Mo2** – **Mo9**, which are poisoned in alcohols and MeCN.

#### 5.3.1.4 Catalyst Decomposition?

It has been determined experimentally that catalytically active species in the epoxidations is only a minor component present in solution (Halpern's rules). While DFT has been used to gain insight into the epoxidation mechanism, computational methods are only ever useful if the starting assumptions with regards to the reactions are correct. In this case the hypothesis is that a derivative of **Mo2** – **Mo11** is the catalytically active species. However, it has been unequivocally shown in this PhD work that these presumptions might be far from reality. As is the case in V catalyzed oxidation of **S6**, where structurally diverse aminophenolato supported V complexes were found to readily decompose and generate a discrete, active catalyst *via* V leaching. As pointed by Finke and co-workers, the concept of “autoxidation-product-initiated chemistry” is widespread in nature, such as in aerobic degradation of

organics, but is rarely detected nor considered in transition metal catalyzed oxidation chemistry.<sup>213</sup>

There are numerous examples of catalyst decomposition in the context of Mo/W catalyzed epoxidation, yielding a catalytically very active species. For example, although based solely on anecdotal evidence it may be possible that **36**, **37** and **86** generate a similar if not the same very active epoxidation catalyst(s) in the presence of TBHP. Similarly, **32** has been shown experimentally to become very active in epoxidation after loss of CpAr<sub>5</sub> ligand under oxidative conditions. Moreover, there is at least one report showing that POMs **84** and **85** lose their polyanionic structure in the presence of H<sub>2</sub>O<sub>2</sub>, generating catalytically very active peroxido species {PO<sub>4</sub>[MO(O<sub>2</sub>)<sub>2</sub>]<sub>4</sub>}<sup>3-</sup> and [M<sub>2</sub>O<sub>3</sub>(O<sub>2</sub>)<sub>4</sub>(H<sub>2</sub>O)]<sup>2-</sup> (M = Mo, W), respectively, *via* W and Mo leaching.<sup>310</sup>

As it stands, the **S1** – **S5** epoxidation reactions catalyzed by **Mo2** – **Mo11** show some aspects that are shared with Finke’s “common catalyst hypothesis” and are thus in principle open for the interpretation of catalyst decomposition. For example, coordinating solvents readily inhibit the epoxidation catalysis, and in the absence of deactivating solvents, the catalytically effective species are seemingly very active, even at 0.01 mol-% loading, much like with **93**. Moreover, the experimental evidence in favor for a “partial ligand dissociation” are in principle consistent with a “complete ligand dissociation” hypothesis as well. For example, the in some respects superior activity of **Mo10** and **Mo11** with regards to **Mo2** – **Mo9** may be explained by a more facile TBHP mediated decomposition of the complexes by virtue of **Mo10** and **Mo11** being less stabilized by tridentate ligands as opposed to tetradentate ones. On the other hand, the poor activity of **Mo9** might be due to the high stability of the pre-catalyst against the effects of TBHP. Since the catalytically active species are invisible using <sup>1</sup>H NMR spectroscopy, as per Halpern’s rules, the fact that **Mo2** – **Mo9**, or some part of them, are visible and unchanged during catalysis cannot be held as evidence for their complete stability. Moreover, the structures of **Mo10** and **Mo11** are immediately altered after treatment with TBHP, with multiple species visible at the end of catalysis. Although **Mo2** – **Mo11** display somewhat different reactivity towards **S1**, the selectivities in the epoxidation **S2** – **S5** are rather comparable. While a similar active catalyst may be imagined for the studied pre-catalyst, **Mo2** – **Mo11** are structurally related aminophenolato complexes after all, the complexes may decompose to form a hypothetical “common epoxidation catalyst” as well. Moreover, the presence of induction periods followed in some cases by sigmoidal (autocatalytic-like) conversion *vs.* time profiles (*cf.* Figures 21 and 24) are very similar to the V-CDO mimetic reactions. Unfortunately, currently it is difficult to differentiate between a “partial ligand dissociation” and “complete ligand dissociation” hypotheses, and future work should be dedicated to conclusively decide between the two.

## 6 Summary and Conclusion

In this PhD thesis I have studied the catalytic properties of several Mo, W and V complexes supported by aminophenolato and similar ligands in catalytic catechol oxidation and alkene epoxidation. In the context of catechol oxidation, it was found that the studied vanadium complexes **V1** – **V9** do not display CO mimetic behavior, as previously thought, but rather primarily CDO mimetic activity. Moreover, mechanistic investigations into the **V1** – **V9** catalyzed catechol oxidation strongly point towards a “common catalyst hypothesis” previously proposed by Finke and co-workers. According to the hypothesis, virtually any H<sub>2</sub>O<sub>2</sub> sensitive V based pre-catalyst is transformed by V leaching into a discrete, catalytically active form, driving the oxidation reaction to a specific outcome. It has been shown here with reasonable evidence that the studied V complexes obey Finke’s common catalyst hypothesis. Moreover, several connections between V catalyzed CO and CDO mimetic chemistry are found when comparing the literature pertaining to older V-CDO and modern V-CO mimetic chemistry, casting some doubts as to the validity of the V-CO mimetic research area as a whole.

However, perhaps most importantly, this PhD thesis highlights some aspects related to the poorly known concept of “true catalyst” evolution *via* “pre-catalyst” decomposition, which may in fact be a far more common phenomenon in the context of catalysis than believed. To quote Finke:

“[The] facile ligand substitution and leaching, especially in the presence of H<sub>2</sub>O<sub>2</sub> and powerfully chelating ligands, such as [3,5-DTBC] dianion, is hereby established as the dominant hypothesis to be disproved for future V-based oxygenation catalysis.”<sup>214</sup>

If anything, it seems that Finke’s “common catalyst hypothesis” has further been reinforced as the dominant hypothesis throughout the work presented herein, encompassing not only new CDO mimetic V compounds, but compounds previously assumed to display different chemistry altogether.

Several aminobisphenolato MoO<sub>2</sub>/WO<sub>2</sub> complexes **Mo2** – **Mo11** and **W2** – **W5** were evaluated in catalytic alkene epoxidation with the primary aim of studying ligand-centered H-bond donating effects on catalysis. As reported by Mösch-Zanetti and co-workers, Mo complexes having H-bond donor capable functionalities in their ligand design, such as amido moieties, display very high catalytic activity at sub 1 mol-% catalyst loadings in alkene epoxidation. Experimental work reveals that most studied Mo complexes indeed remain very active at sub 1 mol-% catalyst loadings, the most widely used standard catalyst loading. Dubbed as the “dilution effect”, the high activity of the complexes at low catalyst loadings was found to be tied to the [Mo]:[TBHP] molar ratio. Pre-equilibration with TBHP was also proposed to account for induction periods in reactions involving **Mo2** – **Mo9**, complexes supported by tetradentate ligands. However, collective catalytic results involving all complexes **Mo2** – **Mo11** reveal that the H-bond donor hypothesis must not hold true for **Mo2** – **Mo5**. Rather, complexes **Mo10** and **Mo11** being supported by a weaker coordinating tridentate aminobisphenolato ligands show identical if not better catalytic activity than the rest of the complexes. Thus, the catalytic activity of the complexes may be governed by ligand hemilability instead. Taking the experimental results together, DFT computational analysis was used to propose an epoxidation mechanism for **Mo2** – **Mo11** that is highly complementary to that proposed by Poli and co-workers for Schiff-base MoO<sub>2</sub> complexes. The mechanism proposes partial ligand dissociation, essentially showing that all complexes react *via* a similar neutral TBHP adduct intermediate, explaining not only the lack of significant structure-activity differences with **S2** – **S5** between the structurally similar but distinct complexes, but the highly competitive activity of **Mo10** and **Mo11** with respect to **Mo2** – **Mo9**.

## 7 Future

In the future, it might be interesting from a purely academic perspective to test the rest of the reported V-CO mimetic pre-catalysts for CDO mimetic activity, and whether they also obey Finke's "common catalyst hypothesis". Unfortunately, the prospects of synthetically utilizing such V complexes may be quite limited with respect to finding the "Holy Grail" general oxygenation catalyst if all V complexes decompose to yield the same catalytically active species, with a rather limited substrate scope. In this regard, other metals such as Fe found in the native CDO enzyme should be focused upon with this goal in mind.

In the context of Mo/W catalyzed epoxidation, the work herein shows that many previously reported aminobisphenolato complexes show high **S1** epoxidation activity below the standard 1 mol-% catalyst loadings. In some cases, the performance of the complexes is poor at 1 or higher mol-% loadings, but significantly increases at lower loadings. While the "dilution effect" mostly applied only for **S1** for the studied Mo complexes, in general it may be worthwhile to adopt a different catalyst loading standard (other than 1 mol-%), or alternatively increase oxidant loadings, even in the case poor catalytic results are obtained at 1 mol-% or higher loadings. Moreover, the extremely high epoxidation activity of **86** at sub 1 mol-% was revealed in the epoxidation of **S1**, which will help to benchmark future complexes.

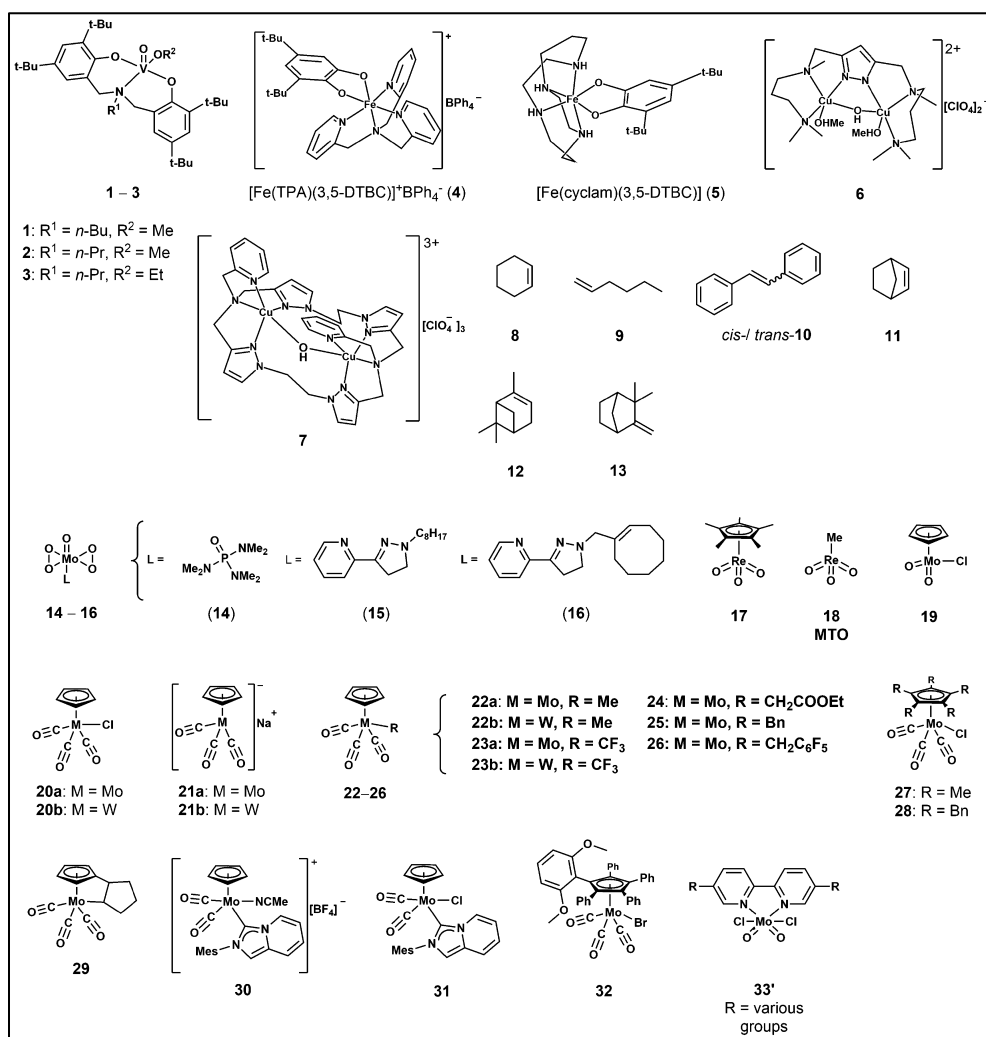
However, designing aminobisphenolato ligands with different pendant arms for use in Mo/W catalyzed alkene epoxidation may be a forgone opportunity if different reactivity is sought, especially if the epoxidation mechanism presented in this PhD thesis is correct. It goes without saying that more work is needed to be done both experimentally and theoretically. For example, experimental mechanistic elucidation using ESI-MS and  $^{19}\text{F}$  NMR spectroscopy might be used to probe speciation during catalytic runs,<sup>311</sup> or EPR might be in turn used to detect radicals during the reactions. In this regard, it might be sensible to design new aminobisphenolato ligands featuring fluorine labels, or ligands whose coordination could be controlled.

Work has already started in our laboratories to study the impact of coordinative hemilability of MoO<sub>2</sub> complexes in alkene epoxidation. Preliminary results have been promising: a structural derivative of **Mo2** with a more loosely coordinated

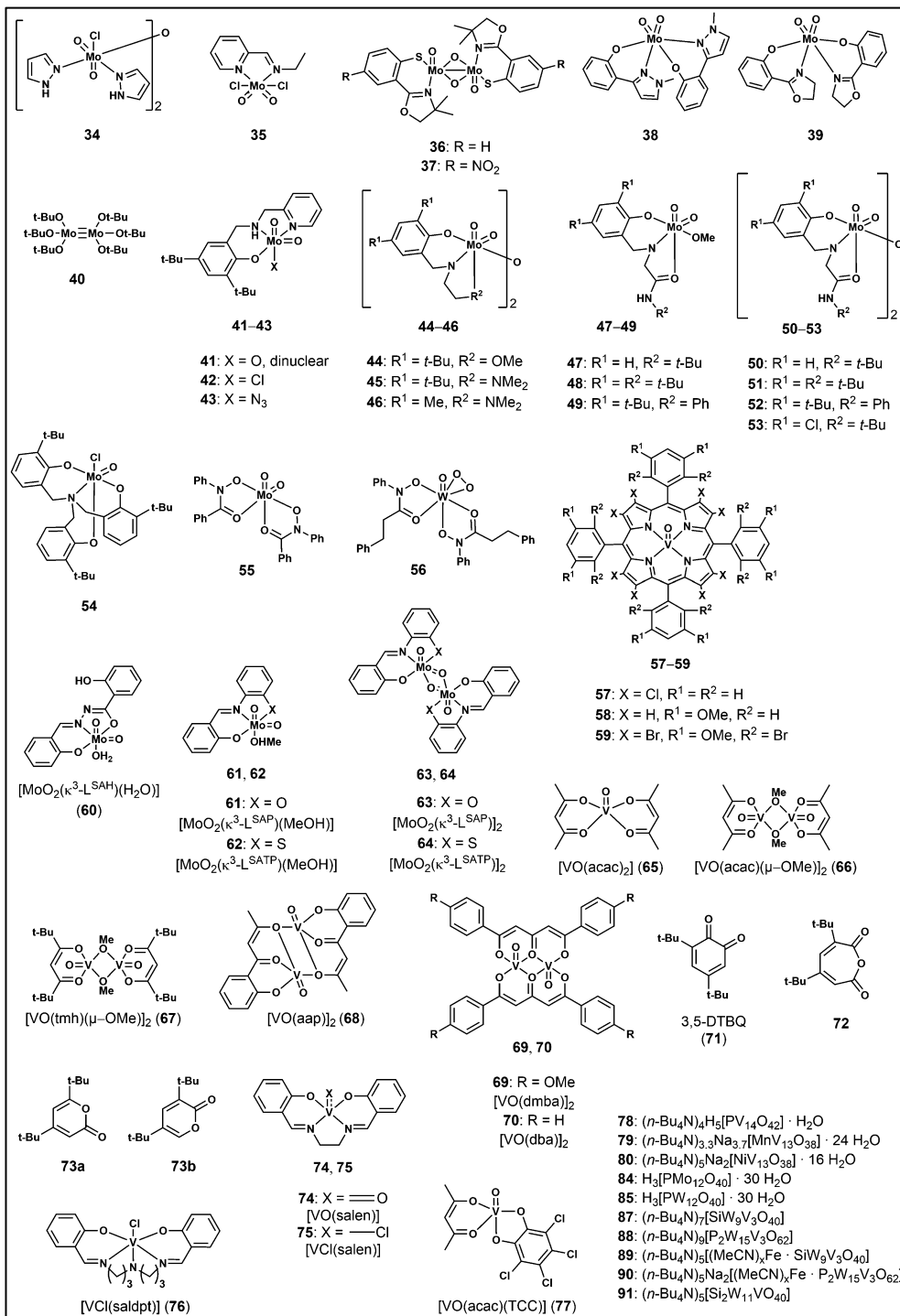
ligand has reached a high initial TOF  $\sim 14000 \text{ h}^{-1}$  at a catalyst loading of 0.001 mol-% in the epoxidation of **S1**. Additionally, a series of V complexes derived from **H<sub>2</sub>L6** – **H<sub>2</sub>L10** are currently investigated as oxidation pre-catalysts.

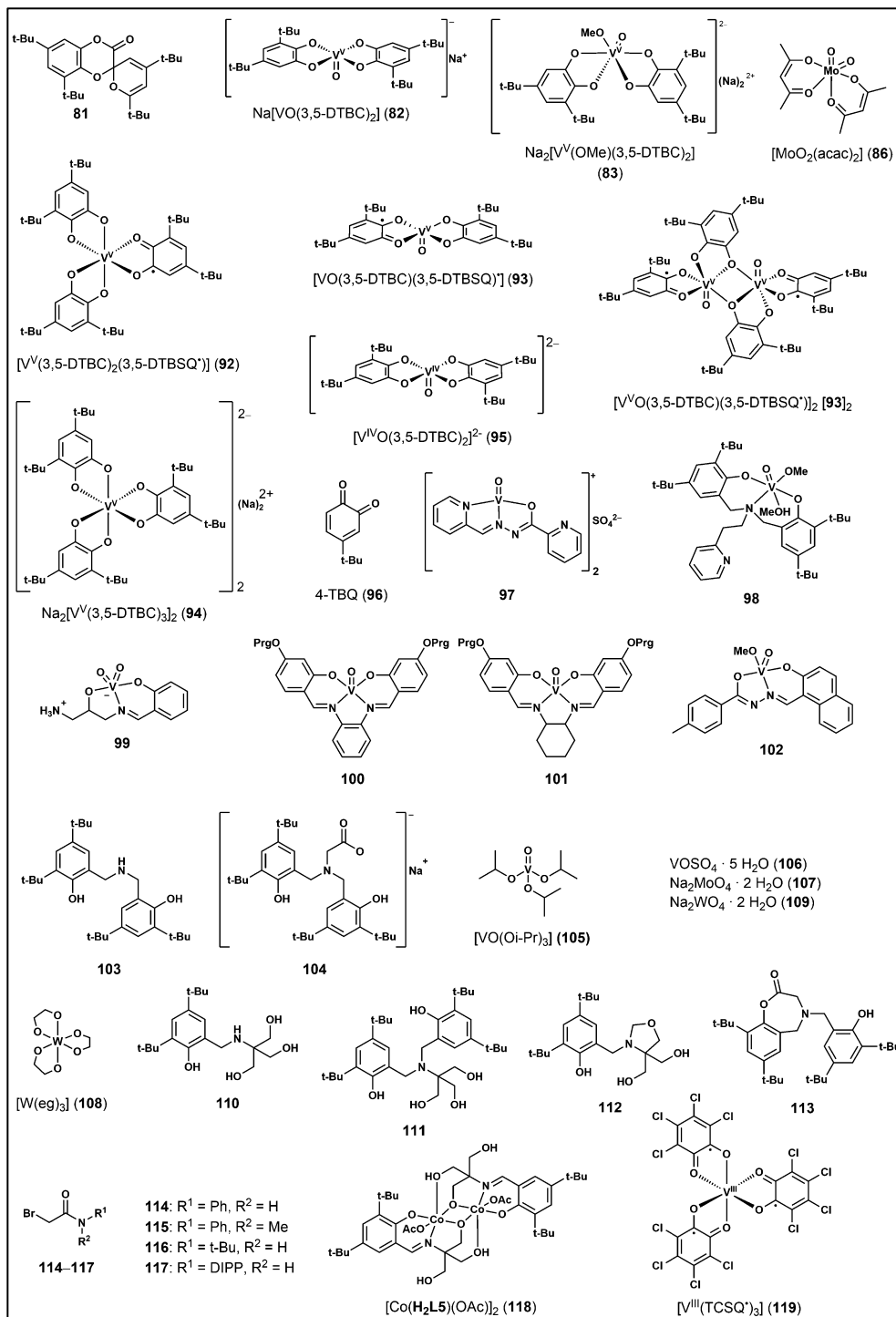
# Appendix

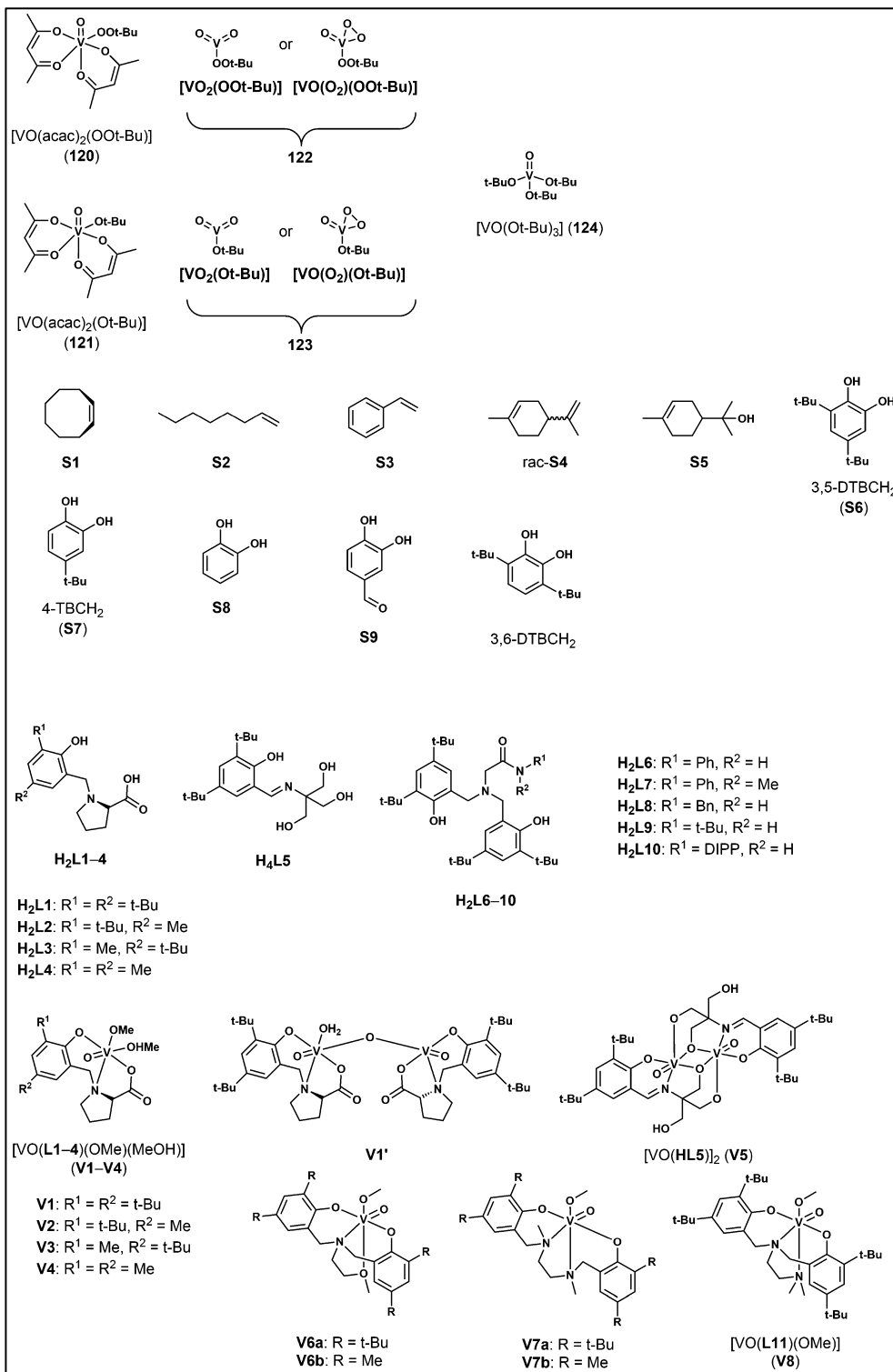
List and structures of all numbered compounds, substrates used in catalysis, as well as proligands and complexes presented throughout this PhD thesis:

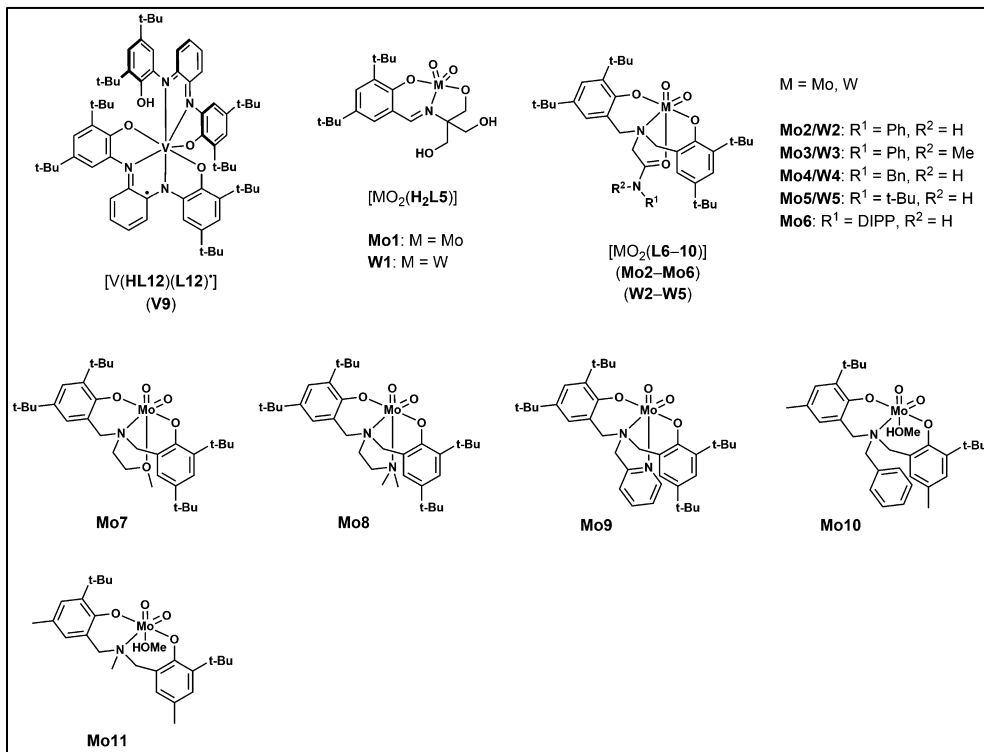












# Acknowledgements

This PhD work was conducted in the Intelligent Materials Chemistry Group (IMCG) laboratories at the Department of Chemistry, University of Turku during 2017 – 2021. The University of Turku Graduate School: Doctoral Programme in Physical and Chemical Sciences (UTUGS: PCS) is greatly acknowledged for full financial support of this project. Additional financial support from UTUGS: PCS, University of Turku Grants and Scholarships, University of Turku Foundation, Fortum foundation and TOP foundation are greatly acknowledged. This support enabled me to present my work at the 2019 Molybdenum and Tungsten Enzyme Conference XI (MoTEC) conference (Potsdam, Germany), as well as make a research visit in Graz, Austria to work in the Mösch-Zanetti research group at the University of Graz.

When I was a little boy, I was fascinated by a children's cartoon called Dexter's Laboratory, one of my favorite TV shows. Dexter had a secret lab hidden in the house, and I used to think that I want to become a scientist when I grow up, just like Dexter. Besides – although obviously lacking a secret lab as a child – I had other things in common with Dexter such as interest in science at a young age, not to mention an annoying big sister. However, part of my decision to choose chemistry instead of building giant death robots must be credited to my upper secondary school chemistry teacher, Jouko “Tane” Tanninen, who was a very inspiring teacher!

First of all, I want to thank the pre-examiners and opponent for finding time to read through my long thesis. My deepest thanks go to my supervisor Dr. Ari Lehtonen who has been very supportive throughout my studies at UTU. You have given me a lot of guidance but also scientific freedom, something I think is very important for a growing scientist to become independent. I will extend my gratitude to the department head Prof. Pasi Virta for all the helpful discussions related to organic synthesis. I then wish to thank my closest work mates and collaborators, starting with Dr. Anssi Peuronen and Dr. Esko Salojärvi. Anssi, you are probably one of the hardest working people I know. Without your expertise related to organic synthesis, single crystal XRD and computational chemistry, my PhD thesis would be but a shadow of what it is now. I think UTU and IMCG in particular are very lucky to have you in their ranks! Thank you Esko for your company in the lab for the past several years, all the helpful discussions and ideas and most of all your

sometimes rather brutal sense of humor! Good luck in your future endeavors. Many thanks to Dr. Risto Savela and Prof. Reko Leino from the Åbo Akademi University (ÅAU) for all the helpful discussions, your contributions and most of all for the opportunity to work at the ÅAU during the first year of my PhD work. Dr. Jari Sinkkonen thank you for showing the ropes concerning NMR spectroscopy, particularly related to  $^{51}\text{V}$  NMR and the various 2D homo- and heteronuclear techniques. Special thanks to Dr. Mika Keränen for a nice introduction into EPR spectroscopy, which proved singularly important in the publication III.

I am very grateful to Prof. Nadia Mösch-Zanetti and Prof. Jörg Schachner from Austria for allowing me to work in Graz in the beginning of 2020 and for your huge contributions to publication IV and in other papers that are yet to come. Thank you Jörg for all the fruitful discussions related to chemistry inside and outside of work; it should be emphasized that the idea for the publication III slowly took shape during the multiple beer/quiz evenings/nights held in Graz.

This separate paragraph is dedicated to the superhumans of the chemistry department, namely Kirsi Laaksonen, Mauri Nauma and Kari Loikas. Thank you Kirsi for your lovely character; it is always a delight to come to chat. You could always be counted on when it came to getting new chemicals. Thank you, IT wizard Kari, for all your help with computer related stuff. It can with reasonable confidence be said that I could not have written my thesis without your help! Thank you, Mauri, for coming to aid when problems occurred in the lab, usually in the form of broken or defective glassware or instruments. Especially I want to thank Mauri for going above and well past his call of duty: he once fixed my bicycle when I fell coming to work during my B.Sc. years, and more recently fixed my coffee maker, without which there was never any real chance for me to finish my PhD work. I wish to also extend my thanks to the Graz equivalent of Kirsi/Mauri/Kari, Doris Eibinger.

I wish to thank my closest friends and colleagues inside and outside of the university who have helped me through my studies in one way or another. A big shoutout not only to all the people at the IMCG, but really the whole chemistry department, for making my time at UTU very enjoyable! I wish to collectively thank the crews of “Ruokaryhmä”, “Maanantain peli-illat” and “Tartsin kiliparyhmä” encompassing Asmo Aro-Heinilä, Oskari Backman, Dr. Ville Eskonen, Tatu Hirvonen, Dr. Jorma Kim, Tapio Lempiäinen, Dr. Ville Tähtinen, Petteri Vainikka, and Saku Valkamaa, and others for the lunch breaks and darts (read: beer) sessions, board game evenings (read: nights), something I always looked forward to! Special thanks go to the crew of HMS Fubar. I want to thank my friends Antti, Atte, Jaakko, Jere, Joel, Juho, Juuso, Lauri, Riku, Ville, Teemu, and others in the Klaani crew. It is always a pleasure meet with you guys! Similarly, I sincerely thank perhaps my oldest friends Santtu Alatalo and Aleksi Saarinen. It is always very enjoyable to meet either person or online; thank you, guys, you are the best! Thank you Dr. Madeleine

Ehweiner and Dr. Carina Vidović, and others including (but not limited to) Fabian, Miljan, Riccardo for your company and for a very memorable stay at Graz!

I sincerely thank my parents Taina and Pekka, and my (not-so-annoying-anymore) big sister Salla and big brother Tero for all your support and just for being there! Although I must admit my mom initially probably never thought I would become a PhD, especially after that one incident involving a certain soup when I was a child.

Last, but certainly not least, I wish to whole-heartedly thank Milla, my companion, friend, and colleague. Throughout my studies at UTU, you have been a constant support and a source of inspiration for me. You have made my days brighter both at home and at work! By the same token, I will also thank our furry and lovely Rosmo-corgi for bringing joy and forcing me outside for walks to cool-off every once in a while.

Turku, October 2021



Pasi Salonen

# List of References

- 1 W. Maret, *Int. J. Mol. Sci.*, 2016, **17**, 66.
- 2 D. H. R. Barton, A. E. Martell and D. T. Sawyer, Eds., *The Activation of Dioxygen and Homogeneous Catalytic Oxidation*, Springer US, Boston, MA, 1993.
- 3 J. A. Brito and M. Archer, in *Practical Approaches to Biological Inorganic Chemistry*, Elsevier, 2020, pp. 375–416.
- 4 R. W. Strange and M. C. Feiters, *Curr. Opin. Struct. Biol.*, 2008, **18**, 609–616.
- 5 W. R. Hagen, *J. Biol. Inorg. Chem.*, 2018, **23**, 623–634.
- 6 K. Wüthrich, *Angew. Chemie Int. Ed.*, 2003, **42**, 3340–3363.
- 7 L. C. Seefeldt, D. R. Dean and B. M. Hoffman, in *Molybdenum and Tungsten Enzymes: Biochemistry*, The Royal Society of Chemistry, 2016, vol. 2017, pp. 274–296.
- 8 L. Que and W. B. Tolman, *Nature*, 2008, **455**, 333–340.
- 9 A. Majumdar and S. Sarkar, *Coord. Chem. Rev.*, 2011, **255**, 1039–1054.
- 10 R. H. Holm, P. Kennepohl and E. I. Solomon, *Chem. Rev.*, 1996, **96**, 2239–2314.
- 11 J. Ibers and R. Holm, *Science (80- )*, 1980, **209**, 223–235.
- 12 A. Butler and J. V Walker, *Chem. Rev.*, 1993, **93**, 1937–1944.
- 13 A. Butler, *Curr. Opin. Chem. Biol.*, 1998, **2**, 279–285.
- 14 A. Butler, *Coord. Chem. Rev.*, 1999, **187**, 17–35.
- 15 A. Butler and J. N. Carter-Franklin, *Nat. Prod. Rep.*, 2004, **21**, 180–188.
- 16 E. J. Allain, L. P. Hager, L. Deng and E. N. Jacobsen, *J. Am. Chem. Soc.*, 1993, **115**, 4415–4416.
- 17 S. Colonna, N. Gaggero, L. Casella, G. Carrea and P. Pasta, *Tetrahedron: Asymmetry*, 1993, **4**, 1325–1330.
- 18 V. M. Dembitsky, *Tetrahedron*, 2003, **59**, 4701–4720.
- 19 A. Messerschmidt and R. Wever, *Proc. Natl. Acad. Sci.*, 1996, **93**, 392–396.
- 20 D. Maity, J. Marek, W. S. Sheldrick, H. Mayer-Figge and M. Ali, *J. Mol. Catal. A Chem.*, 2007, **270**, 153–159.
- 21 V. Conte and G. Licini, *Coord. Chem. Rev.*, 2015, **202–203**, 1–308.
- 22 M. Nozaki, in *Molecular Mechanisms of Oxygen Activation*, Elsevier, 1974, vol. 1955, pp. 135–165.
- 23 A. L. Feig and S. J. Lippard, *Chem. Rev.*, 1994, **94**, 759–805.
- 24 L. Que and R. Y. N. Ho, *Chem. Rev.*, 1996, **96**, 2607–2624.
- 25 M. Costas, M. P. Mehn, M. P. Jensen and L. Que, *Chem. Rev.*, 2004, **104**, 939–986.
- 26 R. A. Sheldon, I. W. C. E. Arends and U. Hanefeld, in *Green Chemistry and Catalysis*, Wiley, 2007, pp. 133–221.
- 27 C. L. Hill and I. A. Weinstock, *Nature*, 1997, **388**, 332–333.
- 28 M. W. Vetting and D. H. Ohlendorf, *Structure*, 2000, **8**, 429–440.
- 29 L. Que, R. C. Kolanczyk and L. S. White, *J. Am. Chem. Soc.*, 1987, **109**, 5373–5380.



- 30 D. D. Cox, S. J. Benkovic, L. M. Bloom, F. C. Bradley, M. J. Nelson, L. Que and D. E. Wallick, *J. Am. Chem. Soc.*, 1988, **110**, 2026–2032.
- 31 H. G. Jang, D. D. Cox and L. Que, *J. Am. Chem. Soc.*, 1991, **113**, 9200–9204.
- 32 A. Dei, D. Gatteschi and L. Pardi, *Inorg. Chem.*, 1993, **32**, 1389–1395.
- 33 C. J. Winfield, Z. Al-Mahrizy, M. Gravestock and T. D. H. Bugg, *J. Chem. Soc. Perkin Trans. 1*, 2000, 3277–3289.
- 34 T. D. H. Bugg and G. Lin, *Chem. Commun.*, 2001, 941–952.
- 35 P. E. M. Siegbahn and F. Haeffner, *J. Am. Chem. Soc.*, 2004, **126**, 8919–8932.
- 36 C. Eicken, B. Krebs and J. C. Sacchettini, *Curr. Opin. Struct. Biol.*, 1999, **9**, 677–683.
- 37 C. Gerdemann, C. Eicken and B. Krebs, *Acc. Chem. Res.*, 2002, **35**, 183–191.
- 38 E. I. Solomon, U. M. Sundaram and T. E. Machonkin, *Chem. Rev.*, 1996, **96**, 2563–2606.
- 39 Q. Wu, D. Yan, Y. Chen, T. Wang, F. Xiong, W. Wei, Y. Lu, W.-Y. Sun, J. J. Li and J. Zhao, *Nat. Commun.*, 2017, **8**, 14227.
- 40 D. Nematollahi and M. Rafiee, *J. Electroanal. Chem.*, 2004, **566**, 31–37.
- 41 M. Corzo-Martínez, N. Corzo, M. Villamiel and M. D. del Castillo, in *Food Biochemistry and Food Processing*, Wiley-Blackwell, Oxford, UK, 2012, pp. 56–83.
- 42 S. K. Dey and A. Mukherjee, *Coord. Chem. Rev.*, 2016, **310**, 80–115.
- 43 I. A. Koval, P. Gamez, C. Belle, K. Selmecezi and J. Reedijk, *Chem. Soc. Rev.*, 2006, **35**, 814.
- 44 J. Ackermann, F. Meyer, E. Kaifer and H. Pritzkow, *Chem. - A Eur. J.*, 2002, **8**, 247–258.
- 45 I. A. Koval, C. Belle, K. Selmecezi, C. Philouze, E. Saint-Aman, A. M. Schuitema, P. Gamez, J.-L. Pierre and J. Reedijk, *JBIC J. Biol. Inorg. Chem.*, 2005, **10**, 739–750.
- 46 E. Monzani, L. Quinti, A. Perotti, L. Casella, M. Gullotti, L. Randaccio, S. Geremia, G. Nardin, P. Faleschini and G. Tabbi, *Inorg. Chem.*, 1998, **37**, 553–562.
- 47 I. A. Koval, K. Selmecezi, C. Belle, C. Philouze, E. Saint-Aman, I. Gautier-Luneau, A. M. Schuitema, M. van Vliet, P. Gamez, O. Roubeau, M. Lützen, B. Krebs, M. Lutz, A. L. Spek, J.-L. Pierre and J. Reedijk, *Chem. - A Eur. J.*, 2006, **12**, 6138–6150.
- 48 S. Mandal, J. Mukherjee, F. Lloret and R. Mukherjee, *Inorg. Chem.*, 2012, **51**, 13148–13161.
- 49 A. Neves, L. M. Rossi, A. J. Bortoluzzi, B. Szpoganicz, C. Wieszicki, E. Schwingel, W. Haase and S. Ostrovsky, *Inorg. Chem.*, 2002, **41**, 1788–1794.
- 50 J. Reim and B. Krebs, *J. Chem. Soc. Dalton Trans.*, 1997, **0**, 3793–3804.
- 51 C. Eicken, F. Zippel, K. Büldt-Karentzopoulos and B. Krebs, *FEBS Lett.*, 1998, **436**, 293–299.
- 52 T. Klabunde, C. Eicken, J. C. Sacchettini and B. Krebs, *Nat. Struct. Biol.*, 1998, **5**, 1084–1090.
- 53 R. Hille, *Dalt. Trans.*, 2013, **42**, 3029–3042.
- 54 R. Hille, *Trends Biochem. Sci.*, 2002, **27**, 360–367.
- 55 R. H. Holm, *Chem. Rev.*, 1987, **87**, 1401–1449.
- 56 R. Hille, J. Hall and P. Basu, *Chem. Rev.*, 2014, **114**, 3963–4038.
- 57 M. K. Johnson, D. C. Rees and M. W. W. Adams, *Chem. Rev.*, 1996, **96**, 2817–2840.
- 58 R. Hille, *Chem. Rev.*, 1996, **96**, 2757–2816.
- 59 C. Kisker, H. Schindelin, A. Pacheco, W. A. Wehbi, R. M. Garrett, K. V. Rajagopalan, J. H. Enemark and D. C. Rees, *Cell*, 1997, **91**, 973–983.
- 60 C. Schulzke, *Eur. J. Inorg. Chem.*, 2011, **2011**, 1189–1199.
- 61 In *IUPAC Compendium of Chemical Terminology*, IUPAC, Research Triangle Park, NC.
- 62 G. Sharma, P. Krishna, V. Doddi, S. Kashyap and P. Reddy, in *Industrial Catalysis and Separations*, Apple Academic Press, 2014, pp. 329–374.
- 63 A. S. Goldman, C. R. Landis and A. Sen, *Angew. Chemie Int. Ed.*, 2018, **57**, 4460–4460.
- 64 C. M. Hagen, L. Vieille-Petit, G. Laurency, G. Süss-Fink and R. G. Finke, *Organometallics*, 2005, **24**, 1819–1831.

- 65 S. Bhaduri and D. Mukesh, *Homogeneous Catalysis: Mechanisms and Industrial Applications*, John Wiley & Sons, Inc., New York, USA, 1st edn., 2000.
- 66 S. Kozuch and J. M. L. Martin, *ACS Catal.*, 2012, **2**, 2787–2794.
- 67 M. Pratt, J. B. Harper and S. B. Colbran, *Dalt. Trans.*, 2007, 2746.
- 68 R. A. Sheldon and J. K. Kochi, in *Advances in Catalysis*, 1976, vol. 25, pp. 272–413.
- 69 L. M. Peschel, F. Belaj, J. A. Schachner and N. C. Mösch-Zanetti, *Eur. J. Inorg. Chem.*, 2017, **2017**, 2808–2817.
- 70 I. W. C. E. Arends and R. A. Sheldon, *Appl. Catal. A Gen.*, 2001, **212**, 175–187.
- 71 P. Anastas and N. Eghbali, *Chem. Soc. Rev.*, 2010, **39**, 301–312.
- 72 S. Enthaler, K. Junge and M. Beller, *Angew. Chemie Int. Ed.*, 2008, **47**, 3317–3321.
- 73 B. Trost, *Science (80-. )*, 1991, **254**, 1471–1477.
- 74 R. A. Sheldon, *Green Chem.*, 2007, **9**, 1273.
- 75 T. A. Nijhuis, M. Makkee, J. A. Moulijn and B. M. Weckhuysen, *Ind. Eng. Chem. Res.*, 2006, **45**, 3447–3459.
- 76 D. Kahlich, U. Wiechern and J. Lindner, in *Ullmann's Encyclopedia of Industrial Chemistry*, Wiley-VCH Verlag GmbH & Co. KGaA, Weinheim, Germany, 2011, p. 100.
- 77 K. Alfonsi, J. Colberg, P. J. Dunn, T. Fevig, S. Jennings, T. A. Johnson, H. P. Kleine, C. Knight, M. A. Nagy, D. A. Perry and M. Stefaniak, *Green Chem.*, 2008, **10**, 31–36.
- 78 M. Castro-Puyana, M. L. Marina and M. Plaza, *Curr. Opin. Green Sustain. Chem.*, 2017, **5**, 31–36.
- 79 J. Muzart, *Adv. Synth. Catal.*, 2006, **348**, 275–295.
- 80 D. Betz, P. Altmann, M. Cokoja, W. A. Herrmann and F. E. Kühn, *Coord. Chem. Rev.*, 2011, **255**, 1518–1540.
- 81 T. P. Thuy Pham, C.-W. Cho and Y.-S. Yun, *Water Res.*, 2010, **44**, 352–372.
- 82 A. Günyar, D. Betz, M. Drees, E. Herdtweck and F. E. Kühn, *J. Mol. Catal. A Chem.*, 2010, **331**, 117–124.
- 83 R. A. Sheldon, in *Studies in Surface Science and Catalysis*, 1990, vol. 55, pp. 1–32.
- 84 R. A. Sheldon, I. W. C. E. Arends and U. Hanefeld, in *Green Chemistry and Catalysis*, Wiley, 2007, pp. 1–47.
- 85 R. Noyori, M. Aoki and K. Sato, *Chem. Commun.*, 2003, **14**, 1977–1986.
- 86 H. Yao and D. E. Richardson, *J. Am. Chem. Soc.*, 2000, **122**, 3220–3221.
- 87 D. E. Richardson, H. Yao, K. M. Frank and D. A. Bennett, *J. Am. Chem. Soc.*, 2000, **122**, 1729–1739.
- 88 J. A. Connor and E. A. V. Ebsworth, in *Advances in Inorganic Chemistry and Radiochemistry*, 1964, vol. 6, pp. 279–381.
- 89 R. A. Sheldon and J. K. Kochi, in *Metal-catalyzed Oxidations of Organic Compounds*, Elsevier, 1981, vol. 261, pp. 271–314.
- 90 K. B. Sharpless and T. R. Verhoeven, *Aldrichim. Acta*, 1979, **12**, 63–74.
- 91 J.-M. Brégeault, *Dalt. Trans.*, 2003, 3289–3302.
- 92 R. A. Sheldon, *J. Mol. Catal.*, 1980, **7**, 107–126.
- 93 S. H. Zhao, O. Samuel and H. B. Kagan, *Tetrahedron*, 1987, **43**, 5135–5144.
- 94 G. Siemel, R. Rieth and K. T. Rowbottom, in *Ullmann's Encyclopedia of Industrial Chemistry*, Wiley-VCH Verlag GmbH & Co. KGaA, Weinheim, Germany, 2000, pp. 8676–8694.
- 95 A. K. Yudin, *Aziridines and Epoxides in Organic Synthesis*, Wiley, 2006.
- 96 K. Faber, M. Mischitz and W. Kroutil, *Acta Chem. Scand.*, 1996, **50**, 249–258.
- 97 A. Archelas and R. Furstoss, in *Biocatalysis - From Discovery to Application*, eds. W.-D. Fessner, A. Archelas, D. C. Demirjian, R. Furstoss, H. Griengl, K.-E. Jaeger, E. Morís-Varas, R. Öhrlein,

- M. T. Reetz, J.-L. Reymond, M. Schmidt, S. Servi, P. C. Shah, W. Tischer and F. Wedekind, Springer Verlag, Berlin, Heidelberg, 200th edn., 1999, pp. 159–191.
- 98 M. G. Clerici, M. Ricci and G. Strukul, in *Metal-catalysis in Industrial Organic Processes*, Royal Society of Chemistry, Cambridge, 2007, pp. 23–78.
- 99 K. Holmberg, in *Ullmann's Encyclopedia of Industrial Chemistry*, Wiley-VCH Verlag GmbH & Co. KGaA, Weinheim, Germany, 2019, vol. 16, pp. 1–56.
- 100 Ericson Polymer Corporation, US Patent 3,876,581, 1975.
- 101 B. M. Lipinski, L. S. Morris, M. N. Silberstein and G. W. Coates, *J. Am. Chem. Soc.*, 2020, **142**, 6800–6806.
- 102 Halcon International, Inc., US Patent 3,351,635, 1967.
- 103 Halcon International, Inc., US Patent 3,350,422, 1967.
- 104 Halcon Industrial Inc., US Patent 3,507,809, 1970.
- 105 N. Prileschajew, *Berichte der Dtsch. Chem. Gesellschaft*, 1909, **42**, 4811–4815.
- 106 D. Swern, in *Organic Reactions*, John Wiley & Sons, Inc., Hoboken, NJ, USA, 2011, pp. 378–434.
- 107 S. A. Hauser, M. Cokoja and F. E. Kühn, *Catal. Sci. Technol.*, 2013, **3**, 552–561.
- 108 U. Neuenschwander and I. Hermans, *J. Org. Chem.*, 2011, **76**, 10236–10240.
- 109 A. Schmidt, N. Grover, T. K. Zimmermann, L. Graser, M. Cokoja, A. Pöthig and F. E. Kühn, *J. Catal.*, 2014, **319**, 119–126.
- 110 J. Morlot, N. Uytendroeck, D. Agustin and R. Poli, *ChemCatChem*, 2013, **5**, 601–611.
- 111 M. Abrantes, A. M. Santos, J. Mink, F. E. Kühn and C. C. Romão, *Organometallics*, 2003, **22**, 2112–2118.
- 112 M. R. Maurya, C. Haldar, A. A. Khan, A. Azam, A. Salahuddin, A. Kumar and J. Costa Pessoa, *Eur. J. Inorg. Chem.*, 2012, **2012**, 2560–2577.
- 113 M. E. Judmaier, C. H. Sala, F. Belaj, M. Volpe and N. C. Mösch-Zanetti, *New J. Chem.*, 2013, **37**, 2139–2149.
- 114 A. O. Chong and K. B. Sharpless, *J. Org. Chem.*, 1977, **42**, 1587–1590.
- 115 P. J. Costa, M. J. Calhorda and F. E. Kühn, *Organometallics*, 2010, **29**, 303–311.
- 116 F. E. Kühn, M. Groarke, É. Bencze, E. Herdtweck, A. Prazeres, A. M. Santos, M. J. Calhorda, C. C. Romão, I. S. Gonçalves, A. D. Lopes and M. Pillinger, *Chem. - A Eur. J.*, 2002, **8**, 2370.
- 117 L. F. Veiros, Â. Prazeres, P. J. Costa, C. C. Romão, F. E. Kühn and M. José Calhorda, *Dalt. Trans.*, 2006, **60**, 1383.
- 118 A. Comas-Vives, A. Lledós and R. Poli, *Chem. - A Eur. J.*, 2010, **16**, 2147–2158.
- 119 C. Dinoi, M. Ciclosi, E. Manoury, L. Maron, L. Perrin and R. Poli, *Chem. - A Eur. J.*, 2010, **16**, 9572–9584.
- 120 J. Zhao, A. M. Santos, E. Herdtweck and F. E. Kühn, *J. Mol. Catal. A Chem.*, 2004, **222**, 265–271.
- 121 F. E. Kühn, W.-M. Xue, A. Al-Ajlouni, A. M. Santos, S. Zang, C. C. Romão, G. Eickerling and E. Herdtweck, *Inorg. Chem.*, 2002, **41**, 4468–4477.
- 122 H. Mimoun, I. Serec de Roch and L. Sajus, *Tetrahedron*, 1970, **26**, 37–50.
- 123 D. V. Deubel, G. Frenking, P. Gisdakis, W. A. Herrmann, N. Rösch and J. Sundermeyer, *Acc. Chem. Res.*, 2004, **37**, 645–652.
- 124 K. B. Sharpless, J. M. Townsend and D. R. Williams, *J. Am. Chem. Soc.*, 1972, **94**, 295–296.
- 125 D. A. Singleton, S. R. Merrigan, J. Liu and K. N. Houk, *J. Am. Chem. Soc.*, 1997, **119**, 3385–3386.
- 126 A. J. DelMonte, J. Haller, K. N. Houk, K. B. Sharpless, D. A. Singleton, T. Strassner and A. A. Thomas, *J. Am. Chem. Soc.*, 1997, **119**, 9907–9908.

- 127 D. V. Deubel, J. Sundermeyer and G. Frenking, *J. Am. Chem. Soc.*, 2000, **122**, 10101–10108.
- 128 M. L. Kuznetsov and J. C. Pessoa, *Dalt. Trans.*, 2009, 5460.
- 129 R. C. Michaelson, R. E. Palermo and K. B. Sharpless, *J. Am. Chem. Soc.*, 1977, **99**, 1990–1992.
- 130 M. G. Finn and K. B. Sharpless, *J. Am. Chem. Soc.*, 1991, **113**, 113–126.
- 131 W. R. Thiel and J. Eppinger, *Chem. - A Eur. J.*, 1997, **3**, 696–705.
- 132 W. R. Thiel and T. Priermeier, *Angew. Chemie Int. Ed.*, 1995, **34**, 1737–1738.
- 133 W. R. Thiel, *J. Mol. Catal. A Chem.*, 1997, **117**, 449–454.
- 134 F. E. Kühn, A. M. Santos and M. Abrantes, *Chem. Rev.*, 2006, **106**, 2455–2475.
- 135 C. Müller, N. Grover, M. Cokoja and F. E. Kühn, in *Advances in Inorganic Chemistry*, 2013, vol. 65, pp. 33–83.
- 136 A. M. Martins, C. C. Romão, M. Abrantes, M. C. Azevedo, J. Cui, A. R. Dias, M. T. Duarte, M. A. Lemos, T. Lourenço and R. Poli, *Organometallics*, 2005, **24**, 2582–2589.
- 137 N. Grover, A. Pöthig and F. E. Kühn, *Catal. Sci. Technol.*, 2014, **4**, 4219–4231.
- 138 L. Graser, R. M. Reich, M. Cokoja, A. Pöthig and F. E. Kühn, *Catal. Sci. Technol.*, 2015, **5**, 4772–4777.
- 139 W. A. Herrmann, J. J. Haider, J. Fridgen, G. M. Lobmaier and M. Spiegler, *J. Organomet. Chem.*, 2000, **603**, 69–79.
- 140 D. Betz, A. Raith, M. Cokoja and F. E. Kühn, *ChemSusChem*, 2010, **3**, 559–562.
- 141 W. A. Herrmann, *Angew. Chemie Int. Ed. English*, 1988, **27**, 1297–1313.
- 142 W. A. Herrmann, R. W. Fischer and D. W. Marz, *Angew. Chemie Int. Ed. English*, 1991, **30**, 1638–1641.
- 143 M. Cousins and M. L. H. Green, *J. Chem. Soc.*, 1964, 1567.
- 144 E. Collange, L. Metteau, P. Richard and R. Poli, *Polyhedron*, 2004, **23**, 2605–2610.
- 145 J. M. O'Connor and C. P. Casey, *Chem. Rev.*, 1987, **87**, 307–318.
- 146 F. E. Kühn, E. Herdtweck, J. J. Haider, W. A. Herrmann, I. S. Gonçalves, A. D. Lopes and C. C. Romão, *J. Organomet. Chem.*, 1999, **583**, 3–10.
- 147 F. E. Kühn, A. D. Lopes, A. M. Santos, E. Herdtweck, J. J. Haider, C. C. Romão and A. G. Santos, *J. Mol. Catal. A Chem.*, 2000, **151**, 147–160.
- 148 F. E. Kühn, A. M. Santos, I. S. Gonçalves, C. C. Romão and A. D. Lopes, *Appl. Organomet. Chem.*, 2001, **15**, 43–50.
- 149 F. E. Kühn, A. M. Santos, A. D. Lopes, I. S. Gonçalves, J. E. Rodríguez-Borges, M. Pillinger and C. C. Romão, *J. Organomet. Chem.*, 2001, **621**, 207–217.
- 150 I. Gonçalves, *J. Organomet. Chem.*, 2001, **626**, 1–10.
- 151 F. E. Kühn, A. M. Santos, A. D. Lopes, I. S. Gonçalves, E. Herdtweck and C. C. Romão, *J. Mol. Catal. A Chem.*, 2000, **164**, 25–38.
- 152 C. C. L. Pereira, S. S. Balula, F. A. Almeida Paz, A. A. Valente, M. Pillinger, J. Klinowski and I. S. Gonçalves, *Inorg. Chem.*, 2007, **46**, 8508–8510.
- 153 D. Martínez-Martínez, M. L. Santiago, R. A. Toscano and M. Amézquita-Valencia, *Eur. J. Inorg. Chem.*, 2021, **2021**, 243–251.
- 154 J. A. Schachner, P. Traar, C. Sala, M. Melcher, B. N. Harum, A. F. Sax, M. Volpe, F. Belaj and N. C. Mösch-Zanetti, *Inorg. Chem.*, 2012, **51**, 7642–7649.
- 155 M. Bagherzadeh, L. Tahsini, R. Latifi and L. Keith Woo, *Inorganica Chim. Acta*, 2009, **362**, 3698–3702.
- 156 S. Krackl, A. Company, S. Enthaler and M. Driess, *ChemCatChem*, 2011, **3**, 1186–1192.
- 157 O. Wichmann, R. Sillanpää and A. Lehtonen, *Coord. Chem. Rev.*, 2012, **256**, 371–392.
- 158 J. M. Mitchell and N. S. Finney, *J. Am. Chem. Soc.*, 2001, **123**, 862–869.

- 159 Y. Wong, Y. Yan, E. S. H. Chan, Q. Yang, T. C. W. Mak and D. K. P. Ng, *J. Chem. Soc. Dalton Trans.*, 1998, **2**, 3057–3064.
- 160 Y.-L. Wong, L. H. Tong, J. R. Dilworth, D. K. P. Ng and H. K. Lee, *Dalt. Trans.*, 2010, **39**, 4602–4611.
- 161 X. Lei and N. Chelamalla, *Polyhedron*, 2013, **49**, 244–251.
- 162 M. K. Hossain, M. Haukka, G. C. Lisensky, A. Lehtonen and E. Nordlander, *Inorganica Chim. Acta*, 2019, **487**, 112–119.
- 163 M. K. Hossain, M. Haukka, R. Sillanpää, D. A. Hrovat, M. G. Richmond, E. Nordlander and A. Lehtonen, *Dalt. Trans.*, 2017, **46**, 7051–7060.
- 164 A. Dupé, M. K. Hossain, J. A. Schachner, F. Belaj, A. Lehtonen, E. Nordlander and N. C. Mösch-Zanetti, *Eur. J. Inorg. Chem.*, 2015, **2015**, 3572–3579.
- 165 M. K. Hossain, J. A. Schachner, M. Haukka, A. Lehtonen, N. C. Mösch-Zanetti and E. Nordlander, *Polyhedron*, 2017, **134**, 275–281.
- 166 M. K. Hossain, J. A. Schachner, M. Haukka, N. C. Mösch-Zanetti, E. Nordlander and A. Lehtonen, *Inorganica Chim. Acta*, 2019, **486**, 17–25.
- 167 M. K. Hossain, PhD thesis: *High Valent Metal Oxo Complexes as Oxidation Catalysts*, Lund University, 2017.
- 168 N. Zwettler, J. A. Schachner, F. Belaj and N. C. Mösch-Zanetti, *Mol. Catal.*, 2017, **443**, 209–219.
- 169 F. Romano, A. Linden, M. Mba, C. Zonta and G. Licini, *Adv. Synth. Catal.*, 2010, **352**, 2937–2942.
- 170 A. U. Barlan, A. Basak and H. Yamamoto, *Angew. Chemie - Int. Ed.*, 2006, **45**, 5849–5852.
- 171 S. K. Maiti, K. M. A. Malik, S. Gupta, S. Chakraborty, A. K. Ganguli, A. K. Mukherjee and R. Bhattacharyya, *Inorg. Chem.*, 2006, **45**, 9843–9857.
- 172 S. K. Maiti, S. Dinda, S. Banerjee, A. K. Mukherjee and R. Bhattacharyya, *Eur. J. Inorg. Chem.*, 2008, **2008**, 2038–2051.
- 173 P. G. Cozzi, *Chem. Soc. Rev.*, 2004, **33**, 410–421.
- 174 A. Syamal and M. R. Maurya, *Coord. Chem. Rev.*, 1989, **95**, 183–238.
- 175 W. Wang, T. Guerrero, S. R. Mercias, H. García-Ortega, R. Santillan, J.-C. Daran, N. Farfán, D. Agustin and R. Poli, *Inorganica Chim. Acta*, 2015, **431**, 176–183.
- 176 W. Wang, T. Vanderbeek, D. Agustin and R. Poli, *Catal. Commun.*, 2015, **63**, 26–30.
- 177 S. M. Bruno, S. S. Balula, A. A. Valente, F. A. Almeida Paz, M. Pillinger, C. Sousa, J. Klinowski, C. Freire, P. Ribeiro-Claro and I. S. Gonçalves, *J. Mol. Catal. A Chem.*, 2007, **270**, 185–194.
- 178 S. N. Rao, N. Kathale, N. N. Rao and K. N. Munshi, *Inorganica Chim. Acta*, 2007, **360**, 4010–4016.
- 179 W. Wang, J.-C. Daran, R. Poli and D. Agustin, *J. Mol. Catal. A Chem.*, 2016, **416**, 117–126.
- 180 Y. Sui, X. Zeng, X. Fang, X. Fu, Y. Xiao, L. Chen, M. Li and S. Cheng, *J. Mol. Catal. A Chem.*, 2007, **270**, 61–67.
- 181 A. Rezaeifard, I. Sheikhsaie, N. Monadi and M. Alipour, *Polyhedron*, 2010, **29**, 2703–2709.
- 182 A. Rezaeifard, I. Sheikhsaie, M. Monadi and H. Stoeckli-Evans, *Eur. J. Inorg. Chem.*, 2010, 799–806.
- 183 J. Pisk, D. Agustin, V. Vrdoljak and R. Poli, *Adv. Synth. Catal.*, 2011, **353**, 2910–2914.
- 184 T. A. Dar, B. Uprety, M. Sankar and M. R. Maurya, *Green Chem.*, 2019, **21**, 1757–1768.
- 185 R. Kumar, N. Chaudhary, M. Sankar and M. R. Maurya, *Dalt. Trans.*, 2015, **44**, 17720–17729.
- 186 W. A. Herrmann, G. M. Lobmaier, T. Priermeier, M. R. Mattner and B. Scharbert, *J. Mol. Catal. A Chem.*, 1997, **117**, 455–469.
- 187 S. N. Rao, K. N. Munshi, N. N. Rao, M. M. Bhadbhade and E. Suresh, *Polyhedron*, 1999, **18**, 2491–2497.

- 188 M. A. Katkar, S. N. Rao and H. D. Juneja, *RSC Adv.*, 2012, **2**, 8071.
- 189 T. D. H. Bugg, *Tetrahedron*, 2003, **59**, 7075–7101.
- 190 J. Mukherjee and R. Mukherjee, *Inorganica Chim. Acta*, 2002, **337**, 429–438.
- 191 U. Casellato, S. Tamburini, P. A. Vigato, M. Vidali and D. E. Fenton, *Inorganica Chim. Acta*, 1984, **84**, 101–104.
- 192 R. R. Grinstead, *Biochemistry*, 1964, **3**, 1308–1314.
- 193 Y. Tatsuno, C. Nakamura and T. Saito, *J. Mol. Catal.*, 1987, **42**, 57–66.
- 194 C. A. Tyson and A. E. Martell, *J. Phys. Chem.*, 1970, **74**, 2601–2610.
- 195 C. G. Pierpont and C. W. Lange, in *Progress in Inorganic Chemistry*, 2007, vol. 41, pp. 331–442.
- 196 C. G. Pierpont and R. M. Buchanan, *Coord. Chem. Rev.*, 1981, **38**, 45–87.
- 197 R. M. Buchanan and C. G. Pierpont, *Inorg. Chem.*, 1979, **18**, 1616–1620.
- 198 P. J. Bosserman and D. T. Sawyer, *Inorg. Chem.*, 1982, **21**, 1545–1551.
- 199 J. P. Wilshire and D. T. Sawyer, *J. Am. Chem. Soc.*, 1978, **100**, 3972–3973.
- 200 M. D. Stallings, M. M. Morrison and D. T. Sawyer, *Inorg. Chem.*, 1981, **20**, 2655–2660.
- 201 M. C. Lim and D. T. Sawyer, *Inorg. Chem.*, 1982, **21**, 2839–2841.
- 202 M. E. Cass, D. L. Green, R. M. Buchanan and C. G. Pierpont, *J. Am. Chem. Soc.*, 1983, **105**, 2680–2686.
- 203 C. L. Simpson and C. G. Pierpont, *Inorg. Chem.*, 1992, **31**, 4308–4313.
- 204 S. R. Cooper, Y. B. Koh and K. N. Raymond, *J. Am. Chem. Soc.*, 1982, **104**, 5092–5102.
- 205 M. E. Cass, N. R. Gordon and C. G. Pierpont, *Inorg. Chem.*, 1986, **25**, 3962–3967.
- 206 C. R. Cornman, G. J. Colpas, J. D. Hoeschele, J. Kampf and V. L. Pecoraro, *J. Am. Chem. Soc.*, 1992, **114**, 9925–9933.
- 207 E. Salojärvi, PhD thesis: *The Optical And Redox-Active d-Block Metal Complexes With Non-Innocent Ligands*, University of Turku, 2021.
- 208 Y. Tatsuno, M. Tatsuda and S. Otsuka, *J. Chem. Soc. Chem. Commun.*, 1982, **1982**, 1100.
- 209 B. Galeffi, M. Postel, A. Grand and P. Rey, *Inorganica Chim. Acta*, 1987, **129**, 1–5.
- 210 T. Funabiki, A. Mizoguchi, T. Sugimoto, S. Tada, T. Mitsuji, H. Sakamoto and S. Yoshida, *J. Am. Chem. Soc.*, 1986, **108**, 2921–2932.
- 211 H. Weiner and R. G. Finke, *J. Am. Chem. Soc.*, 1999, **121**, 9831–9842.
- 212 C. X. Yin and R. G. Finke, *J. Am. Chem. Soc.*, 2005, **127**, 13988–13996.
- 213 C.-X. Yin, Y. Sasaki and R. G. Finke, *Inorg. Chem.*, 2005, **44**, 8521–8530.
- 214 C.-X. Yin and R. G. Finke, *J. Am. Chem. Soc.*, 2005, **127**, 9003–9013.
- 215 K. Nomiya, K. Yagishita, Y. Nemoto and T. Kamataki, *J. Mol. Catal. A Chem.*, 1997, **126**, 43–53.
- 216 K. Nomiya, H. Yanagibayashi, C. Nozaki, K. Kondoh, E. Hiramatsu and Y. Shimizu, *J. Mol. Catal. A Chem.*, 1996, **114**, 181–190.
- 217 A. M. Morris, C. G. Pierpont and R. G. Finke, *J. Mol. Catal. A Chem.*, 2009, **309**, 137–145.
- 218 M. Rolff, J. Schottenheim, H. Decker and F. Tuzcek, *Chem. Soc. Rev.*, 2011, **40**, 4077.
- 219 S. K. Dey and A. Mukherjee, *New J. Chem.*, 2014, **38**, 4985–4995.
- 220 M. Mitra, A. K. Maji, B. K. Ghosh, P. Raghavaiah, J. Ribas and R. Ghosh, *Polyhedron*, 2014, **67**, 19–26.
- 221 M. U. Triller, D. Pursche, W.-Y. Hsieh, V. L. Pecoraro, A. Rompel and B. Krebs, *Inorg. Chem.*, 2003, **42**, 6274–6283.
- 222 S. K. Mal, M. Mitra, H. R. Yadav, C. S. Purohit, A. R. Choudhury and R. Ghosh, *Polyhedron*, 2016, **111**, 118–122.
- 223 C. Balakrishnan and M. A. Neelakantan, *Inorganica Chim. Acta*, 2018, **469**, 503–514.

- 224 M. R. Maurya, B. Uprety, F. Avecilla, P. Adão and J. Costa Pessoa, *Dalt. Trans.*, 2015, **44**, 17736–17755.
- 225 M. R. Maurya, B. Uprety, F. Avecilla, P. Adão, M. L. Kuznetsov and J. Costa Pessoa, *Eur. J. Inorg. Chem.*, 2017, **2017**, 3087–3099.
- 226 B. Baruah and A. Chakravorty, *Indian J. Chem.*, 2003, **42A**, 2677–2679.
- 227 B. Baruah, S. Das and A. Chakravorty, *Inorg. Chem.*, 2002, **41**, 4502–4508.
- 228 S. P. Rath, K. K. Rajak and A. Chakravorty, *Inorg. Chem.*, 1999, **38**, 4376–4377.
- 229 A. A. El-Taras, I. M. EL-Mehasseb and A. E.-M. M. Ramadan, *Comptes Rendus Chim.*, 2012, **15**, 298–310.
- 230 X.-F. Hu and L. Wu, *Chem. Pap.*, 2012, **66**, 211–215.
- 231 S. Ta, M. Ghosh, K. Ghosh, P. Brandão, V. Félix, S. K. Hira, P. P. Manna and D. Das, *ACS Appl. Bio Mater.*, 2019, **2**, 2802–2811.
- 232 G. R. Fulmer, A. J. M. Miller, N. H. Sherden, H. E. Gottlieb, A. Nudelman, B. M. Stoltz, J. E. Bercaw and K. I. Goldberg, *Organometallics*, 2010, **29**, 2176–2179.
- 233 R. K. Harris, E. D. Becker, S. M. Cabral de Menezes, R. Goodfellow and P. Granger, *Magn. Reson. Chem.*, 2002, **40**, 489–505.
- 234 R. R. Gagne, C. A. Koval and G. C. Lisensky, *Inorg. Chem.*, 1980, **19**, 2854–2855.
- 235 CrysAlisPRO, 2014.
- 236 R. W. W. Hooft, Nonius BV, Delft, The Netherlands, 1998.
- 237 Z. Otwinowski and W. Minor, in *Methods in Enzymology*, eds. C. W. J. Carter and R. M. Sweet, New York, USA, 1997, pp. 307–326.
- 238 Bruker (2012), *SADABS*, Bruker ACS Inc., Madison, Wisconsin, USA.
- 239 O. V. Dolomanov, L. J. Bourhis, R. J. Gildea, J. A. K. Howard and H. Puschmann, *J. Appl. Crystallogr.*, 2009, **42**, 339–341.
- 240 G. M. Sheldrick, *Acta Crystallogr. Sect. A Found. Crystallogr.*, 2008, **64**, 112–122.
- 241 G. M. Sheldrick, *Acta Crystallogr. Sect. A Found. Adv.*, 2015, **71**, 3–8.
- 242 G. M. Sheldrick, *Acta Crystallogr. Sect. C Struct. Chem.*, 2015, **71**, 3–8.
- 243 H. Sheykhi and E. Safaei, *Spectrochim. Acta Part A Mol. Biomol. Spectrosc.*, 2014, **118**, 915–920.
- 244 I. S. Belostotskaya, N. L. Komissarova, T. I. Prokof'eva, L. N. Kurkovskaya and V. B. Vol'eva, *Russ. J. Org. Chem.*, 2005, **41**, 703–706.
- 245 D. Wang, S. V. Lindeman and A. T. Fiedler, *Inorganica Chim. Acta*, 2014, **421**, 559–567.
- 246 A. Trapero, A. Pacitto, V. Singh, M. Sabbah, A. G. Coyne, V. Mizrahi, T. L. Blundell, D. B. Ascher and C. Abell, *J. Med. Chem.*, 2018, **61**, 2806–2822.
- 247 T. E. Hurst, R. M. Gorman, P. Drouhin, A. Perry and R. J. K. Taylor, *Chem. - A Eur. J.*, 2014, **20**, 14063–14073.
- 248 A. M. R. Smith, H. S. Rzepa, A. J. P. White, D. Billen and K. K. Hii, *J. Org. Chem.*, 2010, **75**, 3085–3096.
- 249 M. R. Kumar, K. Park and S. Lee, *Adv. Synth. Catal.*, 2010, **352**, 3255–3266.
- 250 A. Leggio, E. L. Belsito, G. De Luca, M. L. Di Gioia, V. Leotta, E. Romio, C. Siciliano and A. Liguori, *RSC Adv.*, 2016, **6**, 34468–34475.
- 251 S. Barroso, P. Adão, A. M. Coelho, J. C. Pessoa and A. M. Martins, *J. Mol. Catal. A Chem.*, 2016, **412**, 107–116.
- 252 G. J. J. Chen, J. W. McDonald and W. E. Newton, *Inorg. Chem.*, 1976, **15**, 2612–2615.
- 253 F. A. Schröder and J. Scherle, *Zeitschrift für Naturforsch. B*, 1973, **28**, 46–55.
- 254 E. Y. Tshuva, I. Goldberg, M. Kol and Z. Goldschmidt, *Organometallics*, 2001, **20**, 3017–3028.

- 255 P. Chaudhuri, M. Hess, J. Müller, K. Hildenbrand, E. Bill, T. Weyhermüller and K. Wieghardt, *J. Am. Chem. Soc.*, 1999, **121**, 9599–9610.
- 256 P. Salonen, A. Peuronen and A. Lehtonen, *Inorg. Chem. Commun.*, 2017, **86**, 165–167.
- 257 D. Maity, A. Ray, W. S. Sheldrick, H. M. Figge, B. Bandyopadhyay and M. Ali, *Inorganica Chim. Acta*, 2006, **359**, 3197–3204.
- 258 M. Debnath, A. Dutta, S. Biswas, K. K. Das, H. M. Lee, J. Vícha, R. Marek, J. Marek and M. Ali, *Polyhedron*, 2013, **63**, 189–198.
- 259 E. Salojärvi, A. Peuronen, M. Lahtinen, H. Huhtinen, L. S. Vlasenko, M. Lastusaari and A. Lehtonen, *Molecules*, 2020, **25**, 2531.
- 260 A. Lehtonen, M. Wasberg and R. Sillanpää, *Polyhedron*, 2006, **25**, 767–775.
- 261 J. A. Schachner, N. C. Mösch-Zanetti, A. Peuronen and A. Lehtonen, *Polyhedron*, 2017, **134**, 73–78.
- 262 T. C. Siu, I. Silva, M. J. Lunn and A. John, *New J. Chem.*, 2020, **44**, 9933–9941.
- 263 A. Peuronen and A. Lehtonen, *Top. Catal.*, 2016, **59**, 1132–1137.
- 264 W. Flaig, T. Ploetz and A. Küllmer, *Zeitschrift für Naturforsch. B*, 1955, **10**, 668–676.
- 265 L. M. Rzepecki and J. H. Waite, *Anal. Biochem.*, 1989, **179**, 375–381.
- 266 K. Ambroziak, Z. Rozwadowski, T. Dziembowska and B. Bieg, *J. Mol. Struct.*, 2002, **615**, 109–120.
- 267 R. M. Claramunt, C. López, M. D. Santa María, D. Sanz and J. Elguero, *Prog. Nucl. Magn. Reson. Spectrosc.*, 2006, **49**, 169–206.
- 268 S. Barroso, P. Adão, F. Madeira, M. T. Duarte, J. C. Pessoa and A. M. Martins, *Inorg. Chem.*, 2010, **49**, 7452–7463.
- 269 J.-B. Wang, L.-P. Lu, J.-Y. Liu, H.-L. Mu and Y.-S. Li, *J. Mol. Catal. A Chem.*, 2015, **398**, 289–296.
- 270 F. Wolff, C. Lorber, R. Choukroun and B. Donnadiou, *Inorg. Chem.*, 2003, **42**, 7839–7845.
- 271 M. R. Maurya, A. Arya, A. Kumar, M. L. Kuznetsov, F. Avecilla and J. C. Pessoa, *Inorg. Chem.*, 2010, **49**, 6586–6600.
- 272 D. Rehder, *Coord. Chem. Rev.*, 2008, **252**, 2209–2223.
- 273 D. Rehder, C. Weidemann, A. Duch and W. Priebsch, *Inorg. Chem.*, 1988, **27**, 584–587.
- 274 A. Lehtonen and R. Sillanpää, *J. Chem. Soc., Dalt. Trans.*, 1995, 2701–2704.
- 275 M. Hoshino, H. Katou, K. Yamaguchi and Y. Goto, *Biochim. Biophys. Acta - Biomembr.*, 2007, **1768**, 1886–1899.
- 276 A. Jimtaisong and R. L. Luck, *Inorg. Chem.*, 2006, **45**, 10391–10402.
- 277 U. Sandbhor, S. Padhye and E. Sinn, *Transit. Met. Chem.*, 2002, **27**, 681–685.
- 278 Y.-J. Jang, S.-J. Mo and B.-K. Koo, *Bull. Korean. Chem Soc.*, 1998, **19**, 587–590.
- 279 G. Asgedom, A. Sreedhara, J. Kivikoski, J. Valkonen, E. Kolehmainen and C. P. Rao, *Inorg. Chem.*, 1996, **35**, 5674–5683.
- 280 D. F. Back, C. R. Kopp, G. Manzoni de Oliveira and P. C. Piquini, *Polyhedron*, 2012, **36**, 21–29.
- 281 C. P. Rao, A. Sreedhara, P. V. Rao, M. B. Verghese, K. Rissanen, E. Kolehmainen, N. K. Lokanath, M. A. Sridhar and J. S. Prasad, *J. Chem. Soc. Dalt. Trans.*, 1998, 2383–2394.
- 282 A. M. Morris, C. G. Pierpont and R. G. Finke, *Inorg. Chem.*, 2009, **48**, 3496–3498.
- 283 L. Gasque, A. Mendieta and G. Ferrer-Sueta, *Dalt. Trans.*, 2020, **49**, 3365–3368.
- 284 M. J. Deery, T. Fernandez, O. W. Howarth and K. R. Jennings, *J. Chem. Soc. Dalt. Trans.*, 1998, 2177–2184.
- 285 S. Ralph, P. Iannitti, R. Kanitz and M. Sheil, *Eur. J. Mass Spectrom.*, 1996, **2**, 173.
- 286 P. C. A. Bruijninx, M. Lutz, A. L. Spek, W. R. Hagen, B. M. Weckhuysen, G. van Koten and R. J. M. K. Gebbink, *J. Am. Chem. Soc.*, 2007, **129**, 2275–2286.



- 287 H. Komatsuzaki, A. Shiota, S. Hazawa, M. Itoh, N. Miyamura, N. Miki, Y. Takano, J. Nakazawa, A. Inagaki, M. Akita and S. Hikichi, *Chem. - An Asian J.*, 2013, **8**, 1115–1119.
- 288 M. Garai, D. Dey, H. R. Yadav, A. R. Choudhury, N. Kole and B. Biswas, *Polyhedron*, 2017, **129**, 114–122.
- 289 C. Bianchini, P. Frediani, F. Laschi, A. Meli, F. Vizza and P. Zanello, *Inorg. Chem.*, 1990, **29**, 3402–3409.
- 290 T. R. Demmin and M. M. Rogic, *J. Org. Chem.*, 1980, **45**, 1153–1156.
- 291 F. R. Hewgill and S. L. Lee, *J. Chem. Soc. C Org.*, 1969, 2080.
- 292 W. A. Herrmann, R. W. Fischer and J. D. G. Correia, *J. Mol. Catal.*, 1994, **94**, 213–223.
- 293 G.-J. ten Brink, I. W. C. E. Arends and R. A. Sheldon, *Chem. Rev.*, 2004, **104**, 4105–4124.
- 294 A. Butler, M. J. Clague and G. E. Meister, *Chem. Rev.*, 1994, **94**, 625–638.
- 295 M. Sutradhar, L. M. D. R. S. Martins, M. F. C. Guedes da Silva and A. J. L. Pombeiro, *Coord. Chem. Rev.*, 2015, **301–302**, 200–239.
- 296 M. Kirihara, *Coord. Chem. Rev.*, 2011, **255**, 2281–2302.
- 297 V. Conte and B. Floris, *Inorganica Chim. Acta*, 2010, **363**, 1935–1946.
- 298 P. Sözen-Aktaş, E. Manoury, F. Demirhan and R. Poli, *Eur. J. Inorg. Chem.*, 2013, **2013**, 2728–2735.
- 299 T. Heikkilä, R. Sillanpää and A. Lehtonen, *J. Coord. Chem.*, 2014, **67**, 1863–1872.
- 300 A. Lehtonen and R. Sillanpää, *Polyhedron*, 2005, **24**, 257–265.
- 301 H. Adolfsson and D. Balan, in *Aziridines and Epoxides in Organic Synthesis*, Wiley-VCH Verlag GmbH & Co. KGaA, Weinheim, FRG, 2006, pp. 185–228.
- 302 M. E. Judmaier, C. Holzer, M. Volpe and N. C. Mösch-Zanetti, *Inorg. Chem.*, 2012, **51**, 9956–9966.
- 303 J. Pisk, B. Prugovečki, D. Matković-Čalogović, R. Poli, D. Agustin and V. Vrdoljak, *Polyhedron*, 2012, **33**, 441–449.
- 304 M. G. Topuzova, S. V. Kotov and T. M. Kolev, *Appl. Catal. A Gen.*, 2005, **281**, 157–166.
- 305 E. P. Talsi, V. D. Chinakov, V. P. Babenko and K. I. Zamaraev, *J. Mol. Catal.*, 1993, **81**, 235–254.
- 306 C. K. Sams, K. A. Jørgensen, S. V. Lindeman and J. Songstad, *Acta Chem. Scand.*, 1995, **49**, 839–847.
- 307 D. K. Steelman, S. Xiong, P. D. Pletcher, E. Smith, J. M. Switzer, G. A. Medvedev, W. N. Delgass, J. M. Caruthers and M. M. Abu-Omar, *J. Am. Chem. Soc.*, 2013, **135**, 6280–6288.
- 308 Y. Nishiyama, Y. Nakagawa and N. Mizuno, *Angew. Chemie - Int. Ed.*, 2001, **40**, 3639–3641.
- 309 J. A. Brito, M. Gómez, G. Muller, H. Teruel, J. C. Clinet, E. Duñach and M. A. Maestro, *Eur. J. Inorg. Chem.*, 2004, 4278–4285.
- 310 C. Aubry, G. Chottard, N. Platzler, J. M. Bregeault, R. Thouvenot, F. Chauveau, C. Huet and H. Ledon, *Inorg. Chem.*, 1991, **30**, 4409–4415.
- 311 S. A. Hauser, M. Cokoja, M. Drees and F. E. Kühn, *J. Mol. Catal. A Chem.*, 2012, **363–364**, 237–244.



**TURUN  
YLIOPISTO**  
UNIVERSITY  
OF TURKU

ISBN 978-951-29-8654-5 (Print)  
ISBN 978-951-29-8655-2 (PDF)  
ISSN 0082-7002 (Print)  
ISSN 2343-3175 (Online)